

การพัฒนาวัสดุกำบังนิวตรอนพลังงานสูงและรังสีแกมมาที่ประกอบด้วยซีเมนต์ผสมยางความ
หนาแน่นสูง



นางสาวปวีตรา เอ็มโอ

จุฬาลงกรณ์มหาวิทยาลัย

บทคัดย่อและแฟ้มข้อมูลฉบับเต็มของวิทยานิพนธ์ตั้งแต่ปีการศึกษา 2554 ที่ให้บริการในคลังปัญญาจุฬาฯ (CUIR)
เป็นแฟ้มข้อมูลของนิสิตเจ้าของวิทยานิพนธ์ ที่ส่งผ่านทางบัณฑิตวิทยาลัย

The abstract and full text of theses from the academic year 2011 in Chulalongkorn University Intellectual Repository (CUIR)
are the thesis authors' files submitted through the University Graduate School.

วิทยานิพนธ์นี้เป็นส่วนหนึ่งของการศึกษาตามหลักสูตรปริญญาวิศวกรรมศาสตรดุษฎีบัณฑิต

สาขาวิชาวิศวกรรมนิวเคลียร์ ภาควิชาวิศวกรรมนิวเคลียร์

คณะวิศวกรรมศาสตร์ จุฬาลงกรณ์มหาวิทยาลัย

ปีการศึกษา 2560

ลิขสิทธิ์ของจุฬาลงกรณ์มหาวิทยาลัย

Development of Innovative High-Energy Neutron and Gamma-ray Shielding
Material Based on High Density Cement and Crumb Rubber



A Dissertation Submitted in Partial Fulfillment of the Requirements
for the Degree of Doctor of Engineering Program in Nuclear Engineering

Department of Nuclear Engineering

Faculty of Engineering

Chulalongkorn University

Academic Year 2017

Copyright of Chulalongkorn University

ปวีตรา เอมโอ : การพัฒนาวัสดุกำบังนิวตรอนพลังงานสูงและรังสีแกมมาที่ประกอบด้วยซีเมนต์ผสมยางความหนาแน่นสูง (Development of Innovative High-Energy Neutron and Gamma-ray Shielding Material Based on High Density Cement and Crumb Rubber) อ.ที่ปริกษานิพนธ์หลัก: รศ. ดร.ดุลยพงศ์ วงศ์แสวง, อ.ที่ปริกษานิพนธ์ร่วม: สมชาย ต้นชราภรณ์, 142 หน้า.

วัสดุที่มีธาตุคาร์บอนและไฮโดรเจนเป็นองค์ประกอบนั้นมีส่วนช่วยในการปรับปรุงประสิทธิภาพของวัสดุป้องกันรังสี คอนกรีตความหนาแน่นสูงผสมยางผงถูกนำมาศึกษาเพื่อใช้เป็นวัสดุกำบังรังสีนิวตรอนและแกมมา การออกแบบวัสดุป้องกันรังสีในงานวิจัยนี้ใช้ โปรแกรม Monte Carlo N-Particle เพื่อศึกษาสัดส่วนของวัสดุป้องกันรังสีที่เหมาะสม วัสดุป้องกันรังสีถูกออกแบบโดยใช้คอนกรีตความหนาแน่นสูงผสมกับยางผงคิดเป็นร้อยละ 5 ถึง 25 โดยปริมาตร และเพิ่มขึ้นร้อยละ 5 โดยใช้ต้นกำเนิดรังสีนิวตรอนจาก Am/Be-241 และต้นกำเนิดรังสีแกมมาจาก Co-60 วัสดุที่ใช้ในงานวิจัยถูกนำมาผสมและขึ้นรูปเพื่อประเมินการลดทอนรังสีนิวตรอนและแกมมาของวัสดุป้องกันรังสี รวมถึงการศึกษาสาเหตุของวัสดุป้องกันรังสีคอนกรีตความหนาแน่นสูงผสมตะกั่วหรือ HDCRL แต่กร้าวโดยใช้เทคนิค X-ray diffraction เพื่อศึกษารูปแบบของฟลักและสารประกอบที่พบในวัสดุป้องกันรังสี HDCRL และได้ทำการศึกษาการเกิดการกระเจิงของรังสีแกมมา และการเกิดรังสีแกมมาทุติยภูมิจากอันตรกิริยา neutron capture โดยการประเมินค่า Buildup factor ของวัสดุ ตลอดจนทำการศึกษากการปลดปล่อยรังสีแกมมาทุติยภูมิจากอันตรกิริยาของรังสีนิวตรอนด้วยเทคนิค Prompt Gamma Neutron Activation Analysis หรือ PGNAA รวมถึงมีการประเมินคุณสมบัติเชิงกลของวัสดุด้วยเครื่อง Compressive Testing Machine ผลการศึกษาพบว่าวัสดุคอนกรีตความหนาแน่นสูงผสมยางผงร้อยละ 5 และตะกั่วร้อยละ 5 โดยปริมาตรมีประสิทธิภาพในการลดทอนรังสีนิวตรอนและแกมมาสูงสุดโดยเปรียบเทียบร้อยละการลดทอนของวัสดุดังกล่าวเทียบกับวัสดุคอนกรีตธรรมดา การลดทอนรังสีนิวตรอนคิดเป็นร้อยละ 64 และการลดทอนรังสีแกมมาคิดเป็นร้อยละ 68 สาเหตุของการแตกร้าวของวัสดุคอนกรีตความหนาแน่นสูงผสมยางและตะกั่วพบมีการเกิดผลึกของ barite, portlandite, quartz, calcite, lead and PbO₂ รวมถึงการยึดเกาะระหว่างวัสดุคอนกรีตความหนาแน่นสูงผสมยางและตะกั่วที่มีการยึดเกาะน้อยจึงเป็นสาเหตุให้เกิดรอยร้าวในวัสดุเกิดขึ้น ด้านการเกิดอันตรกิริยาของรังสีแกมมาและวัสดุคอนกรีตความหนาแน่นสูงผสมยางนั้นมีผลทำให้ค่า Buildup factor ของวัสดุมีค่าสูงขึ้น อย่างไรก็ตามค่า Buildup factor ของวัสดุดังกล่าวมีค่าใกล้เคียง 1 จึงอาจสรุปได้ว่าไม่พบการกระเจิงของรังสีแกมมาและรังสีแกมมาทุติยภูมิ ด้านอันตรกิริยาของรังสีนิวตรอนกับวัสดุคอนกรีตผสมยางผง ผลจากการวิเคราะห์ด้วยเทคนิค PGNAA ไม่พบการเกิดรังสีแกมมาทุติยภูมิในตัวอย่างวัสดุ จากการศึกษาค่าเฉลี่ยแรงอัดของวัสดุพบว่าวัสดุคอนกรีตความหนาแน่นสูงผสมยางผงร้อยละ 5 โดยปริมาตรมีความแข็งแรงมากกว่าสัดส่วนอื่น การเพิ่มปริมาณยางผงในวัสดุคอนกรีตความหนาแน่นสูงมีผลทำให้ความแข็งแรงของวัสดุลดลง วัสดุป้องกันรังสีคอนกรีตความหนาแน่นผสมยางไม่เพียงสามารถนำไปประยุกต์ใช้ทางด้านวิทยาศาสตร์นิวเคลียร์และด้านวิศวกรรมนิวเคลียร์ แต่ยังมีส่วนช่วยในการลดปัญหาสิ่งแวดล้อมที่เกิดจากยางผงได้อีกด้วย

ภาควิชา วิศวกรรมนิวเคลียร์

ลายมือชื่อนิสิต

สาขาวิชา วิศวกรรมนิวเคลียร์

ลายมือชื่อ อ.ที่ปริกษาหลัก

ปีการศึกษา 2560

ลายมือชื่อ อ.ที่ปริกษาร่วม

5771442421 : MAJOR NUCLEAR ENGINEERING

KEYWORDS: NEUTRON AND GAMMA SHIELDING / CRUMB RUBBER / HIGH-DENSITY CEMENT

PAWITRA AIM-O: Development of Innovative High-Energy Neutron and Gamma-ray Shielding Material Based on High Density Cement and Crumb Rubber. ADVISOR: ASSOC. PROF. DOONYAPONG WONGSAWAENG, Ph.D., CO-ADVISOR: SOMCHAI TANCHARAKORN, Ph.D., 142 pp.

The incorporation of carbon and hydrogen-rich material into radiation shielding material can improve its shielding performance. High-density cement mixed with crumb rubber was studied to be a gamma ray and neutron shielding material. Shielding materials were designed using high-density cement mixed with 5 – 25 vol% of crumb rubber. Monte Carlo N-Particle code was employed to simulate radiation shielding performances of the composed materials. The utilized neutron and photon sources were Am-241/Be and Co-60, respectively. These shielding designs were fabricated and experimentally evaluated on the radiation shielding properties. The cracking mechanism of high-density cement mixed with lead (HDCRL) was also investigated. The quantitative X-ray diffraction technique (QXRD) was used to determine the crystalline phases as well as elemental compositions of HDCRL. Buildup factors from gamma ray scattering, prompt and secondary gamma ray emissions from the neutron capture interaction were also evaluated. The prompt and secondary gamma ray emissions were determined using Prompt Gamma Neutron Activation Analysis (PGNAA). In addition, the mechanical properties of samples were evaluated using the Compressive Testing Machine (CTM). The high-density cement mixed with 5 vol% crumb rubber and 5 vol% lead powder demonstrated the highest neutron and gamma ray shielding performances. The neutron and photon attenuations were 64% and 68%, respectively, better than ordinary concrete. Analysis of the cracking mechanism of HDCRL revealed six crystalline phases: barite, portlandite, quartz, calcite, lead and PbO₂. The weak adhesion of lead powder to high-density cement was the main cause of cracking. For photon interaction, the gamma interaction with high-density cement mixed with crumb rubber increased the buildup factor; however, the value was close to unity leading to the conclusion that the secondary gamma ray and prompt gamma ray were not present. For neutron interaction, no prompt or secondary gamma ray emission was detected using PGNAA technique. The average compressive strength indicated that the high-density cement mixed with 5 vol% crumb rubber exhibited higher strength than other specimens and that increasing the crumb rubber content decreased the mechanical property. This innovative composite radiation shielding material not only benefits nuclear science and engineering applications, but also helps solve the environmental issue of waste rubber.

Department: Nuclear Engineering

Field of Study: Nuclear Engineering

Academic Year: 2017

Student's Signature

Advisor's Signature

Co-Advisor's Signature

ACKNOWLEDGEMENTS

At the end of my dissertation, I would like to sincerely thank all those people who have made this dissertation possible and for an unforgettable experience for me.

First of all, I would like to express my deepest sense of gratitude to my thesis advisor, Associate Professor Dr. Doonyapong Wongsawaeng, for his patient, guidance, enthusiastic encouragement and useful critiques of this research work. This dissertation could not have been accomplished without his continuous support throughout the dissertation stages. He has given his knowledge and put in great effort at all time for the benefit of this dissertation. His willingness to give his time so generously has been very much appreciated.

I would like to express my very great appreciation to Synchrotron Light Research Institute (Public Organization) and Ministry of Science and Technology, Royal Thai Government for the financial support of the Ph.D. Scholarship. My very sincere thanks to Prof. Wng. Cmdr. Dr. Sarawut Sujitjorn (Director of SLRI), Dr. Prapong Klysubun, as well as SLRI executive management team for giving me the great opportunity to study the Ph.D. program. I would also like to thank Dr. Somchai Tancharakorn, my co-advisor, for his advice and assistance in keeping my progress on schedule.

I would like to express my sincere appreciation to all lecturers for giving me the valuable knowledge, as well as the assistance of the staff members at the Nuclear Engineering Department, Faculty of Engineering, Chulalongkorn University.

Finally, I take this opportunity to express the profound gratitude from my deep heart to my family, my father and my mother, for the continuous support and encouragement beyond description.

CONTENTS

	Page
THAI ABSTRACT	iv
ENGLISH ABSTRACT	v
ACKNOWLEDGEMENTS	vi
CONTENTS	vii
LIST OF TABLES	12
LIST OF FIGURES	13
CHAPTER I	18
INTRODUCTION	18
1.1 Background and Significance of the Study	18
1.2 Research objective	20
1.3 Scope of dissertation	20
1.4 Expected benefits	21
CHAPTER II	22
THEORY AND LITERATURE REVIEWS	22
2.1 Neutron	22
2.1.1 Nuclear Reactions	22
2.1.2 Charged Particle Reaction	23
2.1.3 Neutron Reaction	24
2.1.4 Neutron Division (by Energy Level)	27
2.1.5 Neutron Interactions	27
2.1.6 Neutron flux	30
2.1.7 Mean free path	31

	Page
2.1.8 Neutron cross section.....	32
2.1.9 Neutron Detection	36
2.2 Gamma ray	37
2.2.1 Gamma interactions.....	38
2.2.2 Interaction processes.....	42
2.3 Gamma ray attenuation.....	43
2.4 Neutron attenuation.....	46
2.5 Monte Carlo Transport Code	47
2.5.1 INP File	48
2.5.2 Cell Cards	49
2.5.3 Surface Cards.....	50
2.5.4 Data Specifications	51
2.5.5 Materials Specification.....	55
2.5.6 Miscellaneous Data Specifications.....	56
2.5.7 Truncation Techniques	57
2.5.8 Statistics.....	57
2.6 Concrete.....	58
2.6.1 Cement	59
2.6.2 Hydration of Portland Cement.....	59
2.6.3 Heat of hydration	62
2.6.4 Portland Cement (American Standard Type).....	62
2.6.5 Mechanical Properties of concrete	63
2.7 Natural Rubber	64

	Page
2.7.1 Tyre.....	65
2.7.2 Waste Rubber Disposal	67
2.7.3 Crumb rubber.....	67
CHAPTER III	68
METHODOLOGY.....	68
3.1 Materials and Instruments	68
3.2 Material analysis.....	70
3.2.1 Material analysis by Scanning Electron Microscope with Energy Dispersive Spectroscopy (SEM:EDS)	70
3.2.2 Material analysis by carbon/hydrogen/nitrogen determinator (CHN determinator)	74
3.2.3 Material analysis by X-ray diffraction.....	75
3.3 Material proportions.....	76
3.4 Shielding materials attenuation simulation by Monte Carlo Simulation (MCNP).....	77
3.5 Shielding materials preparation.....	78
3.6 Gamma attenuation measurement	79
3.7 Neutron attenuation measurement.....	80
3.7.1 Fast neutron attenuation measurement	80
3.8 Lead Adhesion Testing.....	81
3.9 Scattered gamma ray and secondary gamma ray by buildup factor experiment.....	82
3.10 Dose rate measurement	84

	Page
3.11 Prompt gamma ray and secondary gamma ray by Prompt Gamma Neutron Activation Analysis (PGNAA).....	85
3.12 Compressive strength test	86
CHAPTER IV.....	87
RESULTS AND DISCUSSIONS	87
4.1 Material proportions by Monte Carlo Simulation.....	87
4.1.1 Neutron attenuation simulation	87
4.2 Neutron and gamma attenuation experiments	90
4.2.1 Neutron attenuation measurement.....	90
4.2.2 Gamma attenuation measurement.....	91
4.3 Additional material for improving gamma ray shielding performance.....	92
4.4 Additional material for improving neutron shielding performance.....	95
4.5 Radiation transmissions of different shielding thicknesses.....	96
4.5.1 Neutron transmission of high density cement mixed with 5 vol% crumb rubber and boron carbide	96
4.5.2 Gamma ray transmission of high density cement mixed with 5 vol% crumb rubber and lead	97
4.6 Determination of scattered gamma ray and secondary gamma ray from shielding materials.....	98
4.7 Determination of prompt gamma ray and secondary gamma ray of shielding materials	103
4.8 Investigation of the cracking mechanism of high-density cement mixed with crumbed rubber and lead particles.....	104
4.8.1 Lead adhesion result.....	105

	Page
4.8.2 Analysis of elemental composition of high-density cement mixed with 5 vol% crumb rubber and various percentages of lead particles.....	106
4.4 Dose rate evaluation.....	116
4.5 Mechanical property of shielding materials by Compressive Testing Machine (CTM).....	117
4.6 Economic data.....	118
CHAPTER VI.....	120
CONCLUSIONS.....	120
5.1 Conclusions of research.....	120
5.2 Recommendations for future research.....	122
REFERENCES.....	126
APPENDIX B.....	134
APPENDIX C.....	135
EXAMPLE OF MCNP INPUT FILE.....	135
VITA.....	142

LIST OF TABLES

Table 2. 1 Neutron division by energy level.....	27
Table 2. 2 Macrobody available in MCNP [13].....	51
Table 2. 3 Types of tallies available in MCNP [13].....	54
Table 2. 4 Composition of Portland cement with chemical composition and weight percent	60
Table 2. 5 The types of cement are categorized into eight types that are covered in ASTM C150 as the following. [16]	62
Table 2. 6 A Typical Composition by Weight of Tyre [23].....	67
Table 3. 1 Compositions of various shielding materials used in the MCNP simulation.....	77
Table 4. 1 Gamma ray transmissions of narrow beam and broad beam geometries [27] ($I_{ob}=123863.333$ and $I_{0g} = 125572.667$).....	99
Table 4. 2 Weight and atomic percentages of elemental composition of the lead powder based on EDS analysis	105
Table 4. 3 Weight percentages of elemental composition of HDCR25 and HDCR5L8 based on EDS analysis	112
Table 4. 4 Quantitative estimate of weight percentages of the mineral phases in HDCR5 and HDCR5L8 samples based on XRD analysis	115
Table 4. 5 Compressive strengths of different types of shielding materials[27]	118

LIST OF FIGURES

Figure 2. 1 Elastic scattering.....	28
Figure 2. 2 Inelastic scattering.....	28
Figure 2. 3 Radiative Capture (n, γ) of hydrogen to become deuterium.....	29
Figure 2. 4 Radiative Capture (n, γ) of deuterium to become tritium.....	29
Figure 2. 5 Neutron fission.....	30
Figure 2. 6 The relation of neutron flux and energy of research reactor	31
Figure 2. 7 Interaction between neutron beam and target area.....	32
Figure 2. 8 Interaction between neutron beam and Fe-56 target.	33
Figure 2. 9 Three stages of Uranium-238 decay series	38
Figure 2. 10 Photoelectric effect.....	39
Figure 2. 11 Pair production	40
Figure 2. 12 Compton scattering.....	41
Figure 2. 13 Major types of gamma ray interaction and their dependency on Z of absorber and photon energy[9].....	42
Figure 2. 14 Gamma transmissions	43
Figure 2. 15 Neutron transmissions	46
Figure 2. 16 Schematic illustration of the pores in calcium silicate through different stages of hydration.[14].....	61
Figure 2. 17 The chemical structure of natural rubber	64
Figure 2. 18 The cross section of tyre.....	65
Figure 3. 1 (a) Sample analysis preparation (b) Scanning Electron Microscope Instrument.....	70
Figure 3. 2 SEM micrograph of Portland cement type I	71

Figure 3. 3 EDS spectrum of Portland cement type I	72
Figure 3. 4 SEM micrograph of barite.....	72
Figure 3. 5 EDS spectrum of Barite	73
Figure 3. 6 SEM micrograph of lead	73
Figure 3. 7 EDS spectrum of lead particles	74
Figure 3. 8 SEM micrograph of crumb rubber	74
Figure 3. 9 EDS spectrum of crumb rubber	75
Figure 3. 10 (a) Sample packing (b) X-ray diffraction machine.....	76
Figure 3. 11 Mesh Tally Contour Plot of the simulated shielding material.....	78
Figure 3. 12 (a) Material mixing in mortar mixer (b) Mixed materials placed and compacted in the molds.....	79
Figure 3. 13 (a) Specimens before curing in water (b) Shielding material specimens .	79
Figure 3. 14 Gamma attenuation arrangement.....	80
Figure 3. 15 (a) Fast neutron measurement (b) Thermal neutron measurement.....	81
Figure 3. 16 Lead powder on surface of wet shielding	82
Figure 3. 17 Broad beam arrangement.....	83
Figure 3. 18 Narrow beam arrangement.....	83
Figure 3. 19 Gamma dose rate measurement	84
Figure 3. 20 Neutron dose rate measurement	85
Figure 3. 21 PGNAA experimental setup	85
Figure 3. 22 (a) Standard material compression testing machine	86
Figure 4. 1 Simulation result of neutron attenuation of high-density concrete mixed with various volume percentages of waste rubber	88

Figure 4. 2 Simulation result of high-density cement mixed with crumb rubber for photon flux at 0.5 MeV	89
Figure 4. 3 Simulation result of high-density cement mixed with crumb rubber for photon flux at 5 MeV	89
Figure 4. 4 Experimental results of fast neutron transmission for HDC with various vol% of waste rubber[26]	91
Figure 4. 5 Gamma ray attenuation coefficient of HDC mixed with various waste rubber content[26]	92
Figure 4. 6 Simulation result of transmitted photon flux from high-density cement mixed with 5 wt% crumbed rubber and various percentages of lead powder	93
Figure 4. 7 Simulation result of transmitted neutron flux from high-density cement mixed with 5 wt% of crumbed rubber and various percentages of lead powder	94
Figure 4. 8 Gamma ray attenuation coefficient of HDCR5 mixed with various lead contents[26]	95
Figure 4. 9 Experimental results of thermal neutron transmission for HDCR5 with various vol% of boron carbide[26]	95
Figure 4. 10 Simulation results of neutron transmission of HDCR5 with different vol% of boron carbide addition[26]	97
Figure 4. 11 Simulation results of gamma ray transmission of HDCR5 with different vol% of lead addition[26]	98
Figure 4. 12 Mean free path of gamma ray after addition of crumb rubber in high density cement	100
Figure 4. 13 Linear attenuation coefficient of high-density cement mixed with crumb rubber	101
Figure 4. 14 Relationship between linear attenuation coefficient and buildup factor of shielding materials	102

Figure 4. 15 The spectrum of Co-60 background[27].....	103
Figure 4. 16 The spectra of high-density cement with and without crumb rubber compared with Co-60 background spectrum[27]	104
Figure 4. 17 After removal of lead powder from surface of dried shielding	106
Figure 4. 18 SEM micrograph of high-density cement with 5,000x magnification	107
Figure 4. 19 SEM micrograph of high-density cement mixed with 5 vol% crumb rubber at 5,000x magnification.....	107
Figure 4. 20 SEM micrograph of high-density cement mixed with 10 vol% crumb rubber at 5,000x magnification.....	108
Figure 4. 21 SEM micrograph of high-density cement mixed with 15 vol% crumb rubber at 5,000x magnification.....	108
Figure 4. 22 SEM micrograph of high-density cement mixed with 20 vol% crumb rubber at 5,000x magnification.....	109
Figure 4. 23 SEM micrograph of high-density cement mixed with 25 vol% crumb rubber at 5,000x magnification.....	109
Figure 4. 24 SEM micrograph of high-density cement mixed with 5 vol% crumb rubber and 2 vol% lead particles with 5,000x magnification.....	110
Figure 4. 25 SEM micrograph of high-density cement mixed with 5 vol% crumb rubber and 4 vol% lead particles with 5,000x magnification.....	110
Figure 4. 26 SEM micrograph of high-density cement mixed with 5 vol% crumb rubber and 6 vol% lead particles with 5,000x magnification.....	111
Figure 4. 27 SEM micrograph of high-density cement mixed with 5 vol% crumb rubber and 8 vol% lead particles with 5,000x magnification.....	111
Figure 4. 28 EDS spectrum of HDCR25.....	113
Figure 4. 29 EDS spectrum of HDCR5L8	113
Figure 4. 30 XRD spectrum of HDCR5	114

Figure 4. 31 XRD spectra of HDCR5L2, HDCR5L4, HDCR5L6 and HDCR5L8	114
Figure 4. 32 Gamma dose equivalent rate of fabricated shielding materials.....	116
Figure 4. 33 Neutron monitor detector	117



CHAPTER I

INTRODUCTION

1.1 Background and Significance of the Study

Nowadays, the radiation and the nuclear interactions are widely utilized in many medical, research and other fields. The penetrating capability of radiation depends on the type of radiation, energy and strength or radioactivity. The radiation protection has to be considered due to its hazardous effects. As the principle of radiation protection is to reduce it to be as low as reasonably achievable or ALARA, three major factors to be maintained are time, distance and shielding. For this research, the study focused on the shielding of the neutrons and the gamma radiation. Because neutrons and gamma radiation have high penetrating capabilities which can travel through the skin and may cause damages to the tissues or organ in the human body, it is necessary to reduce the radiation risk that may arise for the radiation worker. The radiation shielding is the necessary procedure to provide the radiation workers. Many shielding materials have been utilized to control the radiation exposure to be below the dose limit value as defined by the International Commission on Radiological Protection or ICRP.

For the shielding design, the radiation source consideration is the first priority. Some radiation sources can generate both the gamma rays and the neutron particles. For example, with the superconducting wiggler installed in the storage ring of the synchrotron light source, interaction of high-energy gamma ray with beryllium material results in emissions of neutrons and the gamma ray. This process is called the photonuclear reaction process. [1].

The intensities of sources and the intensities of radiation travelling through materials are evaluated to determine the radiation attenuation by using Beer Lambert's Law. The linear attenuation coefficient has been studied, which is the attenuation parameter for the gamma ray shielding while the removal cross section,

macroscopic cross section or neutron attenuation coefficient is the attenuation parameter for neutron shielding.

Shielding material depends on the type of radiation. Gamma shielding usually composes of heavy elements and high density atoms. Neutron shielding often consists of light elements such as hydrogen and carbon with the characteristic properties to shield against neutron particles. Concrete is the widely preferred material for radiation shielding because of the strength and the cost-effectiveness. This material can attenuate the neutron and gamma radiation. The thick shielding material increases the radiation attenuation. However, in certain locations the thick shielding is not practical due to space limitation. This is the reason why the high density concrete has been utilized as shielding materials more than the ordinary concrete.

Rubber is the biological material which is cost-effective and is cultivated in the southern and eastern of Thailand. There are several research studies using the rubber to be a neutron shielding because rubber contains a lot of hydrogen atoms and carbon atoms. For example, researchers used natural rubber latex mixed with concrete in order to study the high strength concrete [2]. Moreover, the used materials are utilized to mix with concrete. For example, some researchers selected to used tyre rubber as a mixture in concrete in order to study the mechanical properties of concrete [3]. This way, the waste rubber has been recycled into the new product which has contributed to benefit the environment, which is the interesting way to remove the waste. However, most of research studies investigated the mechanical properties of the materials. There has been no research study on the radiation attenuation property. The aim of this research was to design and study the neutron and gamma ray shielding efficiency of the shielding material composing of high-density concrete and waste rubber.

Monte Carlo N-Particle Transport Code was utilized to study the probability of photon and neutron transportation through material and to determine the optimum design of high-density cement mixed with crumb rubber. The results of MCNP simulation were compared with the experiments. The chemical absorbers such as

boron carbide and lead were added to high-density cement mixed with crumb rubber in order to increase the neutron and gamma attenuation efficiency. However, the addition of lead into high-density cement mixed with crumb rubber affected the strength of materials, resulting in cracking problems. The cause of material cracking was investigated in order to improve the strength of the radiation shielding materials, by studying the microstructure and chemical phases in them.

For the application of high-density cement mixed with crumb rubber, two interactions between neutron radiation and gamma radiation occur, resulting in energy loss or transfer of radiation energy which releases radiation. The materials of this research study are utilized for radiation safety, thus, the occurrence of radiation from the interactions need to be investigated. For gamma interactions, the scattered gamma ray and secondary gamma ray may occur from Compton scattering process. Buildup factor is the parameter that was determined to describe this interaction of high-density cement mixed with crumb rubber. For neutron interactions, the prompt gamma ray and secondary gamma ray can be generated from the neutron capture process. The prompt gamma neutron activation analysis technique was used to determine the gamma emission.

The compressive strength was used to describe the mechanical property of this material which can be applied in other engineering works.

1.2 Research objective

To develop an innovative high-energy neutrons and gamma-ray shielding material based on the high density cement and crumb rubber.

1.3 Scope of dissertation

- 1.3.1 Utilize crumb rubber (waste rubber) available in Thailand.
- 1.3.2 Model the composition of shielding materials using MCNP transport code.
- 1.3.3 Develop and fabricate high-energy neutron and gamma-ray shielding material based on the high density cement and crumb rubber.

- 1.3.4 Estimate the neutron attenuation and dose using the neutron source.
- 1.3.5 Estimate the gamma-ray attenuation and dose using the gamma-ray source.
- 1.3.6 Determine the mechanical strength of the designed shielding materials.

1.4 Expected benefits

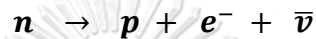
- 1.4.1 The shielding material based on high density cement and crumb rubber which can be effectively used for shielding is obtained. Such material can be used to shield the synchrotron radiation (high-energy neutron and gamma-ray).
- 1.4.2 The low-cost shielding material is obtained and can be fabricated using the materials available domestically.
- 1.4.3 The crumb rubber will be utilized in this innovative shielding material.

CHAPTER II

THEORY AND LITERATURE REVIEWS

2.1 Neutron

Neutron is an unstable particle and its disintegration with a characteristic half-life value can be expressed by the following equation:

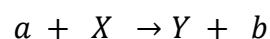


Where $\bar{\nu}$ is the antineutrino according to the quantum mechanics theory. The particles exhibit the wave properties as they are too small to be observed visually. However, they can be studied by their wave functions. In effect, the electron, proton, and neutron have their own characteristic wavelengths, “de Broglie wavelength or λ ,”. For instance, a neutron of 1 MeV energy has the wavelength of $2.86 \times 10^{-4} \text{ \AA}$, while a 0.025 eV thermal neutron has the wavelength of 1.798 \AA .

The fast neutrons from the fission reactions will diffuse in the medium and lose their energy through the collisions until they are in thermal equilibrium with the medium. The energy distribution of the thermal neutrons takes the form of Maxwell-Boltzmann distribution.

2.1.1 Nuclear Reactions

The nuclear reaction happens when the particle such as the proton, the neutron, and the nucleus interact with the other, forming the new nuclei, the new particles and emitting the gamma radiation. The general form of nuclear reaction can be written by:



Where a and X are the particle and the nucleus that interact together, resulting in the nucleus Y and the particle b.

The nuclear reactions are different from the general chemical reactions in that the chemical reactions result in the changes in the electron orbitals when the interaction occurs. For a nuclear reaction, the reaction process has to occur in the nucleus with the size of approximately 10^{-14} to 10^{-15} m which results in the rearrangement of the protons and the neutrons in the nuclear orbitals and, thus, in the new nucleus. The nuclear reactions depend on the types of particles, energy and probability of interactions or cross sections of these reactions such as the Charged Particle Reaction and Neutron Reaction.

2.1.2 Charged Particle Reaction

The charged particles obtained from the particle accelerators can be employed to interact with the nuclei or other particles. Most common charged particles are protons, deuterons and alpha particles. There are several methods to increase the probability of nuclear reactions. For example, increasing the temperature or the energy of an atom or nucleus will provide the energy to overcome the Coulomb or the nuclear force. Particles with sufficiently high energy can result in nuclear interaction. On the other hand, the speed of the particles can be decreased due to energy lost via the scattering process, which is divided into two groups: elastic scattering and inelastic scattering. In addition, the radiative capture can result in new, usually radioactive nuclides, and the produced radioactive nuclides can also emit the particles (charged or uncharged) and gamma radiation. The important particle reactions with the high probability of occurrence are as follows:

1. Proton reaction: (p, n) , (p, d) , (p, α) and (p, γ) . In this reaction, a proton is absorbed by the light element nuclide. The reaction of ${}^7\text{Li}(p, \alpha){}^4\text{He}$ is an example.

2. Deuteron reaction: (d, p), (d, n) and (d, α). For example, the neutron source used to initiate a nuclear reaction operation can come from $^2\text{H}(d, n)^3\text{He}$ and $^9\text{Be}(d, n)^{10}\text{B}$ reactions.
3. Alpha reaction: (α , p) and (α , n). For example, the reaction $^9\text{Be}(\alpha, n)^{12}\text{C}$, which led to a discovery of a neutron particle.
4. Fission reaction: This reaction occurs when a large nuclide is bombarded by the protons, deuterons or alpha particles, and is splitted into two or three daughter nuclides.
5. Spallation. This reaction occurs when a proton is accelerated to more than 10^3 MeV and hits the nucleus of heavy element, separates the nucleus into fragments. This process releases a large number of high energy neutrons.

2.1.3 Neutron Reaction

The uncharged neutrons usually pass through the atoms composing of the medium. The coulomb force does not affect them. However, it has the potential of interaction with their nuclei. While there are several neutron reactions, they can be separated into two processes. The first process is the direct reaction or the potential scattering, which is the basic neutron reaction with the target. The other one is the reaction via the compound nucleus formation where a neutron is absorbed by the nucleus of the target and a new compounded nucleus, which is radioactive, is produced.

Because the neutrons are unstable and beta-decay into the protons with a half-life of approximately ten minutes and because they cannot be stored, they need to be generated via the nuclear reactions. The neutrons can be produced by several ways, which are described as follows.

2.1.3.1 Neutron Sources

The neutrons are emitted from the neutron source. There are various types of neutron sources such as radioactive sources, neutron research facilities and nuclear research reactors, for example. The neutron utilization depends on neutron energy, neutron flux, size of source, costs, etc. The neutron radiation is used to apply in areas of engineering, physics, nuclear power, petroleum exploration, biology, medicine, chemistry and industries, for instance.

In some occasions, a portable source of neutrons is required. Portable neutron sources are normally from the (α, n) reaction or the spontaneous fission. The alpha sources are usually ^{238}Pu , ^{241}Am or ^{242}Cm . The emitted alpha particles interact with beryllium to produce neutrons via the (α, n) reaction. In addition, gamma radiation is also generated.

2.1.3.2 Neutron Generators

Neutron generators are one type of the charged particle accelerators designed to generate a neutron beam from nuclear reaction. Commonly used nuclear reactions are $^3\text{H}(d, n)$ and $^7\text{Li}(p, n)$. The most common one is the $^3\text{H}(d, n)$ reaction. Deuterons are accelerated with the appropriate currents and impinge on the tritium target. The tritium targets are typically Ti with added titanium tritide. This neutron production technique is commonly utilized in the fast neutron activation analysis to determine the light elements.

The spallation neutron sources produce neutrons from the interaction of high energy protons with heavy nuclei such as mercury, which results in the nuclear spallation and releases 20-30 neutrons/proton reaction cascade. These intense neutron fluxes can be utilized in neutron scattering experiments.

2.1.3.3 Accelerators

Accelerators are machines that accelerates the charged particles to increase kinetic energies to overcome the coulomb repulsion force for a nuclear reaction to occur. Several types of machines are designed to accelerate charged particles, for example,

(in the order of increasing final energy) ion sources, electrostatic machines, linear accelerators, cyclotrons and synchrotrons.

Synchrotrons are the high performance machines to produce the electron beams of very high energies. Synchrotrons use the concept of charged particles to generate the synchrotron radiation. Synchrotron radiation is an electromagnetic wave that is emitted from electrons which are accelerated near the speed of light in the magnetic or electric fields. The characteristics of synchrotron radiation are broad spectrum, high brightness, and high degree of collimation, well-defined polarization, pulsed time structure, and others.

The photonuclear reaction can occur in a synchrotron machine from the interaction between the photons and the nuclei. Photons are absorbed by the nuclei of the target forcing it into an excited state and emit particles. Not only will photons be released, but also neutrons, protons, and alpha particles. Thus, the neutron radiation is produced from this interaction.

2.1.3.4 Nuclear fission reactors

The nuclear reactor generates enormous quantities of neutron flux from fission reaction. The uranium-235 fissile isotope is typically used in nuclear power reactors. In such reactors, the only function of the neutrons is to sustain the nuclear fission reaction. On the contrary, nuclear research reactors are primarily designed to generate intense neutron flux and neutron beams for productions of radioisotopes and several other utilizations.

2.1.3.5 Nuclear fusion systems

In nuclear fusion, the hydrogen isotopes are combined. This reaction has the potential to generate large quantities of fast neutrons. Many small-scale experimental fusion reactors for research purposes are available at many academic institutions and laboratories worldwide. Some large-scale nuclear fusion systems also exist such as the

National Ignition Facility (NIF) in the USA, Joint European Torus (JET) in the UK and Thermonuclear Experimental Reactor (ITER) experiment in France.

2.1.4 Neutron Division (by Energy Level)

Different neutron sources offer different neutron energy spectra, which affect the interactions of neutrons with the matter. To understand the neutron behavior, the neutron energy is divided into the following groups as shown in Table 2.1.

Table 2.1 Neutron division by energy level

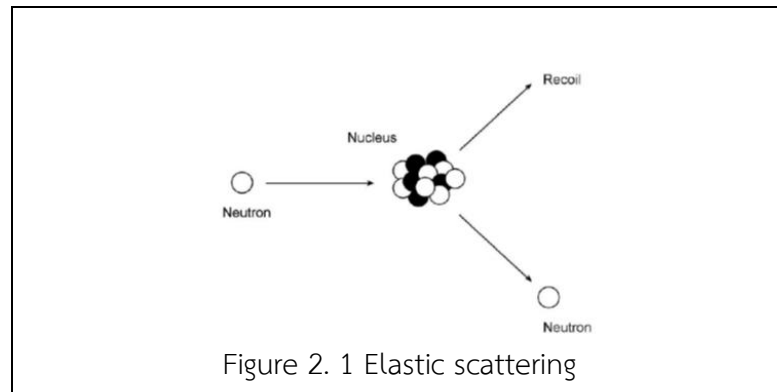
Type of neutron	Energy Level
Slow neutron	0 eV – 10^3 eV
Cold neutron	< 0.01 eV
Thermal neutron	0.01 eV – 0.3 eV
Epithermal neutron	0.3 eV – 10^4 eV

2.1.5 Neutron Interactions

Neutron is a neutral particle because it does not carry any electrical charge; therefore, it is not affected by the nucleus's positive charge. Neutrons interact with the nucleus directly after travelling through the electron cloud. The neutron interactions with nuclei can be one of the following 4 ways [4].

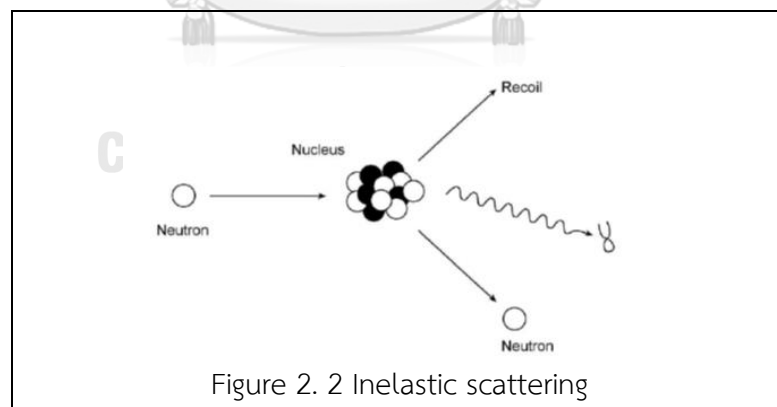
2.1.5.1 Elastic Scattering

For elastic scattering, the neutron scatters with the target nucleus similar to a billiard ball collision as shown in Fig. 2.1. The kinetic energy and momentum of this process are conserved. Normally, the incident neutron transfers some of the kinetic energy to the nucleus of target. The target nucleus gains the kinetic energy from the neutron and travels away with an increased speed. In this case, the nucleus returns to the original ground state. This interaction is abbreviated by the symbol (n, n).



2.1.5.2 Inelastic Scattering

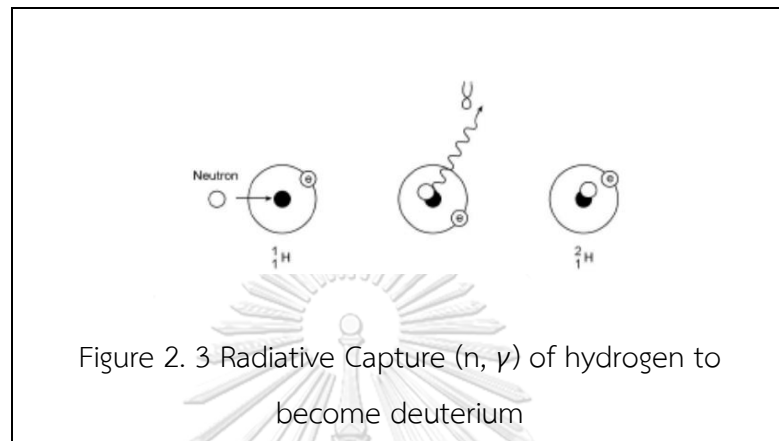
For inelastic scattering, the neutron scatters with the target nucleus like the elastic scattering. However, the difference of this interaction is that some of the incident neutron energy is absorbed by the recoiling nucleus, and the nucleus remains in an excited state as shown in Fig 2.2. The gamma ray, called inelastic gamma ray, is emitted from the excited nucleus. This is, therefore, an endothermic reaction because the energy is absorbed by the nucleus. Inelastic scattering is designated by the symbol (n, n'). This process usually occurs between high-energy neutrons and heavy nuclei and is important for nuclear reactor operation.



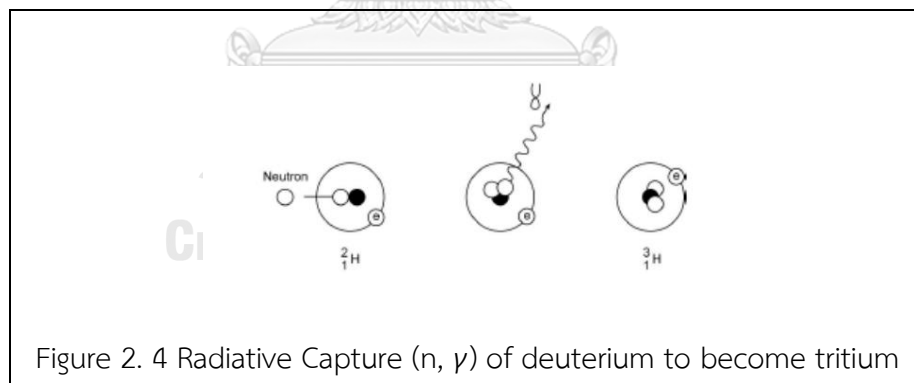
2.1.5.3 Radiative Capture

The radiative capture is a reaction that a neutron is completely captured or absorbed and a compound nucleus is formed. The compound nucleus decays to ground state and emits gamma ray as shown in Fig 2.3. This reaction can happen at all incident

neutron energies. Because the original neutron is absorbed, this interaction is known as absorption reactions process. This is an exothermic interaction and is denoted by (n, γ) . For example, the simple radiative capture occurs when neutron is absorbed by hydrogen atom to produce deuterium or heavy hydrogen.



The deuterium is a stable nuclide. However, there are several radiative capture products that are radioactive and beta-gamma emitters. Deuterium can undergo a radiative capture reaction to form tritium by itself.

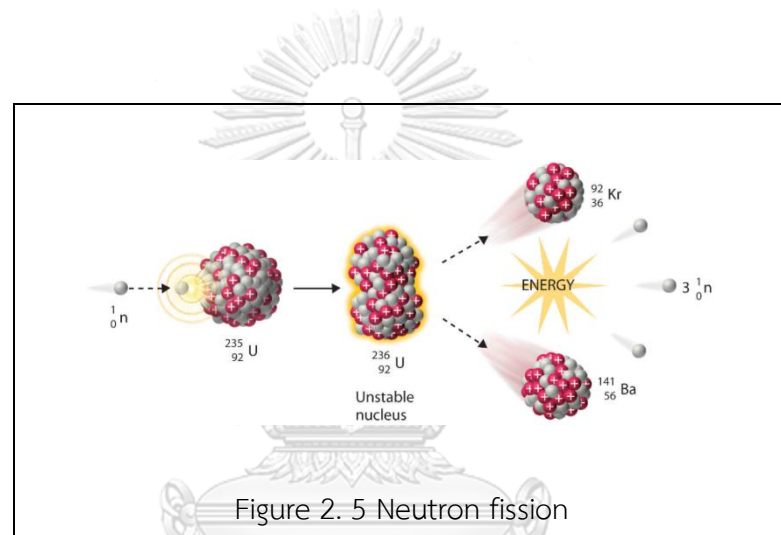


2.1.5.4 Charged-Particle Reactions

The formation of a compound nucleus, which is excited to a high energy level, can release a charged particle while the incident neutron remains in the nucleus. After particle ejection, the remaining nucleus is changed depending on the type of interaction, which normally are (n, α) and (n, p) . Such reactions may be either exothermic or endothermic.

2.1.5.5 Fission

In a fission reaction, a neutron strikes a target nucleus and the nucleus separates into two small, highly-energetic fragments while emitting two or three neutrons and a prompt gamma ray at the same time as shown in Fig 2.5. The fragments, after having stopped in the fuel material, are called fission products. These two nuclei are typically produced with a mass ratio of around 3:2 for normal fissile isotopes. Most of the fissions are binary fission producing two fission products. They range in size from a proton to argon nucleus.



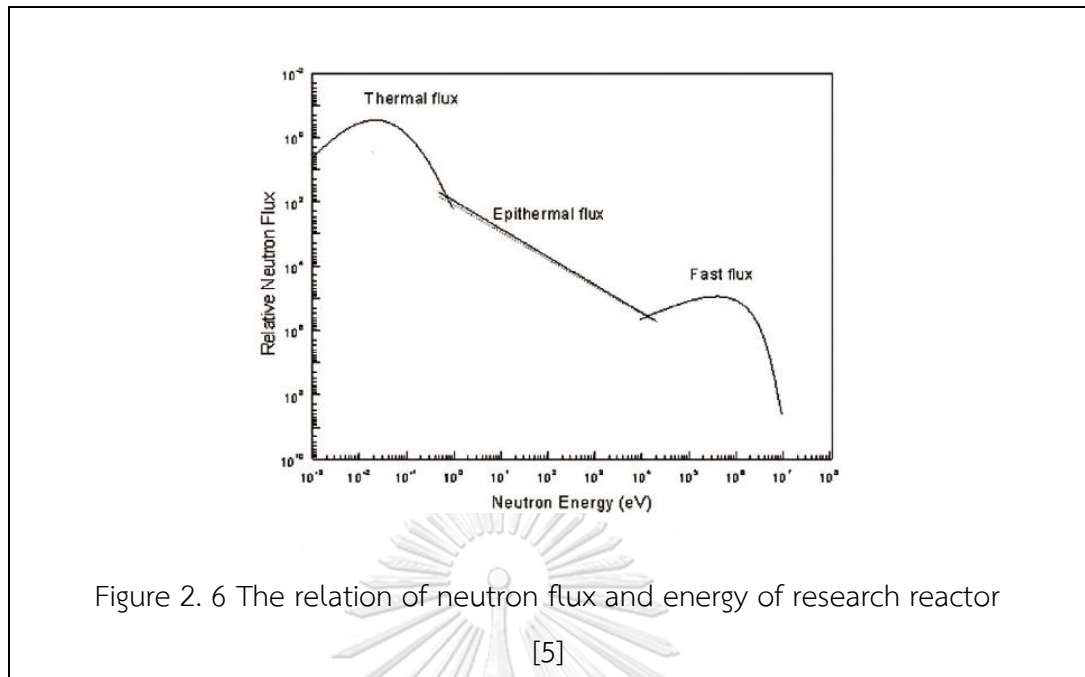
2.1.6 Neutron flux

The neutron flux is defined as the amount of neutron that passes through a unit area per unit time. It is given the symbol ϕ which has the unit in neutrons/cm²-sec. The neutron flux can be calculated from:

$$\phi = nv \quad (1)$$

Where n is the neutron density in neutrons/cm³

v is the neutron velocity in cm/sec



When a beam of neutrons of intensity I strike a thin target, the number of collision per cm^3/sec is given by

$$F = \Sigma_t I \quad (2)$$

Where Σ_t is the total macroscopic cross section.

Because the interaction of neutrons with nuclei is independent of the angle at which the neutrons collide with the nuclei, while n is the neutron density at point of reaction, the total interaction rate is clearly

$$F = \Sigma_t n v \quad (3)$$

Or

$$F = \Sigma_t \phi \quad (4)$$

2.1.7 Mean free path

The mean free path is the average distance travelled by a moving neutron before colliding with another nucleus. The symbol of the mean free path is λ (in cm unit),

which is equal to the average value of x . The distance travelled by a neutron without any interaction, over the interaction probability distribution is [6]:

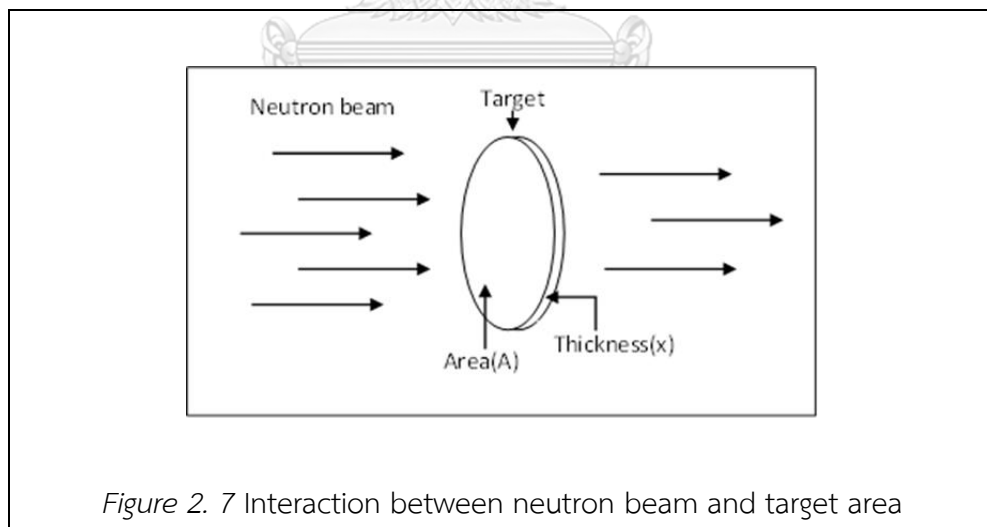
$$\lambda = \Sigma_t \int_0^{\infty} x \cdot e^{-\Sigma_t \cdot x} dx = \frac{1}{\Sigma_t} \quad (5)$$

Or

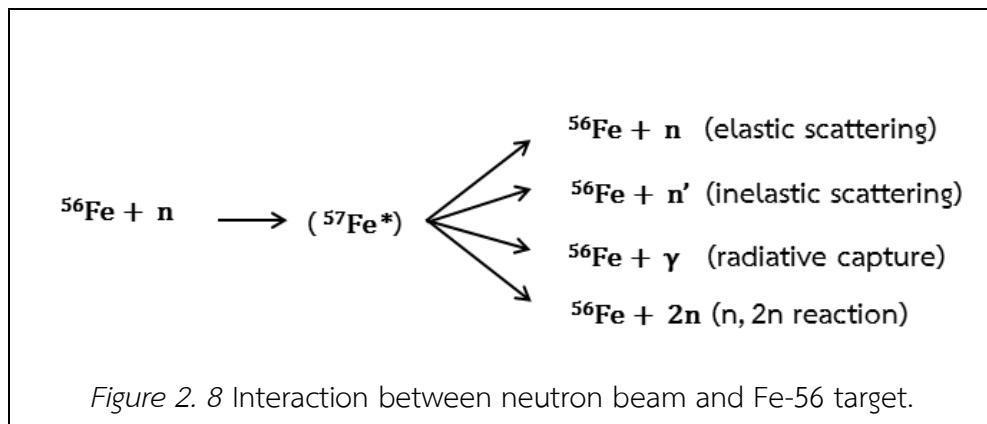
$$\Sigma_t = \frac{1}{\lambda} \quad (6)$$

2.1.8 Neutron cross section

All of the neutron cross sections are functions of the incident neutron energy and the nature of the target nucleus as shown in Fig 2.7. For reactions involving the formation of a compound nucleus, most of the interactions proceed in 2 steps. The incident neutron, upon striking the target nucleus, first coalesces with it to form a compound nucleus.



If the target nucleus is A_Z , the compound nucleus is ${}^{A+1}_Z$. The compound nucleus may then decay in a number of ways. For example, if a Fe-56 target was bombarded with 10 MeV neutrons, the compound nucleus may decay by emitting;



One of the striking features of interactions is that their cross sections display maxima at certain incident neutron energies, the process of compound nucleus formation. The compound nucleus is in excited states with the energy of the neutron after the incident neutron and the nucleus of the target are combined to form a compound nucleus.

When a monoenergetic beam of neutrons travels through the target of thickness x and area A , part of the beam will interact with the target and the rest of the beam will pass through the target. The intensity of the beam can be written as:

$$I = nv \quad (7)$$

Where I is the intensity of the beam

n is the number of neutrons per cm^3 in the beam

v is the speed of the neutrons.

Because the neutron travels a distance of v cm in 1 sec, the volume vA of neutrons will hit the target in 1 sec. Thus, $n \cdot vA$ is the number of neutrons that interact with the target per second, and I is equal to the number of neutrons striking the target per cm^2/sec .

However, most of the neutrons pass through the target without any interaction since nuclei are extremely small and since the target is assumed to be thin. The

number of collisions per second is proportional to the beam intensity, the atom density, the area and the thickness of target as follows:

$$\text{Number of collisions per second} = \sigma INAX \quad (8)$$

Where σ is the microscopic cross section

N is the atom density of the target

A is the interaction area

X is the thickness of target

The total number of nuclei in the target is called the NAX factor. The number of neutron collisions per second with a nucleus is σI . The parameter σ can be calculated from the number of collisions per second with one nucleus divided by the unit intensity of the beam.

The chance of interaction between an incident neutron and a target nuclide, independent of the type of reaction, is expressed with the total cross section σ_t . However, it may be useful to know if the incoming particle bounces off the target (and therefore continues travelling after the interaction) or disappears after the reaction. For that reason, the scattering cross section (σ_s) and absorption cross sections (σ_a) are defined and the total cross section (σ_t) is simply the sum of the two partial cross sections:

$$\sigma_t = \sigma_s + \sigma_a \quad (9)$$

$$\sigma_s = \sigma_{sc} + \sigma_{si} \quad (10)$$

$$\sigma_a = \sigma_r + \sigma_f + \sigma_p + \sigma_\alpha \quad (11)$$

where

σ_{sc} or $\sigma_{(n,n)}$ is elastic scattering cross section

σ_{si} or $\sigma_{(n,n')}$ is inelastic scattering cross section

σ_r or $\sigma_{(n,\gamma)}$ is radiative capture cross section

- σ_{α} or $\sigma_{(n,\alpha)}$ is alpha transmutation cross section
 σ_p or $\sigma_{(n,p)}$ is proton transmutation cross section
 σ_f or $\sigma_{(n,f)}$ is fission cross section

Therefore, the reaction per unit volume per second can be expressed in the collision density (F) as:

$$F = IN\sigma_t \quad (12)$$

The total macroscopic cross section which has cm^{-1} unit can be computed from the total microscopic cross section or σ_t in cm^2 per atom multiplied by the atom density or N in atom per cm^3 as follows:

$$\Sigma = N\sigma_t \quad (13)$$

The macroscopic cross section or Σ is the result of the multiplication between the atomic density (N) and the microscopic cross section in unit cm^{-1} . So the total macroscopic cross section or Σ_t represent $N\sigma_t$. Thus, in terms of total macroscopic cross section, the number of collisions in target can be written by:

$$F = \Sigma_t l \quad (14)$$

The macroscopic cross section of mixed isotope or element can be calculated from

$$\Sigma_t = \frac{\rho N_a}{A} \sigma_t \quad (15)$$

where ρ is the atom density in atom per cm^3

N_a is the Avogadro's number (0.602×10^{24} atom per mole)

A is the atomic mass number.

For compound materials, the number of atoms in materials can be calculated by

$$N_i = \frac{\rho N_i}{M} v_i \quad (16)$$

Where N_i is the atomic number density in compound material, atom per cm^3

M is the molecular weight of compound material, gram per mole

v_i is the atom fraction (abundance) of compound material, the number of atoms of isotope per the total number of atoms of the element

Thus, the macroscopic cross section of mixed elements or compound material can be expressed by:

$$\Sigma_i = \frac{\rho N_a}{M} v_i \sigma_i \quad (17)$$

where σ_i is the microscopic cross section of element i .

Alternatively, the macroscopic cross section of compound material can be written by:

$$\Sigma_{mix} = N_1 \sigma_1 + N_2 \sigma_2 + N_3 \sigma_3 + \dots \quad (18)$$

where

Σ_{mix} = Macroscopic cross section of the mixed material (or isotope)

N_1, N_2, N_3, \dots = Atomic density of isotope or element 1, 2, 3, ..., respectively

$\sigma_1, \sigma_2, \sigma_3, \dots$ = Microscopic cross section of isotope or element 1, 2, 3, ..., respectively.

2.1.9 Neutron Detection

Neutrons can create an ionization track from the elastic scatter which is detectable.

The neutron capture and the elastic scattering are the main processes to detect neutrons.

2.1.9.1 Neutron detection by neutron capture

A common method for detecting neutrons involves converting the energy released from neutron capture reactions into electrical signals. Certain nuclides have a high probability to absorb neutrons. Upon neutron capture, the compound nucleus emits more easily detectable radiation, for example an alpha particle, which is then detected. The nuclides ${}^3_2\text{He}$, ${}^6_3\text{Li}$, ${}^{10}_5\text{B}$, ${}^{233}_{92}\text{U}$, ${}^{235}_{92}\text{U}$, ${}^{237}_{93}\text{Np}$ and ${}^{239}_{94}\text{Pu}$ are useful for this purpose.

2.1.9.2 Neutron detection by elastic scattering

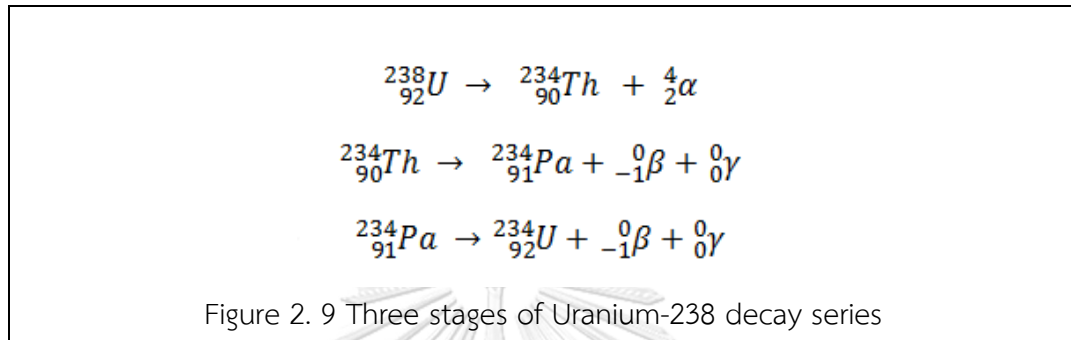
Neutrons can elastically scatter off nuclei, causing the struck nucleus to recoil. The light nuclei such as hydrogen can absorb the neutron energy more than the heavier nuclei. The fast neutron detectors rely on the elastic scattering process. The ionization and excitation of atomic nuclei through collisions can occur from the recoiling nuclei. The signal can be detected via the charge and/or scintillation light.

The moderators such as paraffin or polyethylene are not required for the fast neutron detectors.

2.2 Gamma ray

The most energetic form of the electromagnetic radiation is gamma rays which are the short wavelength electromagnetic radiation emitted from the radioactive atoms. The particular isotope may be stable or unstable depending on the ratio of neutrons to protons within its nucleus. The unstable atom can occur when the binding energy is not strong enough to hold the nucleus of the atom. The high speed particles ejected from the nucleus or gamma rays emitted by either the nucleus or orbital electrons are the ionization radiation.

A nucleus in an excited state may release one or more photons. The effect of moving the nucleus from the higher to the lower energy state results in the gamma ray emission which always follows beta decay, alpha decay and other nuclear decay processes. The following example is the three stages of the uranium-238 radioactivity series.



The beta decay of a Thorium-234 nucleus is initially produced by alpha decay of U-238. Beta decay of Thorium-234 results in a high energy electron being released from the nucleus. The daughter nucleus thus formed has the same mass number of 234 as the parent but is one higher in atomic number as the decaying neutron has changed into a proton which is retained within the nucleus. The protactinium-234 nucleus still contains excess energy which it releases by emitting a high energy gamma radiation.

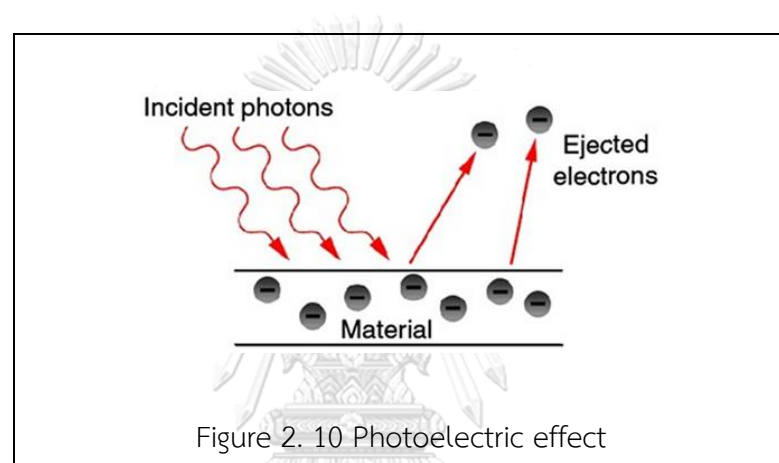
2.2.1 Gamma interactions

There are several ways of gamma rays interaction with matter; however, three processes which are photoelectric effect, pair production, and Compton effect must be taken into account in the nuclear engineering problems [8].

2.2.1.1 The photoelectric effect

In photoelectric effect, the incident gamma ray interacts with an entire atom. One of the atomic electrons is released from the atom and the gamma ray disappears. The recoiling atom carries a low kinetic energy with it in this process. The kinetic energy of the emitted photoelectron is therefore equal to the photon energy less the binding energy of the electron to the atom as shown in Fig 2.11.

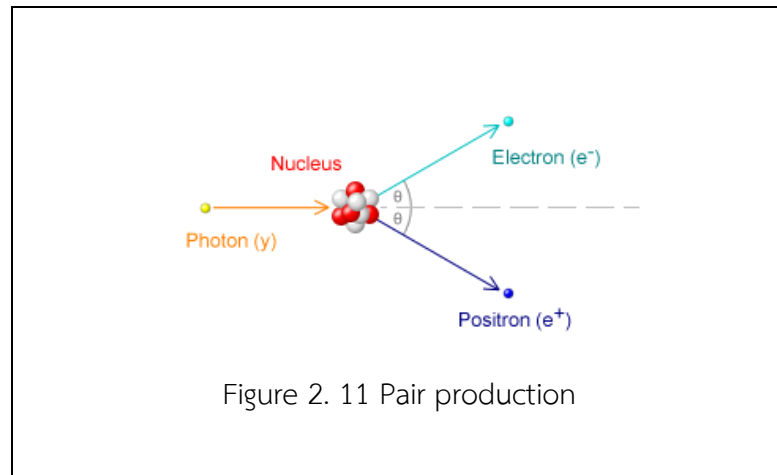
If a gamma ray releases an inner atomic electron, the electronic structure hole is filled by the outer electrons transitioning into the vacant position. This transition is accompanied by the emission of x-rays characteristic of the atom or by the ejection of an Auger electron. The cross section per atom for the photoelectric effect is denoted by the symbol σ_{pe} . This cross section can be used in the same way as the neutron cross sections discussed in the preceding sections. Thus, if I is the intensity of γ rays incident on a thin target containing N atoms per cm^3 , then $IN\sigma_{pe}$ is the number of photoelectric interactions/ $\text{cm}^3\text{-sec}$.



The cross section σ_{pe} depends both on the energy E of the incident photon and the atomic number Z of the atom. The photoelectric cross section is a strong function of Z . Because of the strong dependence of σ_{pe} on Z , the photoelectric effect is most prominent for heavy atoms, such as lead, especially at low photon energies [8].

2.2.1.2 Pair Production

In this process, the photon disappears and a pair of positron and electron is created. Because the total rest-mass energy of the 2 electrons is 1.022 MeV, this effect cannot take place unless the photon has at least this minimum energy. Above this threshold, the pair production cross section, σ_{pp} , increases steadily with increasing photon energy.



Since pair production is an electromagnetic interaction, it can take place only in the vicinity of a Coulomb field. At most gamma ray energies of interest, this is the field of the nucleus, not surrounding electrons.

The combined kinetic energy of the pair of electron and positron is equal to the photon energy minus 1.022 MeV. The created electron interacts with the orbital electrons in the surrounding medium and loses its energy. The positron quickly combines with a negatron, a process called annihilation, after it has slowed down to a very low energy. At the end, the two particles disappear and two photons are released as annihilation radiation with an energy of 0.511 MeV each [8].

2.2.1.3 The Compton effect

The elastic scattering of photon by an electron is called the Compton effect or the Compton scattering, with the conservation of energy and momentum as shown in Fig. 2.13.

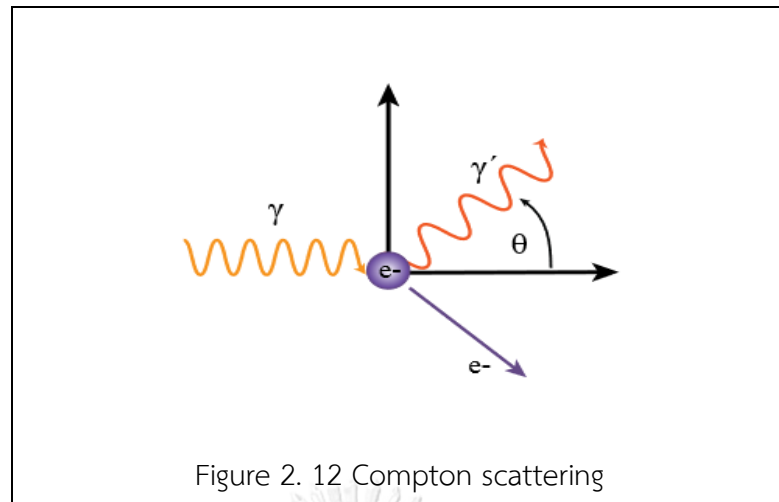


Figure 2. 12 Compton scattering

The incident photon with energy E and wavelength λ is scattered through the angle θ and the struck electron recoils. Since the recoiling electron acquires some kinetic energy, the energy E' of the scattered photon is less than E , and since the wavelength of a photon is inversely proportional to its energy, the wavelength λ' of the scattered photon is larger than λ . By setting up the equations for the conservation of energy and momentum, the following equation is obtained:

$$\lambda' - \lambda = \lambda_c(1 - \cos\theta) \quad (19)$$

In Compton scattering, the photon interacts with individual electrons, and it is therefore possible to define a Compton cross section per electron $e\sigma_c$. The Compton cross section per atom, σ_c is equal to the number of electrons in the atom namely, Z multiplied by $e\sigma_c$. Thus,

$$\Sigma_c = Ze\sigma_c \quad (20)$$

From a practical standpoint, the Compton effect causes difficulties in gamma ray shielding since the photon does not completely disappear as in the photoelectric effect and in pair production. The Compton-scattered photon interacts again in another part of the system. Although X-ray and Auger electrons are released from the

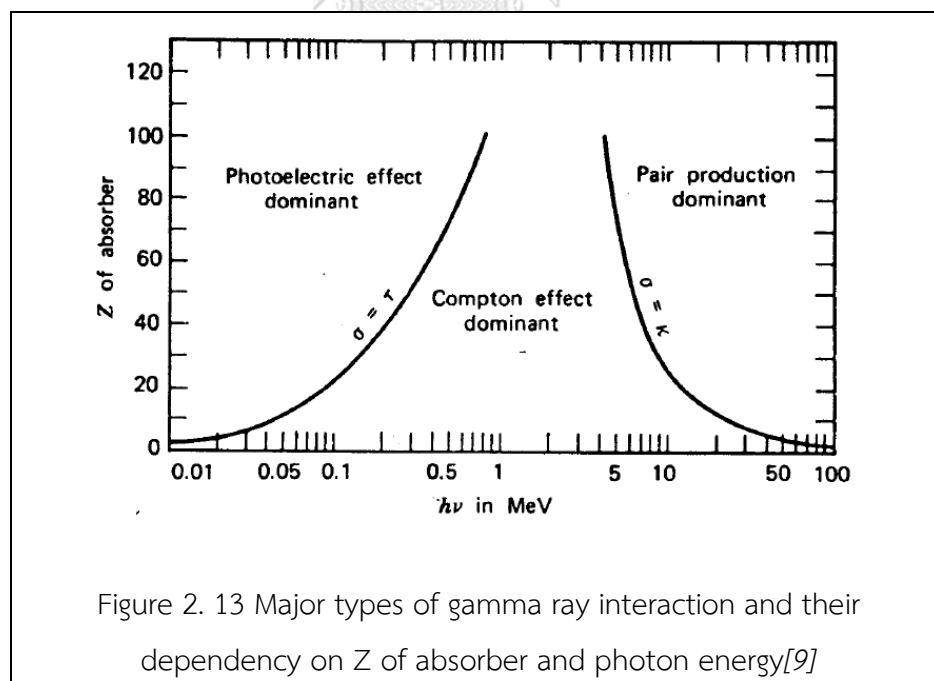
photoelectric effect and although annihilation radiation occurs in a pair production, these radiations are always much less energetic than the initial photons.

2.2.2 Interaction processes

The gamma rays interact with detectors and absorbers by three major processes; photoelectric absorption, Compton scattering, and pair production. In the photoelectric absorption process, the gamma ray loses all of its energy in one interaction. The probability of this process depends very strongly on gamma ray energy E_γ and atomic number Z . In Compton scattering, the gamma ray loses only part of its energy in one interaction. The probability for this process is weakly dependent on E and Z . The gamma ray can lose all of its energy in one pair production interaction.

2.2.2.1 Photoelectric Absorption

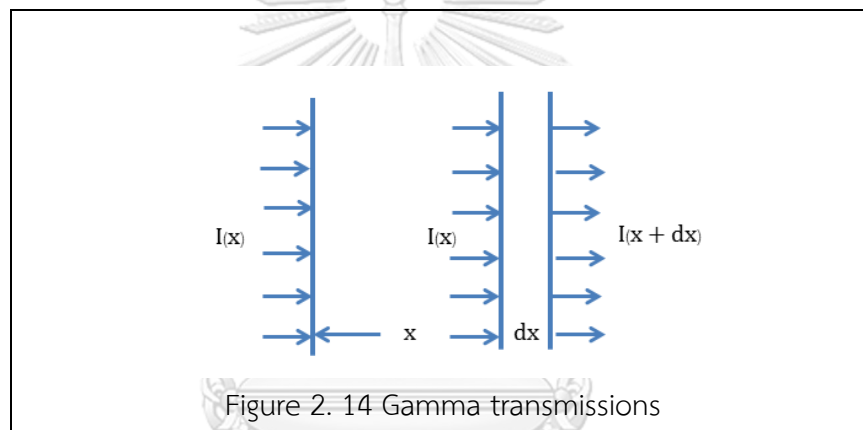
A gamma ray may interact with a bound atomic electron in such a way that it loses all of its energy and ceases to exist as a gamma ray.



Some of the gamma ray energy is used to overcome the electron binding energy, and most of the remainder is transferred to the freed electron as kinetic energy. Because the gamma ray gives up all its energy, the photoelectric absorption is necessary for gamma ray detection.

2.3 Gamma ray attenuation

The gamma attenuation occurs through the interaction of the gamma radiation with matter. The degree of gamma attenuation is dependent upon the incident of gamma ray energy, the atomic number and density of the elements in shielding material including the thickness of the shielding [10].



When a material of thickness x is placed in the path of a gamma ray beam, the intensity of the beam will be attenuated according to Beer-Lambert's law,

$$-dI(x)/I(x) = N\sigma dx \quad (21)$$

Similar to the macroscopic neutron cross section, the macroscopic cross section can also be defined by multiplying σ in Eq. 23 by the atom density N . The macroscopic gamma ray cross sections are commonly called the attenuation coefficient or the linear attenuation coefficient and are represented by the symbol μ [11].

$$\mu = N\sigma \quad (22)$$

Or

$$\mu = \mu_{pe} + \mu_{pp} + \mu_c \quad (23)$$

where μ is the total attenuation coefficient and μ_{pe} , μ_{pp} and μ_c are the attenuation coefficients for the three interaction processes.

$$-dI(x)/I(x) = \mu dx \quad (24)$$

$$I(x) = I_0 e^{-\mu x} \quad (25)$$

where I_0 and I are the incident and attenuated photon intensities, respectively, and μ is the linear attenuation coefficient of material in unit cm^{-1} .

The linear attenuation coefficient has the relationship with the half value thickness (cm). The half value thickness is the thickness at which the intensity of primary photon beam is reduced by $\frac{1}{2}$.

$$HVT = \frac{\ln 2}{\mu} \quad (26)$$

The ratio of the linear attenuation coefficient to the density of the absorbing material (μ/ρ) is called the mass attenuation coefficient with the unit of area per unit mass (cm^2/g). The unit implies that one may think of it as the effective cross sectional area per unit mass of the absorber.

$$I = I_0 e^{-\left(\frac{\mu}{\rho}\right)\rho x} \quad (27)$$

where ρ is the physical density and μ/ρ has the unit of cm^2/g . Also,

$$\mu/\rho = \mu_{pe}/\rho + \mu_{pp}/\rho + \mu_c/\rho \quad (28)$$

The mass attenuation coefficient (μ/ρ) of a compound or mixture material is given by

$$\frac{\mu}{\rho} = \sum_i w_i \left(\frac{\mu}{\rho}\right)_i \quad (29)$$

where ρ is the density of material, and w_i and (μ/ρ) are the weight fraction and mass attenuation coefficient, respectively, of the element i . The attenuation coefficient can be written in terms of a reaction cross section, σ (cm^2) as:

$$\mu = N_0 \times \sigma / A \quad (30)$$

where N_0 is the Avogadro's number (6.02×10^{23} atoms per mole) and A is the atomic weight of the absorber.

The weight fraction of compound material is given by

$$w_i = \frac{a_i A_i}{\sum a_i A_i} \quad (31)$$

where A_i is the atomic weight of element i and a_i is the number of formula units, so the linear attenuation coefficient is given by:

$$\mu = \sum_i \rho_i \left(\frac{\mu}{\rho}\right)_i \quad (32)$$

where ρ_i is the partial density that is mixed the different elements. It is given by the product of the weight fraction of constituent i , w_i , and the density of the compound material, ρ , as the following [11]:

$$\rho_i = w_i \rho \quad (33)$$

The mass attenuation coefficient is independent of density. This coefficient is tabulated more commonly than the linear attenuation coefficient since it indicates the

gamma ray interaction probability of an individual element. Eq. 29 is used to calculate the mass attenuation coefficient for compound materials:

$$\mu = \sum \mu_i w_i \quad (34)$$

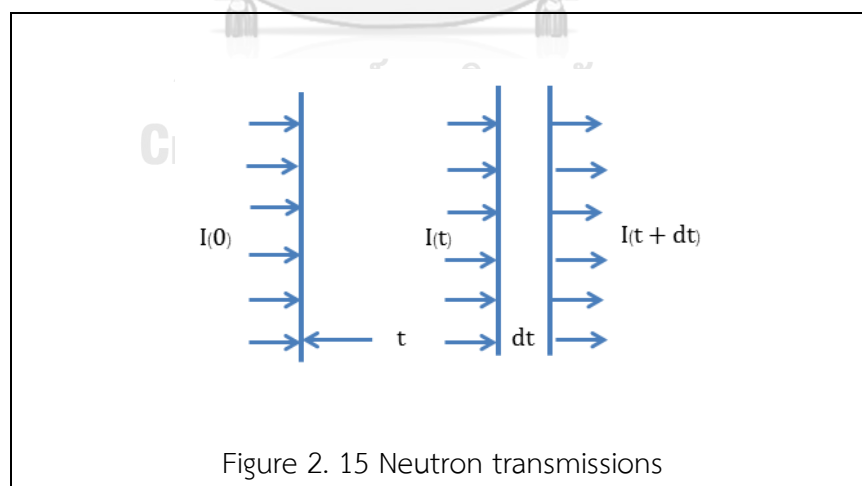
where μ_i = mass attenuation coefficient of element

w_i = weight fraction of element

The gamma ray transmission is the I/I_0 ratio. The increasing gamma ray energy increases the transmission and the increasing absorber thickness decreases the transmission. The attenuation coefficient (μ) depends on the gamma ray energy as well as the atomic number and density of the absorber, which can be measured from the different sources and absorbers.

2.4 Neutron attenuation

Neutron attenuation is similar to gamma ray attenuation. However, the penetrating ability of neutrons is often significantly different from gamma rays.



The following formula, similar to the case of gamma ray, is used to calculate neutron attenuation:

$$-dI = N\sigma I(t)dt \quad (35)$$

The relationship between total macroscopic cross section (Σ) and microscopic cross section (σ) is:

$$\Sigma_t = \sigma N \quad (36)$$

$$-dI(t)/I(t) = \Sigma_t dt \quad (37)$$

$$I(t) = I_0 e^{-N\sigma t} \quad (38)$$

Where I_0 is the incident neutron intensity (flux), I is the attenuated neutron intensity (flux), σ is the microscopic cross section (cm^2), Σ is the macroscopic cross section (cm^{-1}), N is number of nuclei per unit volume (cm^{-3}), and t is material thickness (cm).

The removal cross section for a compound material which is a homogeneous mixture can be computed from the value of each component as follows:

$$\frac{\mu}{\rho} = \sum_i w_i \left(\frac{\mu}{\rho}\right)_i \quad (39)$$

Or

$$\mu = \sum_i \rho_i \left(\frac{\mu}{\rho}\right)_i \quad (40)$$

2.5 Monte Carlo Transport Code

The transportation of neutron, photon, electron as well as coupled neutron/photon/electron can be calculated by Monte Carlo Transport Code or MCNP. MCNP is easy to use for general source, criticality source, and surface source including geometry and output tally plotters. Examples of MCNP applications are such as design of

shielding in accelerator facilities, high-energy dosimetry and neutron detection, transmutation/activation/and burn up in reactor and other systems, nuclear materials detection and others. In using the MCNP tool, the code has to be supplied with an appropriate INP file in order to perform simulation and obtain the output from the simulation.

2.5.1 INP File

An input file has the following form:

Message Block

} Optional

Blank Line Delimiter

One-line Problem Title Card

Cell Cards

•

•

Blank Line Delimiter

Surface Cards

•

•

Blank Line Delimiter

Data Cards

•

•

Blank Line Terminator (optional)

Basic parameters and accompanying units are defined for MCNP calculations

as follows:

1. Lengths (centimeters)
2. Energies (MeV)
3. Times (shakes = 10^{-8} sec)
4. Temperatures (MeV or kT)
5. Atomic densities (atoms/barn-cm)



6. Mass densities (g/cm^3)
7. Cross sections (barns = 10^{-24} cm^2)
8. Heating numbers (MeV/collision)
9. Atomic weight ratio based on a neutron mass of 1.008664967 amu. In these units, Avogadro's number is $0.59703109 \times 10^{24}$ atoms per mole.

2.5.2 Cell Cards

Cells are used to specify the geometry of simulation involving volume of space bounded by surfaces, coordinate system and volumes. All of space must be defined the positions, that is, every xyz point will lie either on a surface or within a uniquely defined cell, where no gap and overlap for cells are allowed. At least one cell will describe the problem exterior. Cells are used for constructing the model, specifying the materials, variance reduction methods, and performing tallies. For lattice ability and repeated structure, cells may contain embedded geometry lattice or repeated structure.

The materials that will be used for cell must be defined by material cards. The overall material density (g/cc or atoms/barn-cm) comes from the cell card where a material is used. Fractions or number densities on a material card are normalized to sum to 1.0.

The next entry is the cell material number. It is arbitrarily assigned by the user. The material is described on a material card (Mn) with the same material number. If the cell is a void, the material number can be entered as zero. Each of the cell and the material numbers cannot exceed 5 digits. The next one is the cell material density. A positive entry is interpreted as the atom density with the unit of $10^{24} \text{ atoms/cm}^3$ while a negative entry is interpreted as the mass density with the unit of g/cm^3 . For a void cell, no density is entered. The following illustrates an example cell card format [12]:

11 -0.0014 -7 IMP:N=1

Cell 1 contains material 1 with density 0.0014 g/cm^3 , is bounded by only one surface (7), and has an importance of 1. For the importance cards, each cell must have an importance for each type of particle such as imp:p for photons, imp:e for electrons, imp:n for neutrons, etc.

2.5.3 Surface Cards

The first entry is the surface number, which must begin in columns 1-5 and must not exceed 5 digits. The following entry is an alphabetic mnemonic indicating the surface type. Following the surface mnemonic are the numerical coefficients of the equation of the surface in the proper order. There are several types of surfaces, for example, plane, rectangular, sphere, cylinder, Ellipsoid hyperboloid Paraboloid, Cylinder Cone Ellipsoid Hyperboloid. The users need to define the arbitrary 3D coordinate to clarify the position of objects [12].

2.5.3.1 Geometry Specifications [13]

The specification of the problem geometry is by first and second degree surfaces in terms of regions or volumes bounded. The intersections, unions and complements of the regions are defined by the user. The cell is build up by using a 3-dimensional (x,y,z) coordinate system. The unit of dimension is in centimeter. The adjacent volumes or cells compose of all space. Each cell is bounded by a surface, multiple surfaces, or by infinity. The positive side and the negative side of every surface describe the cell. These directional senses for a surface are defined formally as follows: any point at which $f(x,y,z) > 0$ is located in the positive sense (+) to the surface, and any point at which $f(x,y,z) < 0$ is located in the negative sense (-) to the surface.

2.5.3.2 Macrobodies

Macrobodies can help the users to define the geometry of simulation easily. MCNP has an alternative way to define cells and surfaces through the use of macrobodies. The macrobodies available in MCNP are shown in Table 2.2.

Table 2. 2 Macrobodyes available in MCNP [13]

Mnemonic	Type of body
BOX	Arbitrarily oriented orthogonal box
RPP	Rectangular paralleliped
SPH	Sphere
RCC	Right circular cylinder
RHP or HEX	Right hexagonal prism
REC	Right elliptical cylinder
TRC	Truncated right-angle cone
ELL	Ellipsoid
WED	Wedge
ARB	Arbitrary polyhedron

About tallies with macrobodyes, the surfaces of most macrobodyes are formed by several distinct components. Specific facets must be specified for surface tallies. Facet numbers are fixed with respect to the macrobody. For example, for rectangular paralleliped or RPP:

- 1 right side
- 2 left side
- 3 front
- 4 back
- 5 top
- 6 bottom

2.5.4 Data Specifications

The type of particles, problem materials and radiation sources are defined by the block of input cards. The level of detail for the physics of particle interactions, variance reduction techniques, cross section libraries, the amount and type of output interpret the results of score and tally. A particle designator to distinguish between input data for photons, electrons and neutrons are required in the several data cards. The particle

designator consists of the symbol : (colon) and the letter N or P or E immediately following the name of the card. For example, to enter neutron importance, use an IMP:N card. Thus, the IMP:P card and the IMP:E cards are for photon importance and electron importance, respectively [12].

MCNP card name

1. mode, MODE
2. cell and surface parameters, IMP:N
3. source specification, SDEF
4. tally specification, Fn, En
5. material specification, and Mn
6. problem cutoffs. NPS

2.5.4.1 MODE Card

This card is used to identify the type of problem, for instance, type of source particles to be tracked. Several different modes of MCNP can be executed:

- MODE N — neutron transport only
- N P — neutron and neutron-induced photon transport
- P — photon transport only
- E — electron transport only
- P E — photon and electron transport
- N P E — neutron, neutron-induced photon, and electron transport

2.5.4.2 Cell and Surface Parameter Cards [12]

Most of these cards describe values of cell parameters. Entries correspond in order to the cell or surface cards that appear earlier in the INP file. Some method of specifying relative cell importance is required; the majority of the other cell parameter cards are for optional variance reduction techniques. The number of entries on a cell or surface parameter card must equal the number of cells or surfaces in the problem or MCNP prints out a WARNING or FATAL error message. In the case of a WARNING, MCNP

assumes zeros. The IMP:N card is used to specify relative cell importance in the sample problem. There are four cells in the problem, so the IMP:N card will have four entries. The IMP:N card is used (a) for terminating the particle's history if the importance is zero and (b) for geometry splitting and Russian roulette to help particles move more easily to important regions of the geometry. An IMP:N card for the sample problem is

```
IMP:N 1110
```

Cell parameters also can be defined on cell cards using the keyword=value format. If a cell parameter is specified on any cell card, it must be specified only on cell cards and not at all in the data card section.

2.5.4.3 Source specifications

The source and type of radiation particles for MCNP problem are specified by the SDEF command. The SDEF command has many variables or parameters that are used to define all the characteristics of all sources in the problem. There are many of source variables for SDEF command [13]. For example

ERG is the energy (MeV) which starting energy default is 14 MeV.

POS is the reference point for positioning sampling which x y z (0 0 0)

RAD is the radial distance of the position from POS or AXS.

PAR is the type of particle source emits.

CEL is the starting cell number

WGT is the starting weight, default is 1;

TME is the time, default is 0;

PAR is the source particle type 1 for N, N P, N P E; 2 for P, P E; 3 for E.

The CEL entry is not always required as MCNP will determine the starting cell number for a point isotropic source. The default source particles starting direction is isotropic. For instance, a fully specified source card is

```
SDEF POS = 0-2-3.5 CEL = 1 ERG = 12 WGT = 1 TME = 0 PAR = 1
```

Neutron particles will start at the center of the oxygen sphere (0 -2 -3.5), in cell 1, with an energy of 12 MeV, and with weight 1 at time 0. [12]

2.5.4.4 Tally Specifications

MCNP produces k-eff and various information that have only limited information about fluxes, spectra, reaction rates, etc. In fixed-source problems, MCNP gives no physical results by default. Tallies are analogous to measurement devices in the experiments. These are often called edits in many other codes such as fluxes, currents, and reaction rates.

The tallies are identified by tally type and particle type. Tallies are given the numbers 1, 2, 4, 5, 6, 7, 8, or increments of 10 thereof, and are given the particle designator :N or :P or :E (or :N,P only in the case of tally type 6 or P,E only for tally type 8). Each with different energy bins such as F4:N, F14:N, F104:N, and F234:N are all legitimate neutron cell flux tallies; they could all be for the same cell(s) but with different energy or multiplier bins, for example. Similarly F5:P, F15:P, and F305:P are all photon point detector tallies. Having both an F1:N card and an F1:P card in the same INP file is not allowed. The tally number may not exceed three digits [12].

There are many technical descriptions of the various types of tallies permitted in MCNP calculations. Table 2.3 summarizes the available tallies in MCNP.

Table 2. 3 Types of tallies available in MCNP [13]

Mnemonic	Tally Type	Particles pl	Fn Units	*Fn Units
F1:pl	Surface current	N or P or N,P or E	#	MeV
F2:pl	Average surface flux	N or P or N,P or E	#/cm ²	MeV/cm ²
F4:pl	Average flux in a cell	N or P or N,P or E	#/cm ²	MeV/cm ²
F6:pl	Energy deposition	N or P or N,P	MeV/g	Jerks/g
F7:pl	Fission energy deposition in a cell	N	MeV/g	Jerks/g
F8:pl	Pulse height distribution in a cell	P or E or P,E	pulse	MeV

The current at a surface (F1), the average flux at a surface (F2), the flux at a point or ring (F5), and the flux averaged over a cell (F4) are the most frequently used tallies. The various tallies of energy deposition (F6 and F7) are similar to the flux tallies over a cell. The one source particle excluding tallies F6 and F7 normalized with an FM card. Multiple tally Fn:pl cards can be used with a unique value of n for each tally. The last digit n determines the type of tally. Thus, for instance, F2:N, F12:P and F22:E can be used to give the average surface flux of neutrons, photons and electrons, respectively [13].

At every collision makes a deterministic estimate of flux. X, Y, and Z are position of tally where flux is desired. Tallies require volumes or areas for tallies (except F5) to be valid. MCNP must know a volume or area to perform the division. Sometimes, MCNP will be unable to calculate the volume of cells or areas of surfaces so the user must provide this information. MCNP normalizes flux tallies by dividing by area, volume, or mass.

For cell flux tallies or F4 must divide by volume
 For surface flux tallies or F2 must divide by area.
 For energy deposition or F6 must divide by mass.
 For fission heating or F7 must divide by mass.

Cards for optional tally features

The MCNP manual lists many optional tally commands. The sorting a tally into energy bins (En card), multiplying a tally by some quantity (FMn card), and multiplying each tally contribution by a conversion factor (Den and DFn cards) are the tally modification commands.

2.5.5 Materials Specification

Specification of materials filling the various cells in MCNP involves the following elements [13]:

- a) Defining a unique material number.

- b) The elemental or isotropic composition
- c) The cross section compilations to be used.

The density is not specified here. Instead, density is specified on the cell definition card. This permits one material to appear at different densities in different cells.

The cards in this section specify the material's isotopic composition as well as the cross-section evaluations to be used in the cells. The following describes the materials specification.

a. Material (Mm) Card: The following card is used to specify a material for all cells containing material m, where m cannot exceed 5 digits:

Mm ZAID1 fraction1 ZAID2 fraction2 ...

The m on a material card corresponds to the material number on the cell card. The consecutive pairs of entries on the material card consist of the identification number (ZAID) of the constituent element or nuclide followed by the atomic fraction (or weight fraction).

b. VOID Card: All materials and cross sections can be removed by the VOID card and be set all nonzero importance to unity. It is used to find the errors in the geometry description since all particles will be run in the short time [12].

2.5.6 Miscellaneous Data Specifications

Time or History Cards

The common method for limiting the amount of time that MCNP can run is to specify either the maximum number of source particle histories or the maximum execution time. The maximum number of histories N is specified on the card by NPS command. Furthermore, another option is CTME command that is used for the computing time cut off T in minutes.

2.5.7 Truncation Techniques

This technique reduces the time per particle history by either simplifying the geometry or the physics used to generate the random walk for each particle.

Energy, Time and Weight Cut off

The CUT command is used to specify a minimum energy time, or particle weight below which the particle is killed. For example

CUT:p j 0.025 \$ kill photons with E<25 keV

Thus, whenever a photon energy falls below 25 keV, it is killed. The CUT command consists of 5 parameters. The first is a time limit for an individual history, which in the above example is specified as j to jump over the default value of a very large time.

2.5.8 Statistics

In assessing the results, the influence of statistical noise must be considered when assessing the reliability of Monte Carlo results. MCNP provides uncertainties and performs statistical checks to attempt to assess whether or not the results are reliable.

Average, standard deviation, relative error

Let X_k = the value of a tally for the k^{th} history
 N = number of histories run

Average tally, after N histories

$$\bar{X} = \frac{1}{N} \sum_{k=1}^N X_k \quad (41)$$

Standard deviation of average tally, after N histories is,

$$S_{\bar{X}} = \frac{1}{\sqrt{N-1}} \sqrt{\frac{1}{N} \sum_{k=1}^N X_k^2 - \bar{X}^2} \quad (42)$$

2.6 Concrete

Concrete is composed of cement and other cementitious materials such as fly ash, slag cement, aggregate and water. The cement paste which is the adhesive properties with sand and stone is the reaction of cement. The cement paste is changed to the concrete form in the mold. Concrete will be set in the solid state after 24 hours of the concrete mixing period has passed. There are two major groups of concrete composition which are the cement paste and the strength of concrete. The cement paste consists of cement, water and void due to the chemical reaction between cement and water. This is the important process that helps to combine admixtures together and contribute to increase the strength of concrete. The quality of cement paste affects the strength of concrete, which involves the concrete composition including the water per cement ratio that has been mixed in concrete.

Aggregate can be categorized by size as the following;

1. *Fine Aggregate* is the material size less than 4.5 mm. or the admixture that can pass through a standard sieve number 4 which the fine aggregate size is more than 0.07 mm.

2. *Coarse Aggregate* is the material size larger than fine aggregate which is more than 4.5 mm. Or it could not pass through the standard sieve number 4 such as gravel or millstone.

Furthermore, to increase concrete properties, admixture blend may be added into concrete such as chemical admixture or mineral admixture.

Concrete that is used to apply with construction work may be categorized into the following 3 groups:

1. *Plain concrete*

Plain concrete only uses concrete and no steel reinforcement is embedded, and only its compressive strength is taken. For example, thick concrete for machine basement or dam which uses the weight of barrier against pressure.

2. *Reinforced concrete*

Reinforcement is steel embedded into the concrete in such a manner that the two materials act together in resisting forces and tensile and compressive strength is taken.

3. *Prestressed concrete*

Prestressed concrete is the great strength concrete that is used to apply with the bridge and building construction.

2.6.1 Cement

Cement is a very fine powder that is manufactured from the element mixtures that are found in the natural materials such as limestone, clay, sand and/or shale. The major chemical compounds are calcium and aluminum silicate. Portland cement is the hydraulic cement. When it is mixed with water with the specific portion, it can develop to solid state in water because the hydration reaction of cement and water is activated. The rate of concrete forming, as well as the generated heat, depend on the chemical compounds and sizing of cement powder. The strength and durability of concrete involve the concrete proportions and moisture during concrete forming.

2.6.2 Hydration of Portland Cement

Concrete is prepared by mixing cement, water and aggregate together to make a workable paste. It is molded or placed, consolidated, and then left to harden. Concrete does not need to dry out in order to harden.

Concrete requires moisture to hydrate and cure. When concrete dries, it stops getting stronger. Concrete with too little water may be dry since it is not reacted fully. The properties of such concrete would be less than that of a wet concrete. The reaction of water with the cement in concrete is very important to its properties and reactions may continue for many years.

Portland cement consists of 5 major compounds and some minor compounds. The typical composition of a Portland cement is listed in Table 2.4.

When water is added to cement, each compound undergoes the hydration process and contributes to the final concrete product. Only the calcium silicates contribute to strength. Tricalcium silicate is responsible for most of the early strength in the first 7 days. Dicalcium silicate, reacting more slowly, contributes to the strength at later times.

Table 2. 4 Composition of Portland cement with chemical composition and weight percent

Cement compound	Weight Percentage	Chemical Formula
Tricalcium silicate	50%	Ca_3SiO_5 or $3\text{CaO}.\text{SiO}_2$
Dicalcium silicate	25%	Ca_2SiO_4 or $2\text{CaO}.\text{SiO}_2$
Tricalcium aluminate	10%	$\text{Ca}_3\text{Al}_2\text{O}_6$ or $3\text{CaO}.\text{Al}_2\text{O}_3$
Tetracalcium aluminoferrite	10%	$\text{Ca}_4\text{Al}_2\text{Fe}_2\text{O}_{10}$ or $4\text{CaO}.\text{Al}_2\text{O}_3.\text{Fe}_2\text{O}_3$
Gypsum	5%	$\text{CaSO}_4.2\text{H}_2\text{O}$

The reaction for the hydration of tricalcium silicate is as follows:



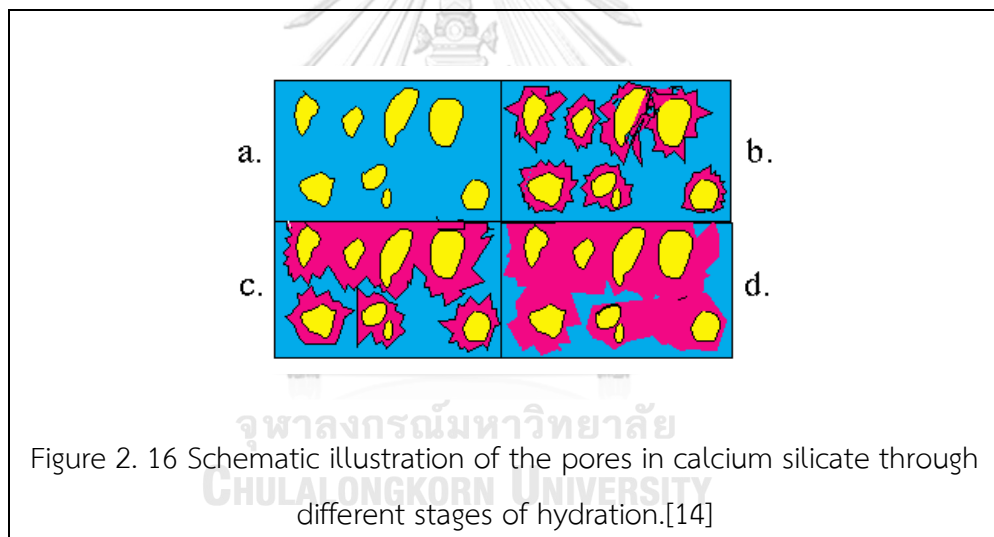
When water is added, tricalcium silicate rapidly reacts to release calcium and hydroxide ions as well as a large amount of heat. The pH quickly climbs to > 12 due to the release of OH^- ions. This initial hydrolysis slows down rapidly after it starts, resulting in a decrease in heat released.

The reaction continues slowly, generating calcium ion and hydroxide ion until the system reaches saturation. After this condition occurs, calcium hydroxide begins to crystallize. Simultaneously, calcium silicate hydrate starts to form. Ions precipitate out of solution accelerating the reaction of tricalcium silicate to calcium and hydroxide ions.

The calcium hydroxide and calcium silicate hydrate crystals is formed to be “seeds” which depend upon the amount of calcium silicate hydrate. The crystals

which are the calcium silicate hydrate grow larger until they reach the unhydrated tricalcium silicate. The speed of the reaction is now controlled by the rate at which water molecules diffuse through the calcium silicate hydrate coating. This coating thickens over time causing the production of calcium silicate hydrate to become slower.

Figure 2.16 shows the pore formation as calcium silicate hydrate is formed. Diagram (a) shows the pores filled with water. Diagram (b) illustrates the beginning of hydration. Diagram (c) is when the hydration process occurs and the empty space are filled with water and calcium hydroxide. Diagram (d) depicts the nearly hardened cement paste. The hydration will continue as long as water is present and as long as there are still unhydrated compounds in the cement paste.



Dicalcium silicate also influences the concrete strength from its hydration. Dicalcium silicate reacts with water in a similar manner to tricalcium silicate. However, the reaction is much more slowly. The liberated heat is also less than that released by the hydration of tricalcium silicate because the dicalcium silicate is much less reactive. The hydration products of dicalcium silicate are the same as those for tricalcium silicate:



The other major components of Portland cement, tricalcium aluminate and tetracalcium aluminoferrite, also react with water. Their hydration chemistry is more complicated as they involve reactions with the gypsum as well. However, these reactions do not contribute significantly to strength. The hydration rate of a compound may be altered by adjusting their concentrations.

2.6.3 Heat of hydration

It is the amount of heat released or absorbed when one mole of an anhydrous or a partially hydrated salt combines with the required number of moles of water to form specific hydrates. The main product involved in the binding of cement and water is heat, which is released when the concrete is being hardened. This process is known as the heat of hydration. Heat of hydration can be managed while designing and pouring concrete, during the process of curing and hardening. However, if designers do not allow for the heat, it can cause serious issues with cracking and can also disturb the structural integrity of the concrete. Heat of hydration can generate high temperature within the internal structure when a large amount of concrete is poured quickly or due to a very high cement to water ratio. During construction, if the heat of hydration is not properly managed, it can create significant cracks. This will further weakens the structural integrity of the concrete due to cracks formed by expansion of concrete [15].

2.6.4 Portland Cement (American Standard Type)

Table 2. 5 The types of cement are categorized into eight types that are covered in ASTM C150 as the following. [16]

Cement Type	Use
I	General purpose cement, when there are no extenuating conditions.
II	Aids in providing moderate resistance to sulfate attack.
III	When high-early strength is required
IV	When a low heat of hydration is desired
V	When high sulfate resistance is required

Table 2. 6 The types of cement are categorized into eight types that are covered in ASTM C150 as the following.(Continued)

Cement Type	Use
IA	A type I cement containing an integral air- entraining agent
IIA	A type II cement containing an integral air- entraining agent
IIIA	A type III cement containing an integral air-entraining agent

2.6.5 Mechanical Properties of concrete

The performance of concrete can be evaluated from the mechanical properties, which include the compressive strength, tensile strength, flexural strength and modulus of elasticity. The most important characteristic is the compressive strength which has to be considered to improve the mechanical properties [17] .

2.6.5.1 Compressive strength

The maximum compressive stress is called the compressive strength that a given solid material can sustain without fraction during under a gradually applied load. The compressive strength can be calculated by dividing the maximum load by the specimen's cross-section area in a compression testing [18].

2.6.5.2 Tensile strength

The ability of material to withstand a pulling or tensile force is called tensile strength. The tensile strength measurement is in the unit of force per cross-section area. This is a significant concept in engineering fields, especially the field of material science, mechanical engineering and structural engineering. The ability to resist breaking under tensile stress is widely measured properties of materials used in structural applications. This is important to describe the brittle materials more than ductile materials [19].

2.6.5.3 Flexural strength

The measure of the tensile strength of concrete beams or slabs is called flexural strength that identifies the amount of stress and force and unreinforced concrete

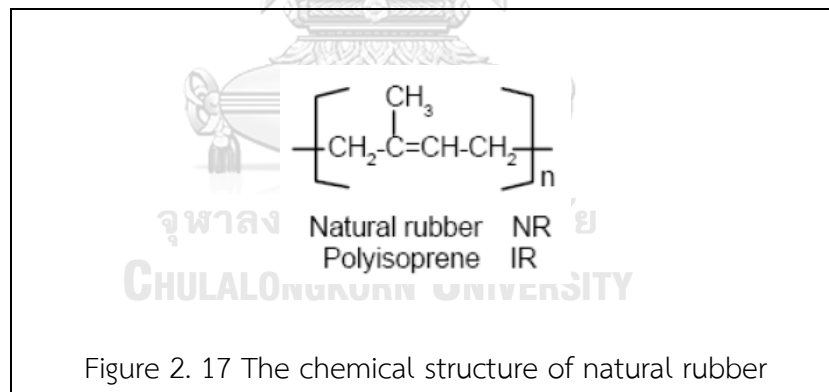
slab, beam or other structure can resist any bending failures. Flexural strength is also known as bend strength or modulus of rupture or fracture strength [20].

2.6.5.4 Elastic modulus

The number that measures an object or substance's resistance to being deformed elastically when a stress is applied to it is called elastic modulus (also known as modulus of elasticity). The stress is the force causing the deformation divided by the area to which the force is applied and strain is the ratio of the change in some parameter caused by the deformation to the original value of the parameter [21].

2.7 Natural Rubber

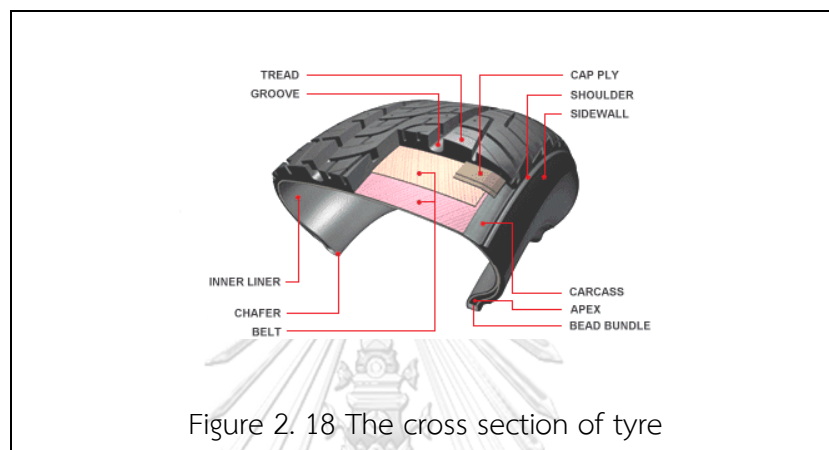
Natural rubber is the elastomers. It is extracted in the form of latex from the bark of the Hevea tree. The rubber is collected from the latex involving preservation, concentration, coagulation, dewatering, drying, cleaning, and blending. The natural rubber polymer is cis-1,4 polyisoprene function which the chemical structure is:



One of the fundamentally important properties of natural rubber is the elasticity. Rubber is unique in the extent to which it can be distorted, and the rapidity which it recovers to its original shape and dimensions. Raw natural rubber has low tensile strength and abrasion resistant. Furthermore, it can absorb the large quantities of water.

2.7.1 Tyre

An essential part of most ground vehicles is a ring shape covering the boundary of a wheel, which is a tyre that is used to protect the wheel from wear and tears as well as to provide a friction between the vehicle and the road. There are several parts in tyre. A typical tyre cross section is shown in Figure 2.19.



Tread : The part of the tyre that contacts with the road surface is called tread. It is produced from the rubber with carbon black and other chemicals which not only has to provide grip and cornering stability but must also resist abrasion, cutting, and impacts, as well as withstand high temperatures.

Groove: The channel within the tread to improve driving stability, pulling and braking ability.

Cap ply: Steel cords to stabilize the tyre shape against internal pressure.

Shoulder: The transitioning section between the edge of the tread and the sidewall.

Sidewall: A bridge between tread and bead to protect the carcass and improve ride quality by allowing the tyre to expand and compress with the terrain.

Carcass: The inner cord of the tyre that supports the weight and absorbs impact. It is made of fabric embedded in rubber, optionally steel chords.

Apex: The filler providing cushion between bead, inner liner and body ply.

Bread bundle: Rigid bands of steel wire in rubber compound to establish press fit of the tyre to the wheel.

Belt: Layers of rubber made of steel or textile fabric. It's closely spaced steel chords provide strength while remaining flexible.

Chaffer: Protects direct contact between the steel cords and the wheel rim, prevents dirt and moisture from getting into the rim.

Inner liner: An airtight rubber lining attached to hold high-pressure air inside.

The vulcanized rubber and various reinforcing materials were carried out to manufacture the tyres. The key element of tyre is natural rubber due to its unique elastic properties. The natural rubber is used to blend with synthetic rubber or elastomers such as Styrene-Butadiene Rubber (SBR), Butadiene Rubber (BR), Isoprene Rubber (IR), Ethylene Propylene Terpolymer (EPT) and Isobutylene Isoprene Rubber (IIR) in order to improve the elasticity of the material. In addition to the rubber compound, tyres contain:

1. Reinforcing fillers such as carbon black in order to increase the strength of rubber and make tyre have more abrasion resistance.

2. Reinforcing fibers such as textile or steel fibers. Textile is made of natural cotton and synthetic textile is made of nylons and polyesters. It is usually in the form of a cord which is used to provide the reinforcing strength or tensile component in tyres.

3. Extenders such as petroleum oils which are used to control viscosity, decrease internal friction during processing, and develop low temperature flexibility in the vulcanized product.

4. Vulcanizing agents such as organo-sulphur compounds which is a catalyst for the vulcanization process. Zinc oxide and stearic acid are used to activate the curing (cross-linking) system and to preserve cured properties [22]. The raw materials used in tyre manufacture are shown in Table 2.7.

Table 2. 7 A Typical Composition by Weight of Tyre [23]

Component	Car tyre (%)	Truck tyre (%)
Rubber/elastomers	48	45
Carbon black	22	22
Black metal	15	25
Textile	5	-
Zinc oxide	1	2
Sulphur	1	1
Additives	8	5

2.7.2 Waste Rubber Disposal

The principle of waste rubber disposal is to make waste rubber utilization of either the old product or the new product. Mostly this process is called recycle. There are many recycling methods such as fuel, reuse, and reprocess in order to obtain the main compound of product.

2.7.3 Crumb rubber

Crumb rubber is the name given to any material derived from reducing scrap tires or other rubber into uniform granules with the inherent reinforcing materials such as steel and fiber. There are several processes for manufacturing crumbed rubber. Mechanical process is one of the ways to recycle waste rubber into crumbed rubber. Grinding is the process to separate the rubber, metal, and fabric components of the tyre. Whether using granulation equipment or cracker mills, the first processing typically reduces the waste rubber to small chips. The next process will grind the chips to remove the rubber from the fabric and metal. After each processing, the raw materials are classified by screens to separate the size. Magnets are used throughout to remove wire and other metals. In the last step, fabric is removed by air separator.

CHAPTER III

METHODOLOGY

3.1 Materials and Instruments

3.1.1 Portland Cement Type I

3.1.2 Crumb rubber (Union commercial development Co., Ltd., Thailand.)

3.1.3 Lead powder

3.1.4 Boron carbide powder

3.1.5 Barium sulphate (P and S Barite Mining Co., Ltd.)

3.1.6 Water

3.1.7 MCNP transport code

3.1.8 Neutron source (Americium-241/Beryllium-9, $^{241}\text{Am}/\text{Be}$)

3.1.9 Gamma ray source (Cobalt-60, Co-60)

3.1.10 Material Analysis

3.1.10.1 *Scanning Electron Microscope with Energy Dispersive Spectroscopy or SEM:EDS*

3.1.10.2 *Carbon/hydrogen/nitrogen determinator*

3.1.10.3 *Quantitative X-ray diffraction technique (QXRD)*

3.1.11 Gamma attenuation experiment

3.1.11.1 *Nal(Tl)Scintillation Detector (CANBERRA Model 802-2x2, crystal size 2x2 inches)*

3.1.11.2 *Counting system: Pre-amplifier, Multi-channel analyser (MCA), Amplifier, High Voltage Power Supply*

3.1.11.3 *Lead bricks*

3.1.12 Neutron attenuation experiment

3.1.12.1 Boron Trifluoride (BF_3) Neutron Detector

3.1.12.2 Counting system: Pre-amplifier, Amplifier, High Voltage Power Supply, Multi-Channel Analyzer (MCA)

3.1.12.3 Polyethylene shields

3.1.12.4 Acrylic slabs

3.1.12.5 Lead plates

Buildup factor experiment

3.1.13.1 NaI (Tl) Scintillation Detector (CANBERRA Model 802-2x2, crystal size 2x2 inches)

3.1.13.2 Counting system: Pre-amplifier, Multi-channel analyzer (MCA), Amplifier, High Voltage Power Supply

3.1.13.3 Lead collimators

3.1.14 Prompt Gamma Neutron Activation Analysis Experiment (PGNAA)

3.1.14.1 High Purity Germanium Detector model GC3021 (HpGe)

3.1.14.2 Counting system: Multichannel analyser, Amplifier, High Voltage Power Supply

3.1.14.3 Polyethylene shields

3.1.15 MGP Model HDS101 handled search and isotope identification device

3.1.15.1 CsI(Tl) scintillator for low gamma dose rate measurement

3.1.15.2 Silicon Diode for high gamma dose rate measurement

3.1.15.3 LiI(Eu) scintillator for neutron measurement

3.1.16 Neutron monitor NT-35-03

3.1.17 Compressive Testing Machine (CTM)

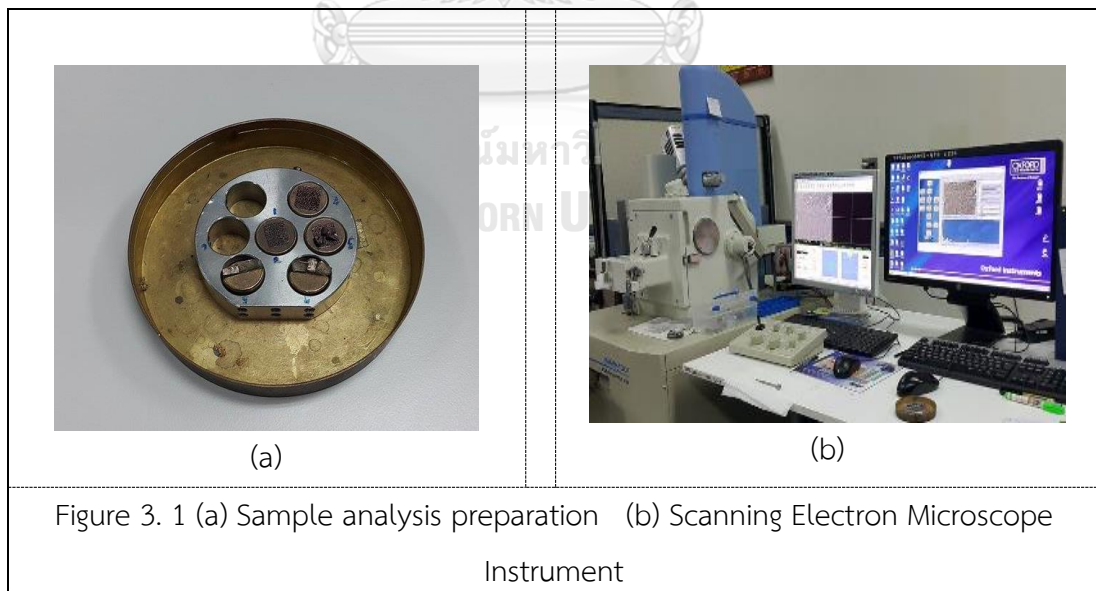
3.1.18 Mortar Mixer

3.2 Material analysis

3.2.1 Material analysis by Scanning Electron Microscope with Energy Dispersive Spectroscopy (SEM:EDS)

The key factor of radiation shielding concrete is the atomic compositions. For neutron and gamma ray shielding, the most effective shielding material is obtained from a mixture of hydrogenous materials, heavy metal elements and other neutron absorbers. The 3 major materials that have been selected to use in this research were portland cement, crumb rubber and barite. Material analyses were carried out to investigate the elemental composition in materials in order to obtain the corrective data to use in Monte Carlo Simulation program and to know what elements influenced neutron and photon shielding capability.

SEM images are produced with the appearance of the realistic topography. In this analysis, the electrons travel to the surface of the sample in the vacuum condition in a raster pattern. The electrons impinge on the surface and emit the secondary electrons that are collected by a fixed in-column detector [24].



SEM was utilized to determine elements in or on the surface for qualitative information and to measure elemental composition. The analysis was performed at

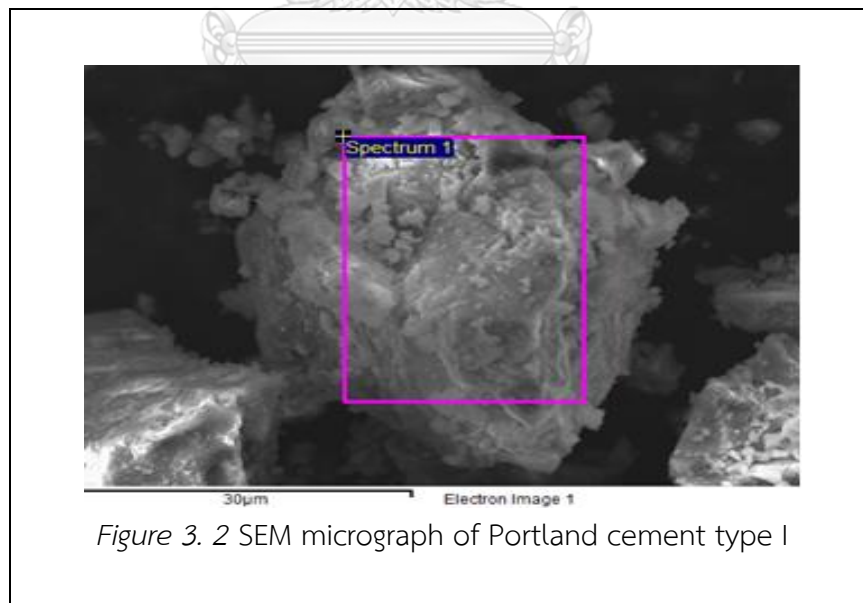
Scientific and Technological Research Equipment Centre Chulalongkorn University using scanning electron microscope model JSM6610LV (JEOL) with Energy Dispersive Spectroscopy (EDS).

Energy-dispersive spectrometer or EDS utilizes the pulse height analysis of the detector. The output pulses proportional in height to the X-ray photon energy is analysed in a pulse height analyser. A solid state detector is used for better energy resolution. The incident photons from the X-ray source cause the ionization in the detector that produces an electrical charge, which is amplified by a sensitive pre-amplifier that is located close to the detector. Both of detector and pre-amplifier are cooled with liquid nitrogen in order to minimize the electronic noise [25], resulting in a spectrum with peaks at the characteristic energies for the elements present.

1) Material analysis results by using SEM:EDS

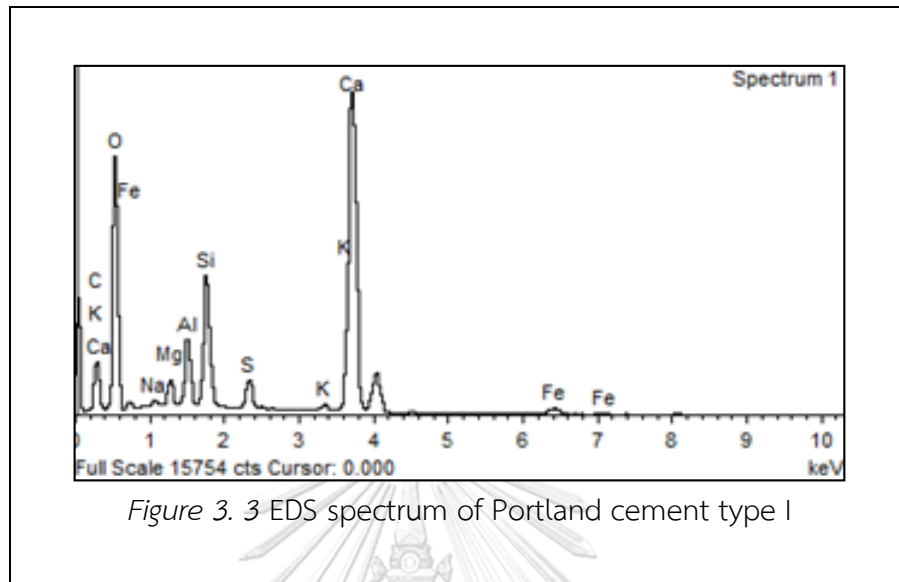
a) Portland cement type I

The analysis of Portland cement type I is presented. The SEM micrograph revealed a complex microstructure as shown in Fig 3.2.



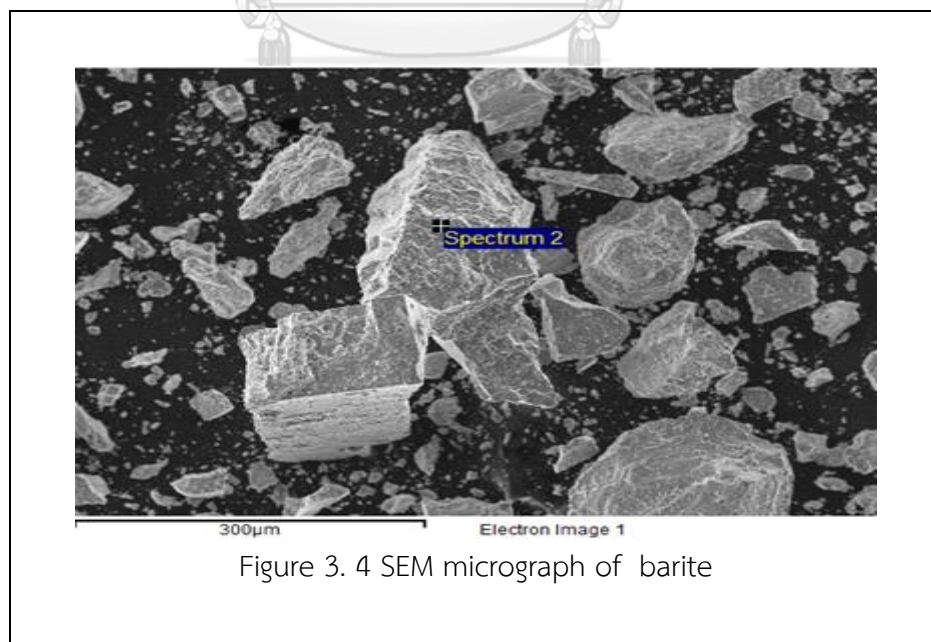
The EDS spectrum described the quantity of elements present in Portland cement type I. The result revealed the presence of the following elements: Ca (33.67), O

(47.74 wt%), Si (5.56 wt%), C (9.62 wt%), Al (2.63 wt%), Mg (1.07 wt%) and S (1.55 wt%).

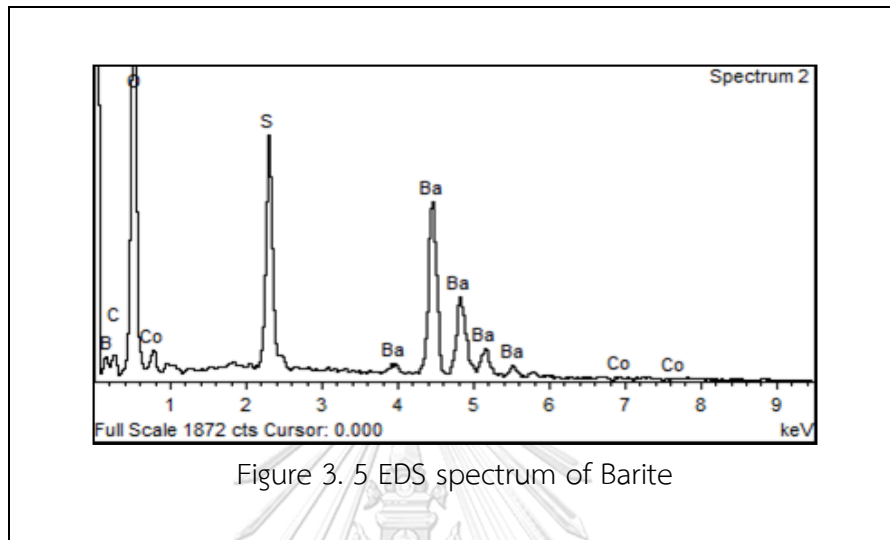


b) Barite

The analysis of barite is presented. The SEM micrograph revealed a complex microstructure as shown in Fig 3.4.

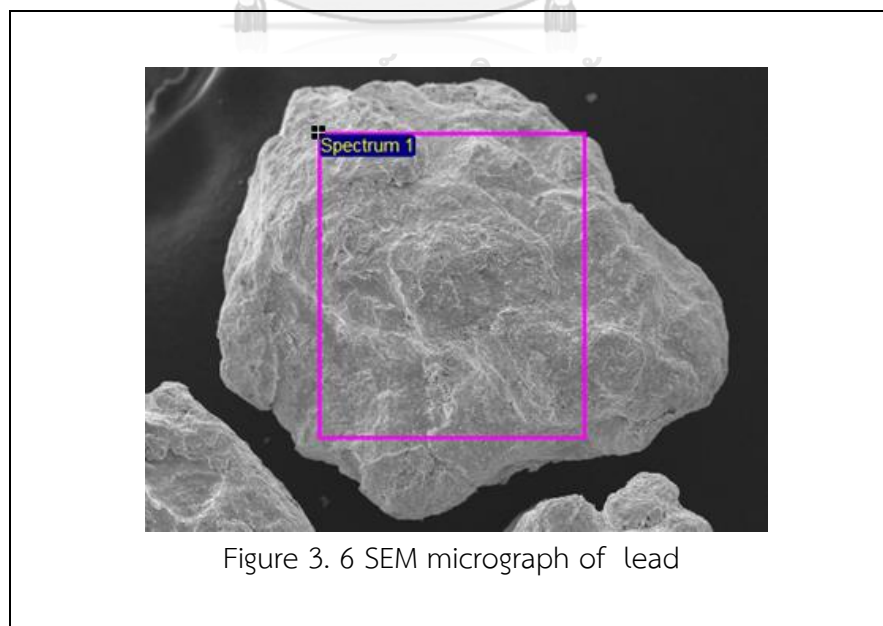


Barite is a mineral consisting of barium sulfate. The elemental composition in Barite consists of Ba (45 wt%), O (25 wt%), S (12 wt%) and others as shown in the EDS spectrum Fig 3.5.



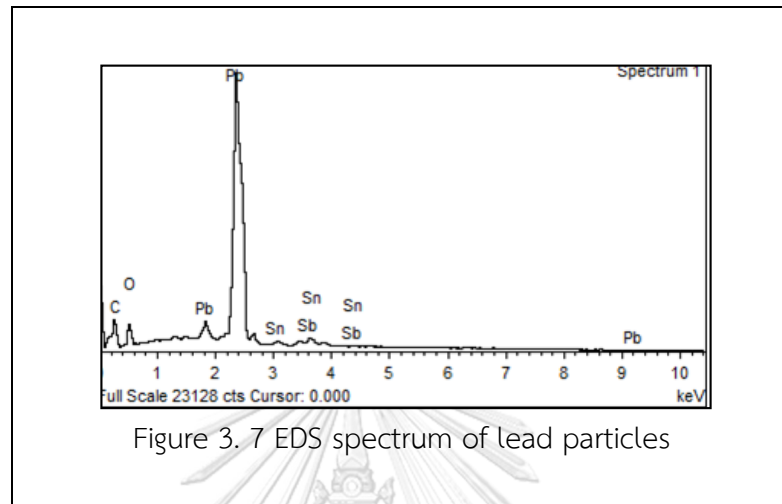
c) Lead particles

The analysis of lead is presented. The SEM micrograph showed a complex microstructure as shown in Fig 3.6.



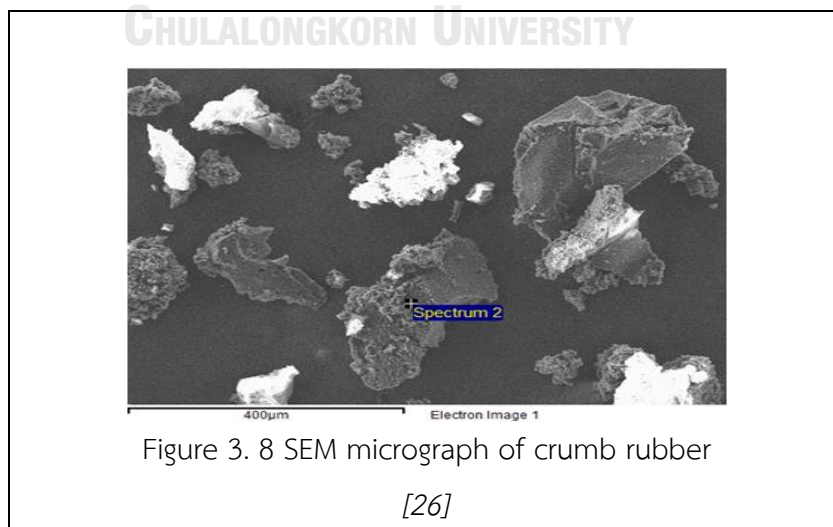
EDS spectrum indicated the presence of the following elements in lead particles used in the experiment: O (7.84 wt%), Sn (2.88 wt%), Sb (3.52 wt%) and Pb (85.74%).

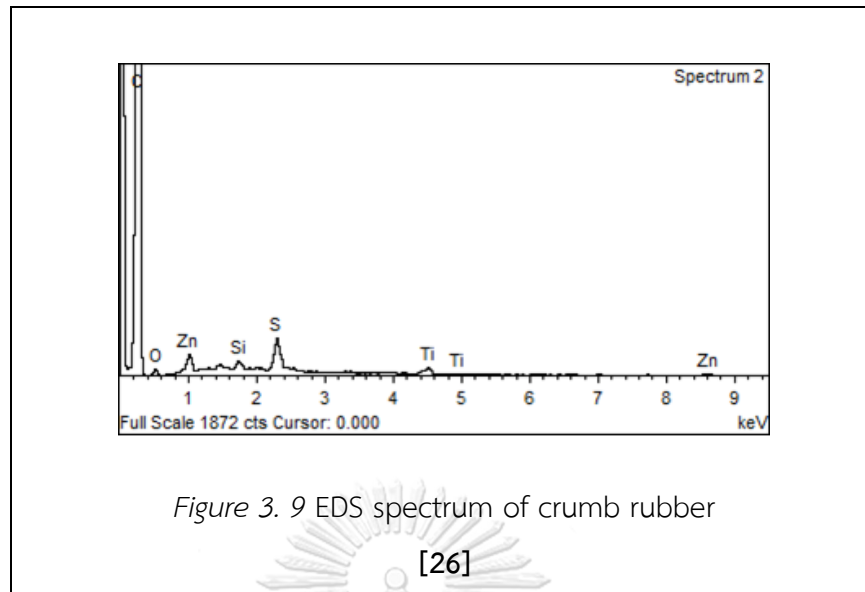
The EDS spectrum is shown in Fig 3.7.



3.2.2 Material analysis by carbon/hydrogen/nitrogen determinator (CHN determinator)

The analysis of crumb rubber is presented. The SEM micrograph revealed a complex microstructure as shown in Fig 3.8. The analysis result indicated the presence of the following elements C (80.79 wt%) and H (9.03 wt%) using C/H/N determinator Serial No. 3525.

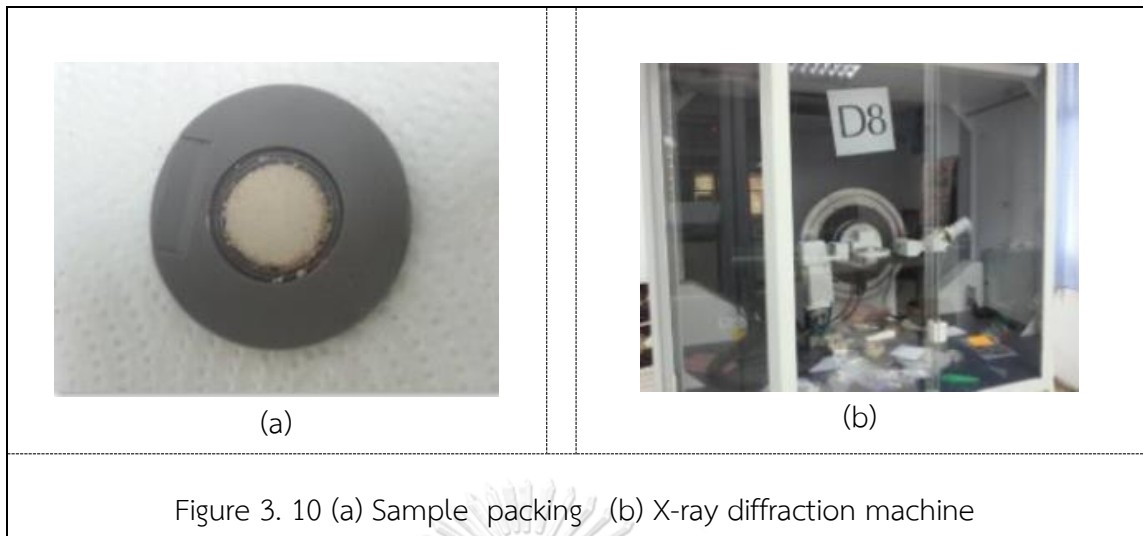




3.2.3 Material analysis by X-ray diffraction

In this research study, the X-ray diffraction technique was utilized to investigate the crystalline phase of shielding materials. X-ray diffraction is a technique used for the characterization and identification of crystalline phases. When X-ray beam interacts with a crystalline phase, Bragg diffraction occurs, producing a characteristic diffraction pattern. The pattern is unique for each particular phase, similar to a fingerprint, and so can be used to identify the substance.

In this study, the X-ray source operated at 40 kV and 40 mA. Scans were typically collected from 5 degree 2θ to 80 degree 2θ using step size of 0.017 degree at a scan time of 2 hrs.



3.3 Material proportions

The elemental compositions of the concrete shielding materials depended on the mix proportions and the chemical composition of the materials used. Shielding materials were designed in 4 types as follows:

1. Type I, High Density Cement (HDC)
2. Type II, composing of High Density Concrete mixed with Crumb Rubber (HDCR)

HDCR shielding materials were designed with the following percentages of crumb rubber: 0, 5, 10, 15, 20 and 25 vol%.

3. Type III, composing of High Density Concrete mixed with crumb rubber and lead powder (HDCRL)

High Density Concrete mixed with 5 vol% crumb rubber was selected to mix with lead powder at various percentages (2, 4, 6 and 8 wt%). These mixtures were used in the MCNP simulation.

4. Type IV, composing of High Density Concrete mixed with crumb rubber and boron carbide (HDCRB)

High Density Concrete mixed with 5 vol% crumb rubber was selected to mix with boron carbide at various percentages (2, 4, 6 and 8 wt%). These mixtures were used in the MCNP simulation.

The following Table shows the compositions of various shielding materials used in the MCNP simulation.

Table 3. 1 Compositions of various shielding materials used in the MCNP simulation

Specimen	Waste Rubber (gram)	Cement (gram)	Barite (gram)	Absorber (gram)	Water (gram)	Density (gram/cm ³)
HDC	-	1,000	5,763	-	450	3.350
HDCR5	94.22	1,000	5,669	-	450	2.831
HDCR10	188.25	1,000	5,370	-	450	2.782
HDCR15	282.67	1,000	5,070	-	450	2.733
HDCR20	376.91	1,000	4,771	-	450	2.636
HDCR25	471.00	1,000	4,472	-	450	2.587
HDCR5L2	94.22	1,000	5,669	464.98	450	2.957
HDCR5L4	94.22	1,000	5,669	929.96	450	3.080
HDCR5L5	94.22	1,000	5,669	1,162.45	450	3.154
HDCR5L6	94.22	1,000	5,669	1,394.94	450	3.219
HDCR5L8	94.22	1,000	5,669	1,859.92	450	3.350
HDCR5B2	94.22	1,000	5,669	103.23	450	2.812
HDCR5B4	94.22	1,000	5,669	206.47	450	2.798
HDCR5B6	94.22	1,000	5,669	309.71	450	2.785
HDCR5B8	94.22	1,000	5,669	412.95	450	2.771

3.4 Shielding materials attenuation simulation by Monte Carlo Simulation (MCNP)

The Monte Carlo Transport Code was used to assess the radiation attenuation efficiency of shielding materials in order to determine the optimum material compositions. Am-241/Be was selected to be the neutron source and Co-60 was selected to be the gamma source. In this work, an isotropic Am/Be source was used to study the neutron transmission of shielding materials between energy 5.0×10^{-7} and 1.0×10^2 MeV. The source was placed at the front center of the shielding material. The radiation shield with dimensions $12.7 \times 12.7 \times 12.7$ cm³ was developed according to the

British standard for concrete cubes. The surface flux tally of F2 was used to track particles through the matter with the unit of number of particles/cm²/source particle. The standard deviation errors were considered from the MCNP simulation. Dose Energy or DE and Dose Function or DF were carried out to convert flux to total dose equivalent rate in unit of (rem/hr)/(particle/cm²-s). The simple geometry was designed to simulate the problems.

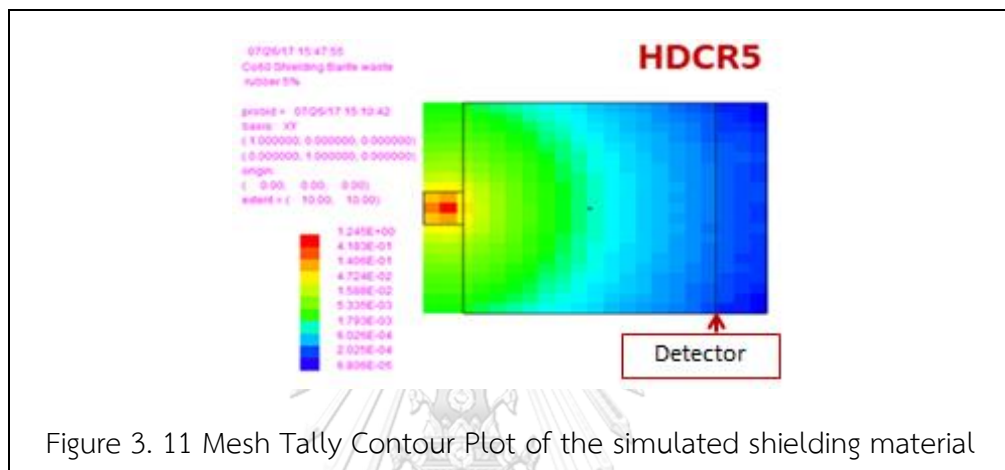


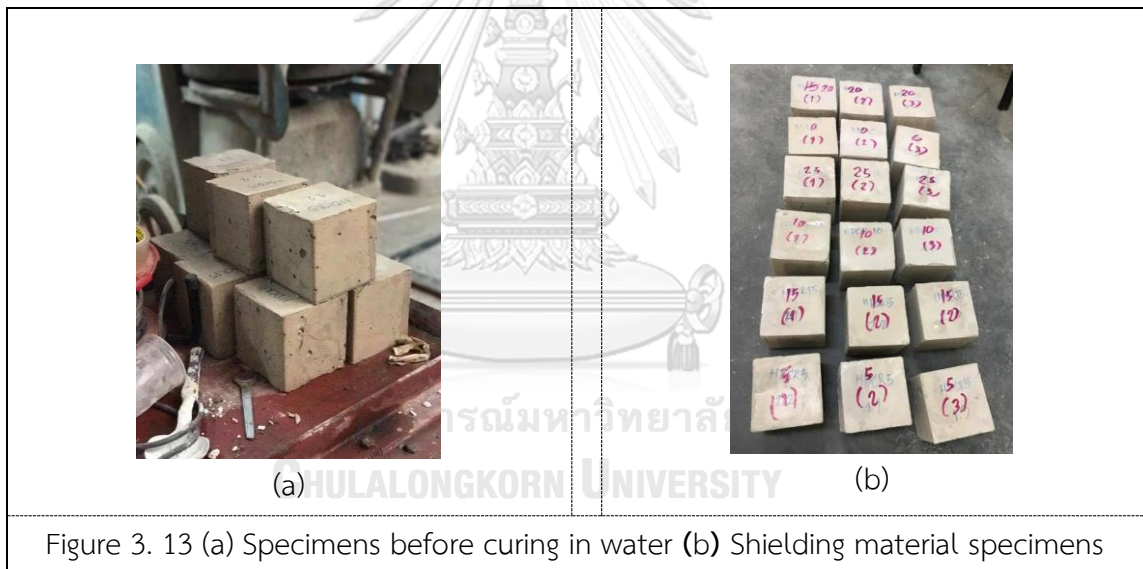
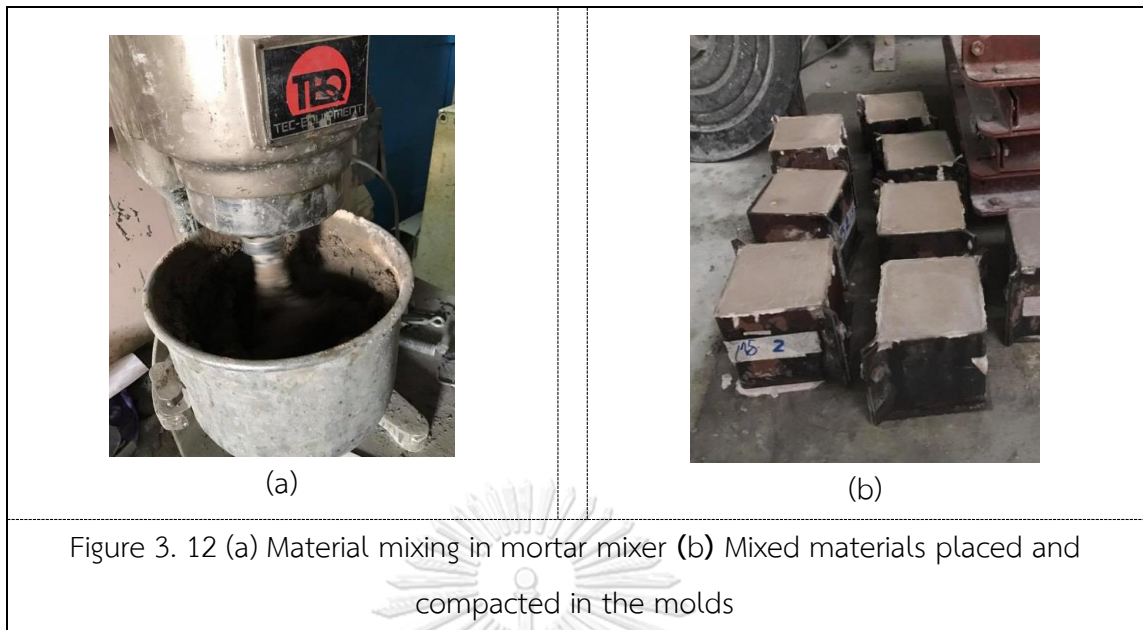
Figure 3. 11 Mesh Tally Contour Plot of the simulated shielding material

The isotropic source was installed in front of the shield at the center position. The shield with thickness 12.7 cm was placed between the isotropic source and the detector. The detector was placed at the back center of the shield to detect radiation passing through the shield.

To study the neutron and photon penetration through each material thickness, the shielding was also designed to have different thicknesses as follows: 6.35, 12.7, 19.05 and 25.4 cm.

3.5 Shielding materials preparation

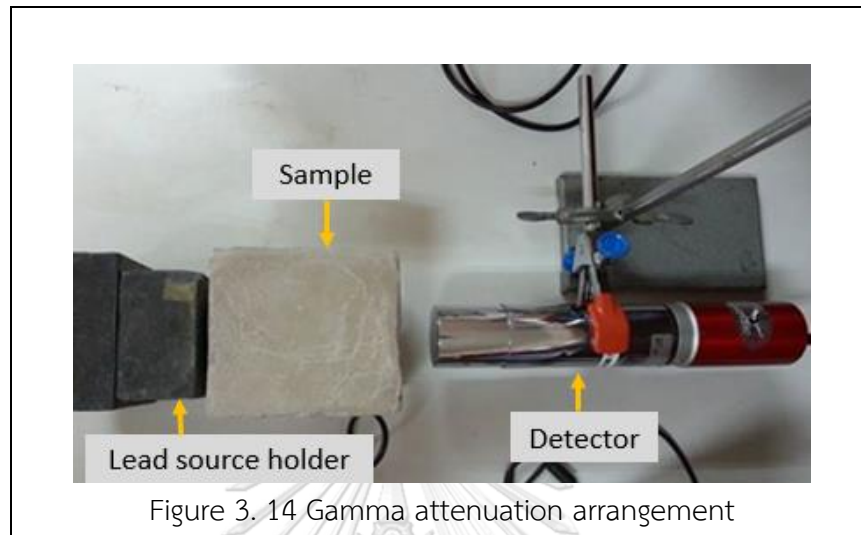
After all the components of HDCR with specific portions have been thoroughly mixed in a mortar mixer, waste rubber and fine aggregates were added to HDCR and were bonded to Portland cement through the hydration process in the molds. The molds were removed after 24 hours and the shielding blocks were submerged in water for 7 days of curing, after which they were tested for radiation attenuation.



3.6 Gamma attenuation measurement

All of the radiation measurements were carried out at the Radiation Measurement Laboratory at Nuclear Engineering Department, Faculty of Engineering, Chulalongkorn University to assess the shielding performances. Co-60 was selected to be the isotropic gamma source to measure the gamma attenuation. The scintillation detector, Canberra model 802-2 x 2 serial no. 01067803, was used to measure gamma radiation. A linear setup with the gamma source and the detector separated by 17 cm was used as shown

in Fig. 3.14. The counting time was 1 minute per measurement. Two gamma energies were considered in the gamma attenuation studies.



3.7 Neutron attenuation measurement

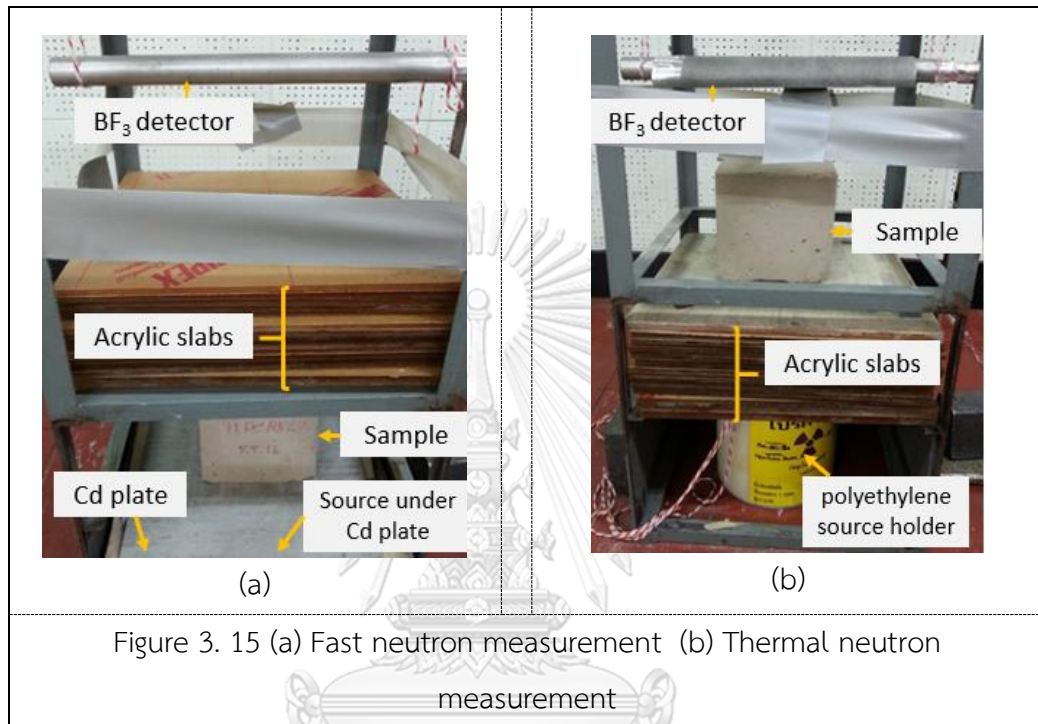
3.7.1 Fast neutron attenuation measurement

The Am-241/Be neutron source with strength $3.08 \times 10^3 \text{ n cm}^{-2} \text{ s}^{-1}$ was placed in the polyethylene source holder under the specimen. The acrylic slabs, each with thickness 10.5 cm, were placed between the shielding block and the thermal neutron detector to thermalize fast neutrons into thermal energy to be suitable for the thermal neutron detector. The thermal neutron detector, boron trifluoride (BF_3) detector, was used in this experiment. In order to prevent radiation scattering from the floor, a lead sheet was utilized. The distance from the lead sheet to the neutron detector was 51.5 cm. The counting time was set at 10 minutes by the rate meter Model 2200 Serial No. 211137. The operating voltage was 4.3 keV.

3.7.2 Thermal neutron attenuation measurement

The Am-241/Be neutron source with strength $3.08 \times 10^3 \text{ n cm}^{-2} \text{ s}^{-1}$ was placed in the polyethylene source holder under the acrylic slabs, each with thickness 10.5 cm. The specimen was placed on the acrylic slabs. The thermal neutron detector, boron

trifluoride (BF_3) detector, was used in this experiment. The distance from the bottom of the specimen to the neutron detector was 21 cm. The counting time was set at 10 minutes by the rate meter Model 2200 Serial No. 211137. The operating voltage was 4.3 keV.



3.8 Lead Adhesion Testing

Even though the addition of lead powder to HDCR5 increased the gamma attenuation, increasing amount of lead to more than 2 wt% resulted in cracking of the shielding materials. It was suspected that the added lead powder may play an important role in cracking via reduced adhesion inside concrete. Thus, the adhesion between lead particles and high-density cement mixed with 5 wt% crumb rubber was investigated by the lead adhesion testing. Lead powder was spread over the surface of the wet shielding as shown in Fig 3.16. After the shielding became dried, the lead adhesion was assessed by wiping over the surface of the shielding and observing the amount of lead power that became unattached from the shielding surface.

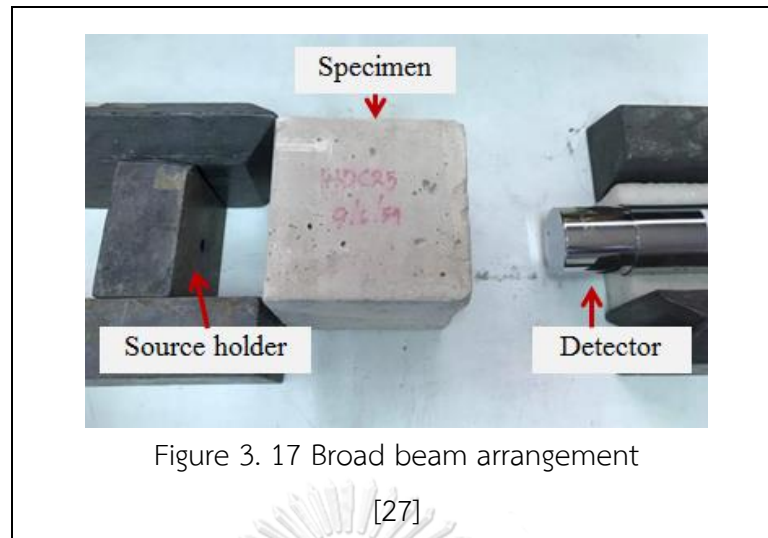


Figure 3. 16 Lead powder on surface of wet shielding

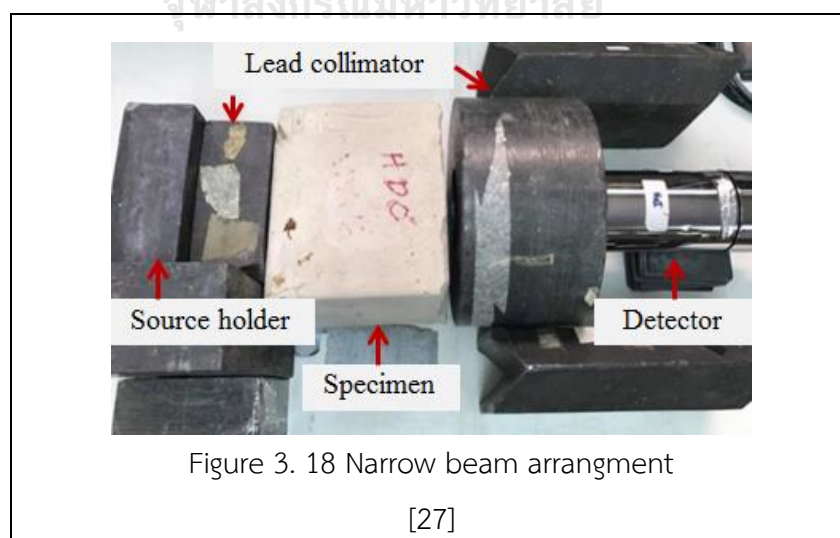
3.9 Scattered gamma ray and secondary gamma ray by buildup factor experiment

The gamma rays interact with matter via three processes, which are photoelectric effect, Compton scattering and pair production. Scattered gamma ray and secondary gamma ray can be released after gamma ray interacts with material through the Compton scattering process. The purpose of this research study was to design shielding materials for radiation safety, so the scattered gamma ray and secondary gamma ray emissions from materials had to be considered by studying the buildup factor parameter.

Two geometries, broad beam (poor-geometry) and narrow beam (good-geometry), were arranged to determine the buildup factor. For broad beam (poor-geometry), some photons are scattered while travelling from the source to the detector because there is no collimator or lead shield, which is unrealistic. For narrow beam (good-geometry), no photons are scattered from gamma ray transportation from the source to the detector because the gamma radiation has been collimated by lead shield, which is idealistic. This is why the two geometries had to be investigated.

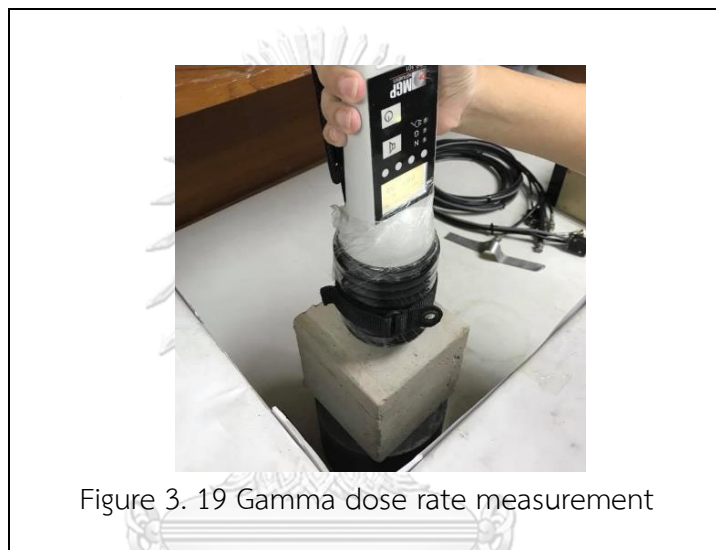


For the narrow beam geometry, lead collimators were used to collimate gamma ray. The lead brick for the source holder was 5 cm thick and 4.5 cm height with 1 cm central hole diameter. Gamma radiation travelling to the detector was collimated with the cylindrical lead shield with the central hole diameter of 3 cm and the outside diameter of 16 cm. The distance between the isotropic source and the detector was 17 cm. The distance between the isotropic source and the shielding material was 12 cm. The broad beam geometry was obtained by simply excluding both collimators. Figures 3.17 and 3.18 show the narrow beam and broad beam arrangements, respectively.

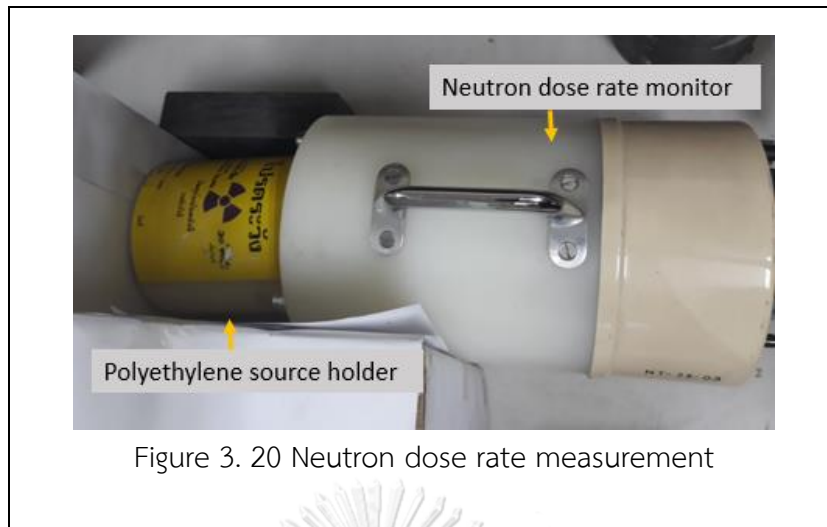


3.10 Dose rate measurement

The photon and neutron sources which were Co-60 and Am-241/Be, respectively, were selected for the measurement of photon and neutron dose equivalent rates. For gamma dose rate evaluation, the photon source was placed at the center of lead shield. The height of the shield from the bottom was 4 inches. The shielding material specimen was placed above the lead shield as shown in Fig 3.19.

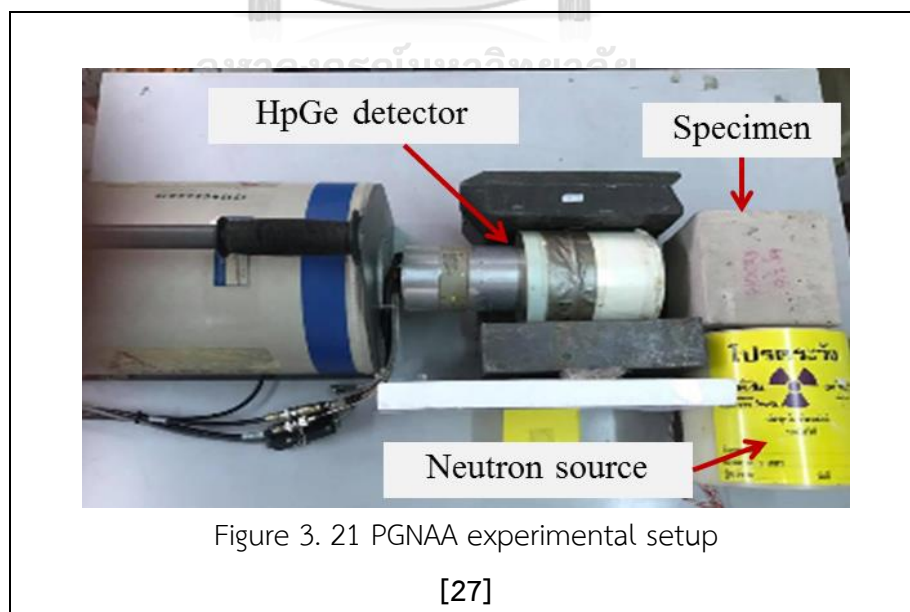


The photon transmissions were measured using the dose rate detector MGP Model HDS101 G/GN in unit micro-sievert per hour. The CsI(Tl) scintillator was used for low gamma dose rate measurement and Silicon Diode was used for high gamma dose rate measurement. Neutron dose rate evaluation was performed by using the neutron monitor NT-35-03 in unit micro-sievert per hour and the dose rate detector MGP Model HDS101 G/GN in unit count per sec which utilized LiI (Eu) scintillator for neutron measurement. The neutron source was installed in the central hole of the polyethylene shield. The specimen was placed between the polyethylene shield and the neutron detector as shown in Fig. 3.20.



3.11 Prompt gamma ray and secondary gamma ray by Prompt Gamma Neutron Activation Analysis (PGNAA)

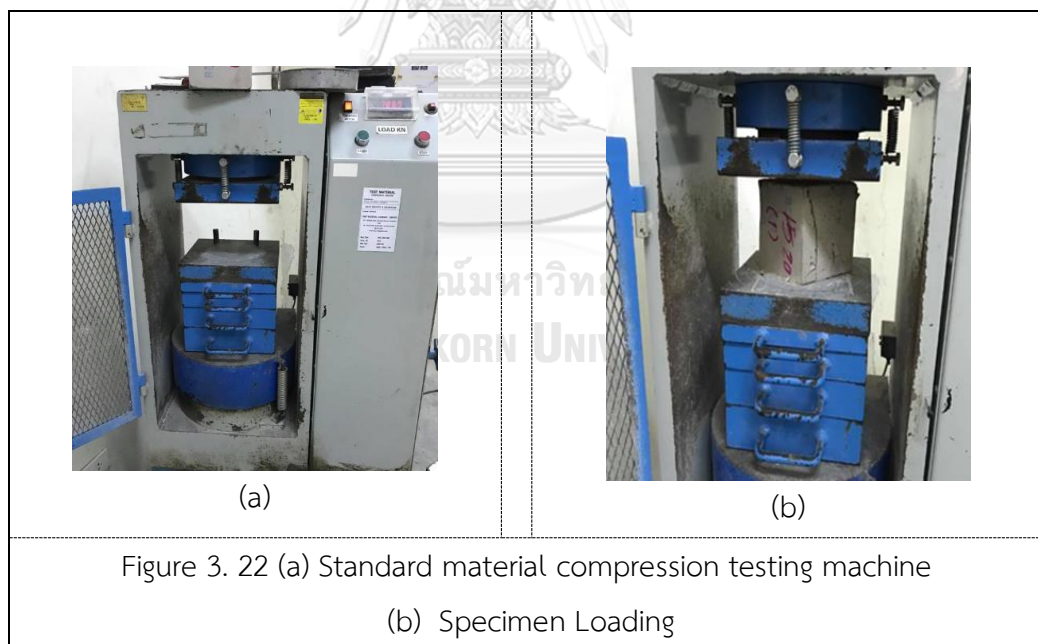
A non-destructive elemental analysis technique for measuring prompt gamma ray and secondary gamma ray is Prompt Gamma Neutron Activation Analysis. The Am-241/Be isotopic source was selected and a high-purity germanium (HpGe) detector model GC3021 with 30% relative efficiency at 1.1732 and 1.3325 MeV was used to detect prompt gamma ray emitted from the specimen during neutron irradiation.



The neutron source was placed in front of the specimen with the distance of 12 cm, while the specimen was placed 3 cm from the detector. A polyethylene sheet was used to cover the HpGe detector to minimize undesirable neutron radiation that may approach the detector from the side, potentially causing detector damage, as shown in Fig 3.21. The operating high voltage for measurement was 2,900 V. The specimen was irradiated with neutron radiation for 1 hour by using the Am-241/Be neutron source. The gamma spectrum from 20 to 5,300 keV was recorded.

3.12 Compressive strength test

The most important engineering property of hardened concrete is the compressive strength. Other properties such as tensile strength, flexural strength and modulus of elasticity are closely related to the compressive strength [28]. The specimens with a cubical shape were evaluated for the compressive strength [29] as illustrated in Fig. 3.22 .



The compressive strength test was performed after 28 days of curing time since the effective strength of materials increased with curing time [2]. A compression testing machine (CTM) was utilized to evaluate the compressive strength.

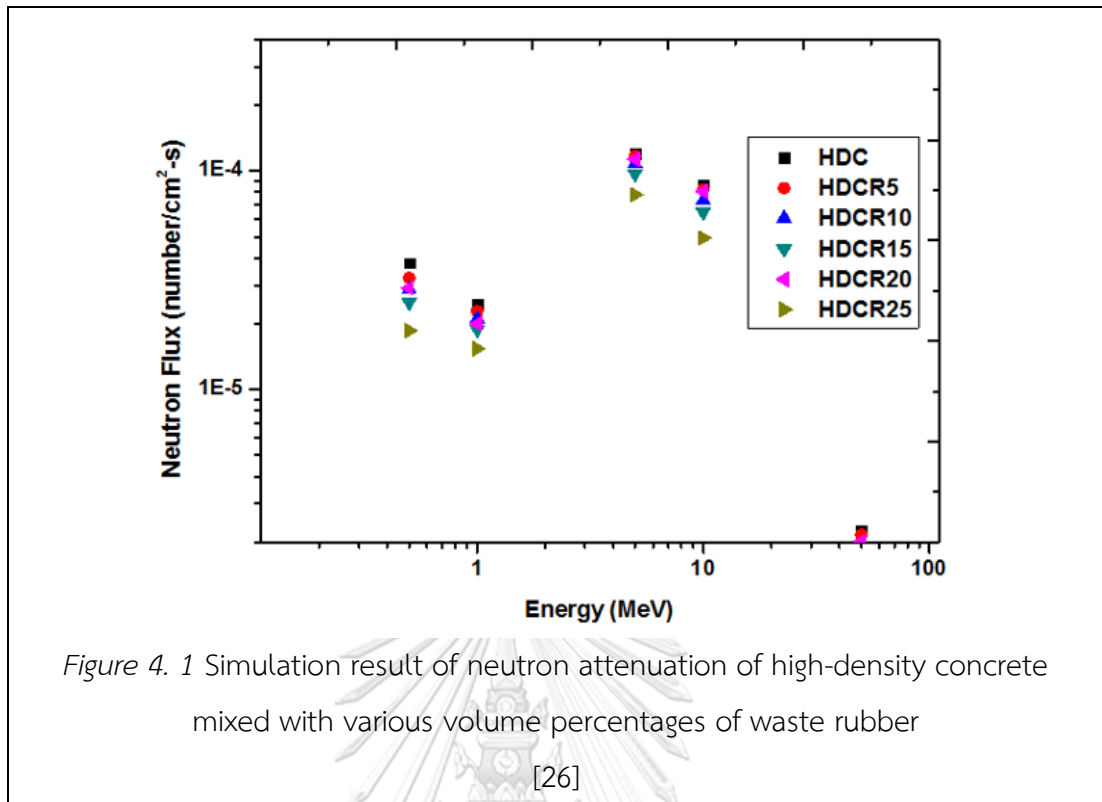
CHAPTER IV

RESULTS AND DISCUSSIONS

4.1 Material proportions by Monte Carlo Simulation

4.1.1 Neutron attenuation simulation

To determine the best composition of high-density cement mixed with crumb rubber, the MCNP simulation was performed firstly. The addition of crumb rubber in high-density cement with varying volume percentages of 5, 10, 15, 20 and 25 was studied. HDC denotes high-density cement; HDCRx denotes high-density cement mixed with x volume percent of crumb rubber. HDCR5, HDCR10, HDCR15, HDCR20 and HDCR25 shielding materials were investigated for the neutron attenuation using MCNP simulation program. The simulation results showed that incorporation of crumb rubber into high-density cement assisted in increasing the neutron attenuation. The minimum percentage of transmitted neutron flux occurred with 25 vol% crumb rubber for all simulated neutron energies as illustrated in Fig. 4.1. Because the fast neutrons could undergo elastic scattering interaction with carbon atoms and hydrogen atoms which were present at 80.79 and 9.03 wt% in crumb rubber, respectively, the combination of material proportions between heavy elements (barium) and low elements (carbon and hydrogen atoms) in crumb rubber improved the ability of neutron shielding.



4.1.2 Gamma attenuation simulation

As the purpose of shielding materials was not only for neutron radiation attenuation, but also for gamma radiation attenuation, the gamma shielding effectiveness had to be evaluated as well. MCNP computer simulation was carried out to investigate the most suitable portion of high density cement mixed with crumb rubber for gamma ray shielding. HDCR5, HDCR10, HDCR15, HDCR20 and HDCR25 were simulated to study gamma radiation attenuation. The simulation results indicated that the addition of crumb rubber into high density cement reduced the gamma attenuation as shown in Figs. 4.2 and 4.3. The comparison of high-density cement mixed with crumb rubber at low photon energy of 0.5 MeV is indicated that Fig.4.2. The simulation results revealed that increasing the crumb rubber content resulted in the increased transmitted photon flux, reaching the highest value of 3.5305×10^{-5} particle/cm² for the high-density cement mixed with 25 vol% crumb rubber. Fig. 4.3 showed the simulation result of high-density cement mixed with crumb rubber under the high photon energy of 5 MeV. The results exhibited the same trend compared to the case of low photon energy. The

minimum photon flux occurred when high density cement was mixed with 5 vol% crumb rubber. Thus, this specific proportion of crumb rubber was used throughout the remaining studies when adding additives to improve the performance of the shielding material.

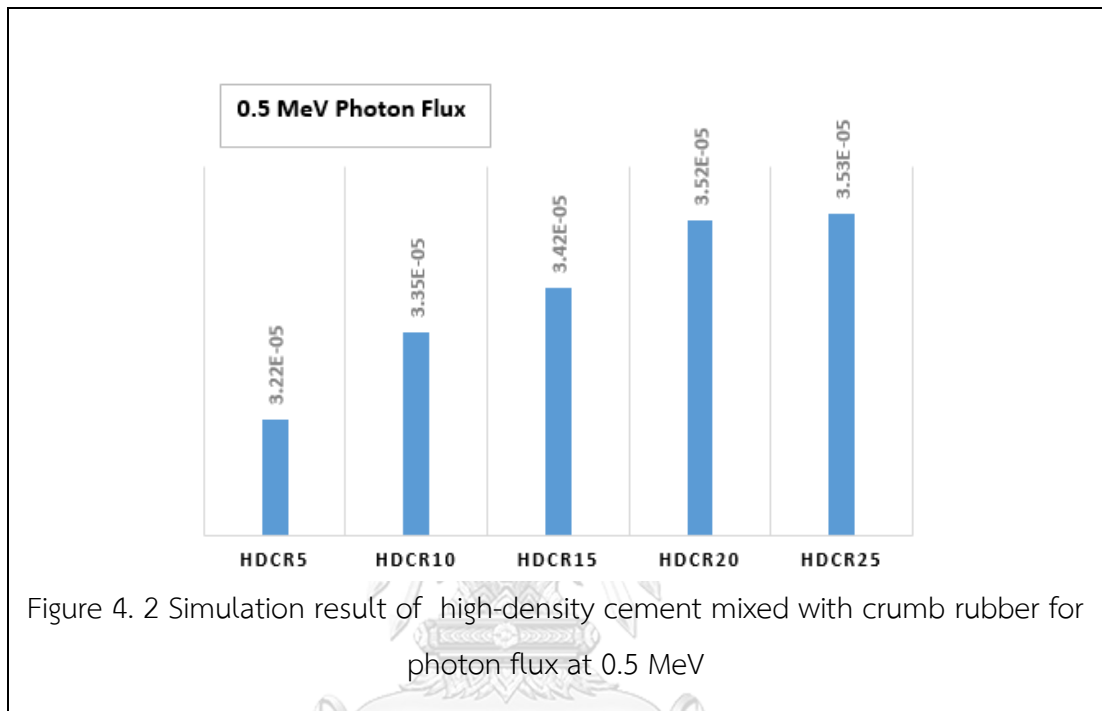


Figure 4. 2 Simulation result of high-density cement mixed with crumb rubber for photon flux at 0.5 MeV

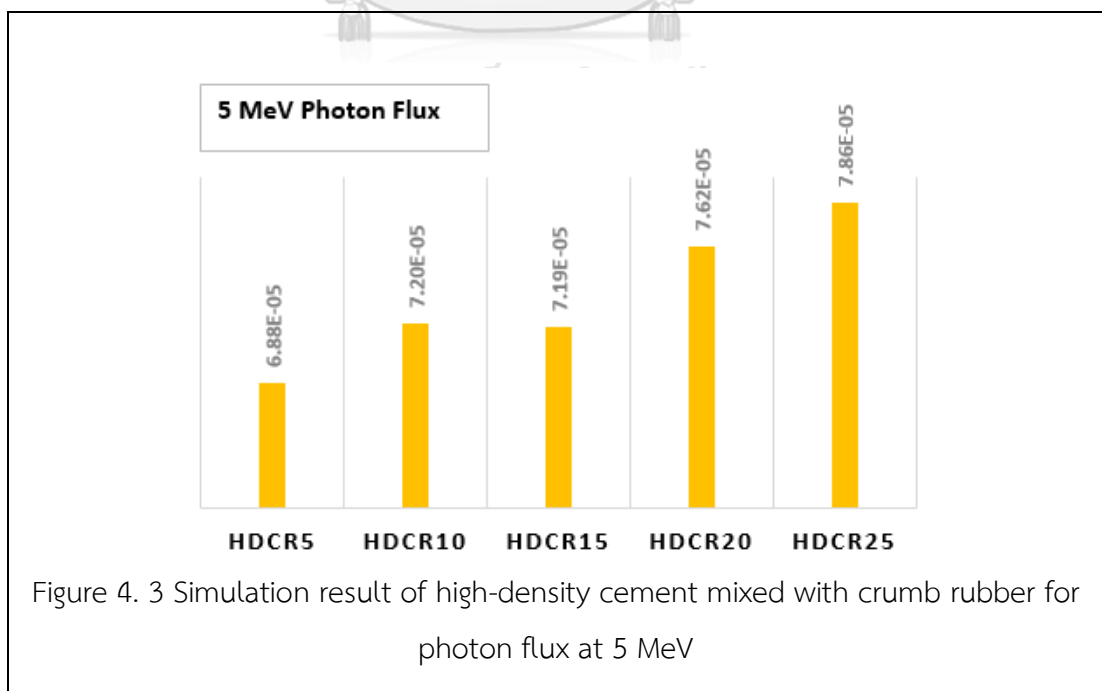


Figure 4. 3 Simulation result of high-density cement mixed with crumb rubber for photon flux at 5 MeV

4.2 Neutron and gamma attenuation experiments

4.2.1 Neutron attenuation measurement

The results of neutron attenuation experiment revealed that high-density cement mixed with 5, 10, 15, 20 and 25 vol% of crumb rubber was more effective against fast neutron radiation than high-density cement alone, and that the neutron transmission increased when the incorporation of crumb rubber was greater than 5 vol% as shown in Fig. 4.4, with the removal neutron cross section of 1.842×10^{-2} barn. Crumb rubber consists of large quantities of carbon and hydrogen atoms that exhibit excellent fast neutron attenuation. The energies of fast and intermediate energy neutrons were reduced via the scattering process with carbon and hydrogen atoms. This crumb rubber content in high density cement of 5 vol% did not agree with the simulated result in Fig 4.1. The reason why the fast neutron attenuation reduced when increasing the amount of crumb rubber to more than 5 vol% was the reduction of barium content in the shielding material. BaSO_4 , commonly called Barite, constituted 45.5 % by weight in high density cement. The decrease in Ba atoms in the shielding material, as a result of increasing crumb rubber percentage, decreased the number of inelastic scattering interactions of fast neutron with Ba. In addition, during fabrication, after all materials were mixed, the cement started to swell because of water absorption into crumb rubber, resulting in increasing the volume of the sample. Consequently, some part of the sample could not be contained in the mold and a certain amount of the rubber was not included in the shielding material. This problem intensified with increasing crumb rubber content in high-density cement.

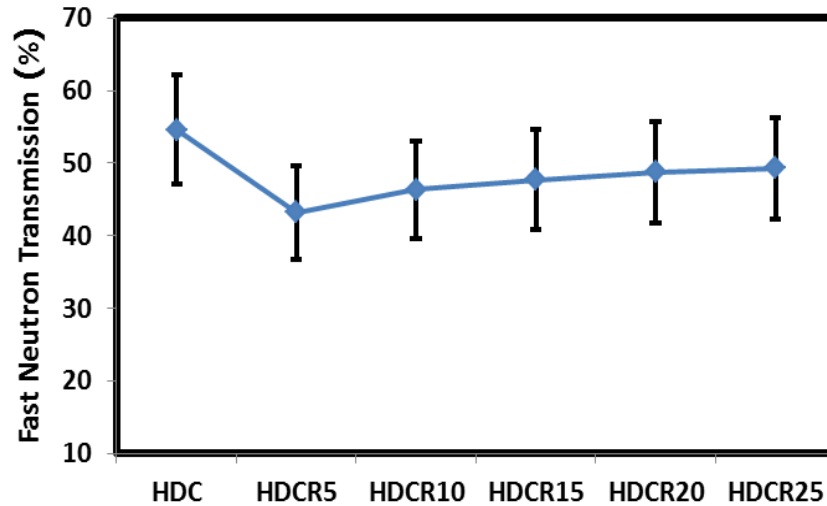
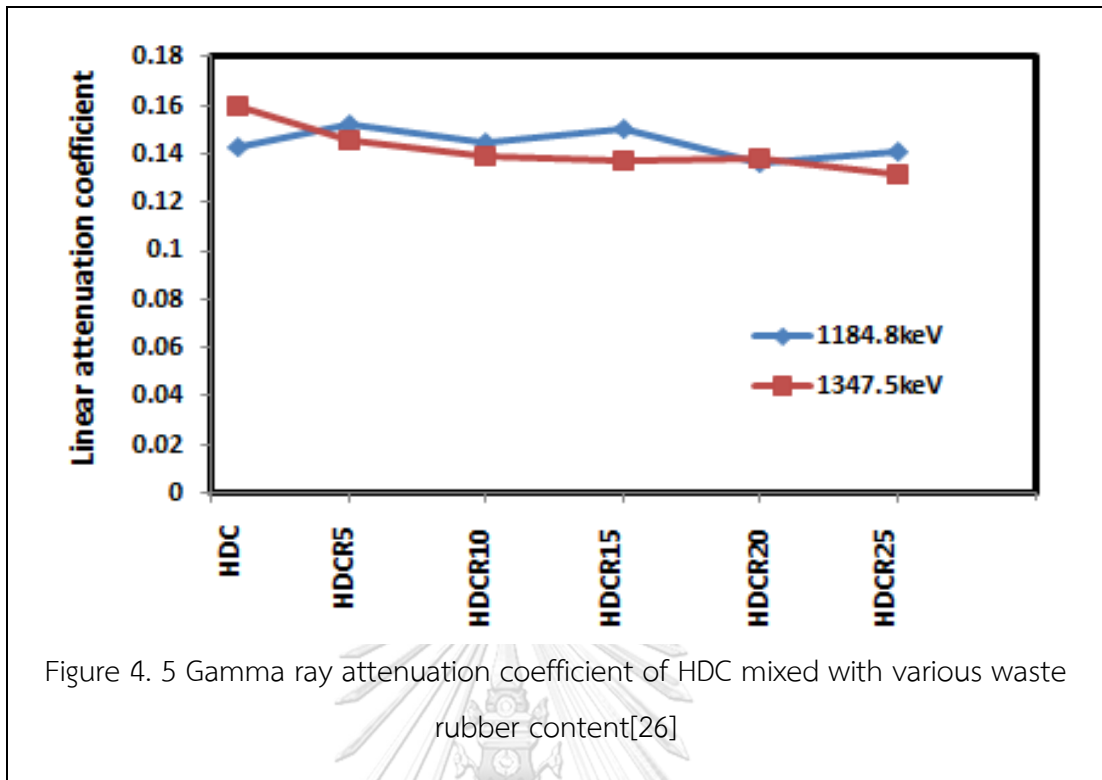


Figure 4. 4 Experimental results of fast neutron transmission for HDC with various vol% of waste rubber[26]

4.2.2 Gamma attenuation measurement

The addition of crumb rubber in high density cement at 5, 10, 15, 20 and 25 vol% was investigated for the gamma attenuation efficiency. The experimental results revealed that the incorporation of crumb rubber into HDC resulted in a slight decrease in the attenuation coefficient for 1,184.8 keV gamma ray as shown in Fig. 4.5. For the gamma ray energy of 1,347.5 keV, the linear attenuation coefficient decreased slightly more than for the case of 1,184.8 keV gamma ray as shown in Fig 4.5. Because Barite, the heavy element composition of HDC, was reduced by the addition of crumb rubber, thus, the gamma attenuation decreased. Moreover, the scattered gamma ray and secondary gamma ray that can be released from the gamma radiation interacting with shielding materials through Compton scattering process were absorbed by carbon and hydrogen atoms in crumb rubber.



4.3 Additional material for improving gamma ray shielding performance

Incorporation of lead particles into high density cement mixed with 5 vol% crumb rubber was studied to improve the gamma ray shielding performance. Various percentages of lead particles from 2 to 8 vol% with 2 vol% increment were studied. HDCR5 denotes high-density cement mixed with 5 vol% crumb rubber; HDCR5Lx denotes high-density cement mixed with 5 vol% crumb rubber and x volume percent of lead particles.

The gamma ray attenuation and neutron attenuation of HDCR5x were simulated by the MCNP program. Co-60 and Am-241/Be were selected to be the isotropic source of photon simulation and neutron simulation, respectively. The results revealed that lead particles played an important role to improve the photon shielding which is shown in Fig. 4.6, where the lowest transmitted photon flux was for the high-density cement mixed with 5 vol% crumb rubber and 8 vol% of added lead particles (HDCR5L8). HDCR5L6, HDCR5L4 and HDCR5L2 exhibited progressively lower photon

attenuation, respectively. This is because the high-Z materials have large absorption cross sections in the fast neutron region.

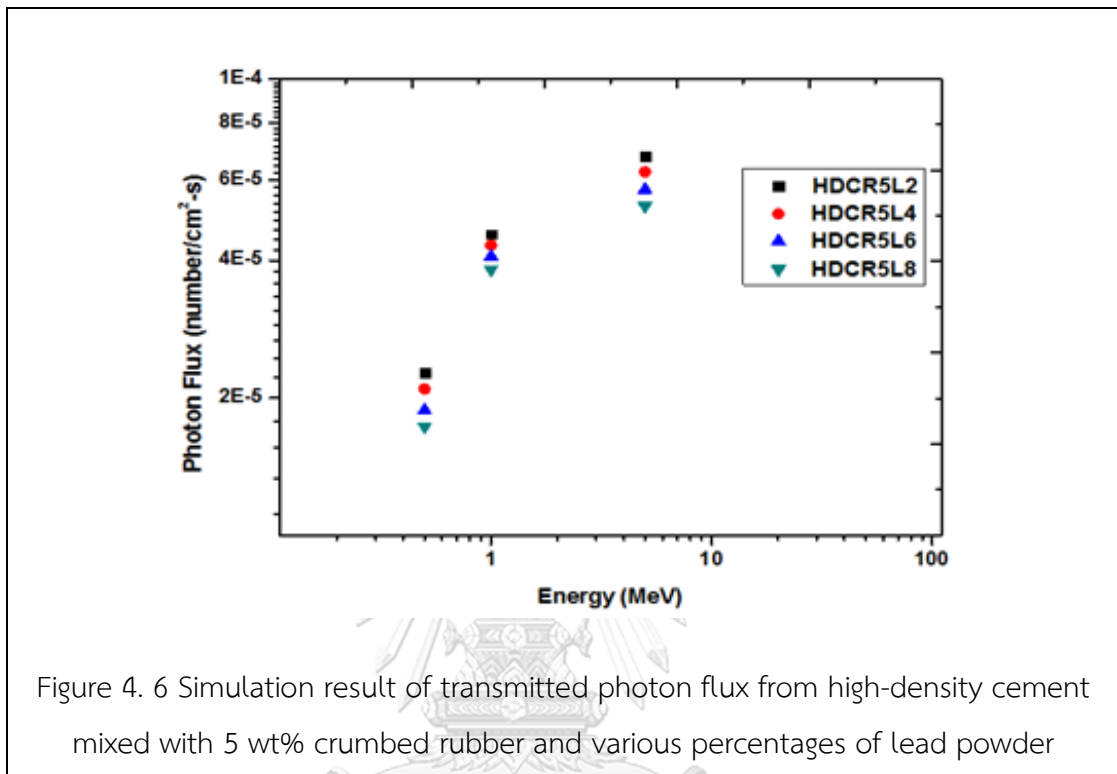
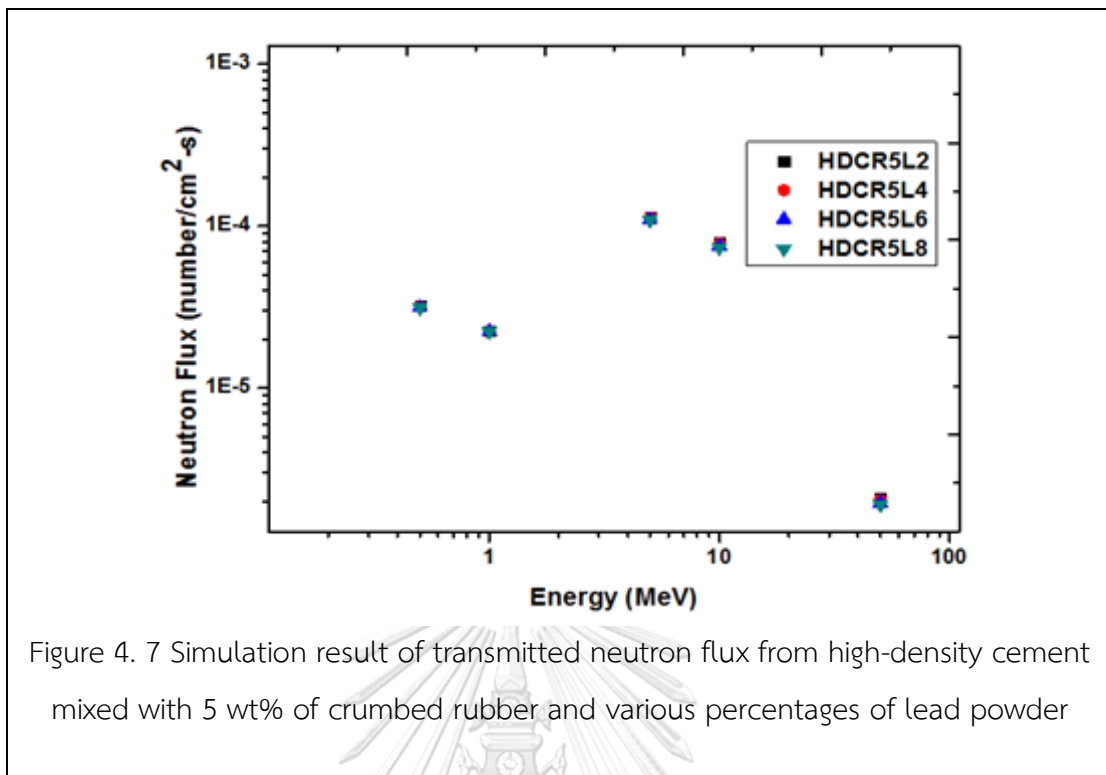


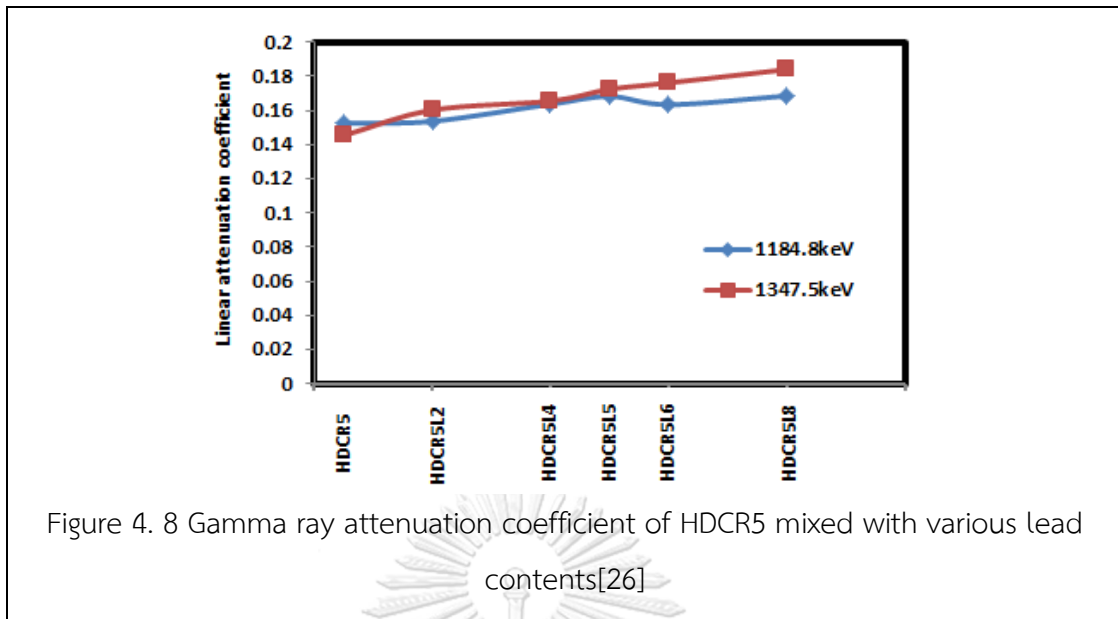
Figure 4. 6 Simulation result of transmitted photon flux from high-density cement mixed with 5 wt% crumbed rubber and various percentages of lead powder

The simulation result of neutron attenuation was illustrated in Fig. 4.7. The addition of lead particles in HDCR5Lx had no effect on neutron shielding ability. The transmitted neutron flux of HDCR5L2, HDCR5L4, HDCR5L6 and HDCR5L8 were very similar. This outcome was expected because lead exhibits a very low neutron attenuation capability compared to hydrogenous materials.



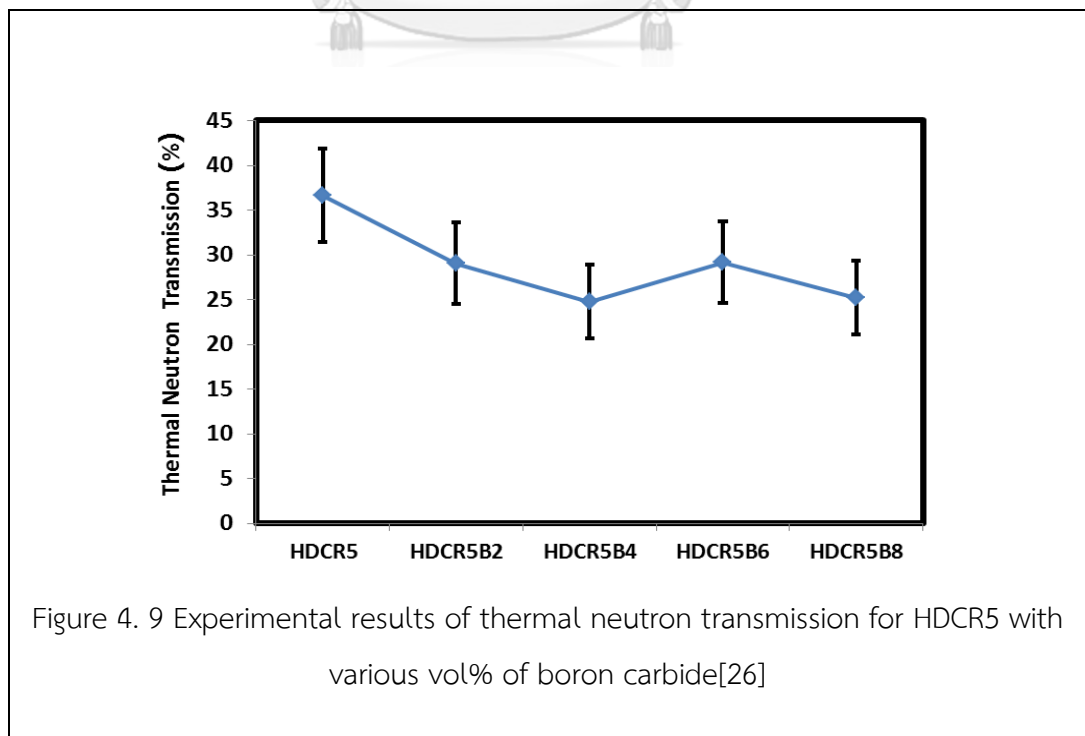
The experimental results of gamma ray attenuation indicated that the addition of lead content in high-density cement mixed with crumb rubber improved the gamma attenuation as illustrated in Fig. 4.8. Thus, the simulation results of gamma ray attenuation was confirmed by the experimental results.

The attenuation of gamma ray at 1,347.5 keV was better than at 1,184.8 keV as shown by the linear attenuation coefficients in Fig. 4.8. In addition, increasing the amount of lead particles improved the photon attenuation as lead is a heavy element with the characteristic property to attenuate gamma radiation very effectively.



4.4 Additional material for improving neutron shielding performance

To improve the efficiency of neutron attenuation, boron carbide (B_4C) was selected to be the neutron absorber since boron has a very high neutron absorption cross-section ($^{10}B = 3,843$ barns). Boron was added to high-density cement mixed with 5 vol% crumb rubber by various percentages from 2 to 8 vol% with 2 vol% increment.



Experimental results revealed that boron carbide played an important role in decreasing thermal neutron radiation as shown in Fig 4.9. Thermal neutron transmission was substantially reduced after incorporation of boron carbide absorber into the shielding material compared to high-density cement mixed with crumb rubber alone (HDCR5). The graph in Fig. 4.9 exhibited a downward trend. Although thermal neutron transmissions for different percentages of boron carbide addition did not show a clear trend, this is because the epithermal neutrons (10^{-5} - 10^{-2} MeV) could undergo elastic scattering with hydrogen atoms in crumb rubber and water to thermal energies. However, the percentages of transmitted thermal neutrons were in the range of standard deviation in the overall. Since the design purpose of this shielding material was to shield against high energy neutrons, this result only applies to thermal neutron shielding applications.

4.5 Radiation transmissions of different shielding thicknesses

Different shielding thicknesses of 6.38, 12.7, 19.08 and 25.46 cm were simulated for neutron and gamma ray transmissions. For all simulations, HDCR5 was used as a base with added boron carbide (B_4C) for neutron transmission and lead for gamma ray transmission.

4.5.1 Neutron transmission of high density cement mixed with 5 vol% crumb rubber and boron carbide

The transmitted fast neutron intensity in the presence of the shielding with different thicknesses was investigated. The results revealed that the $\ln(I/I_0)$ value reduced substantially when the shielding thickness increased in accordance with the Beer Lambert's law as shown in Fig. 4.10. Also, different boron carbide (B_4C) percentages only slightly affected the $\ln(I/I_0)$ value of fast neutron.

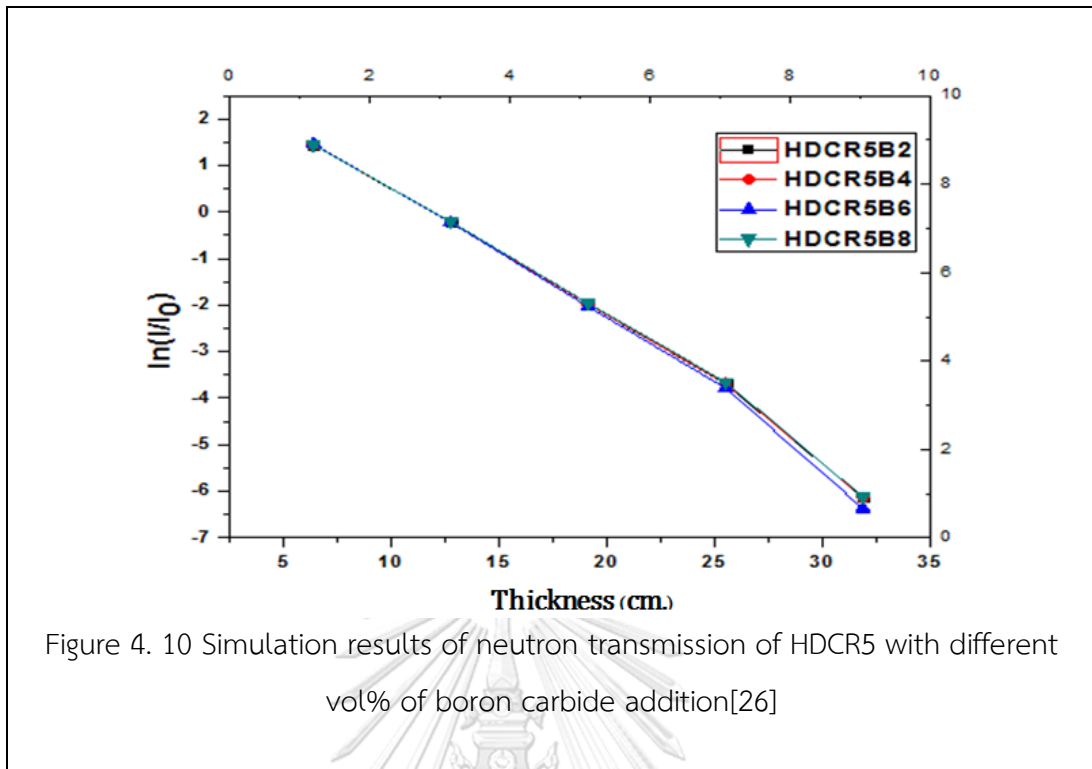


Figure 4. 10 Simulation results of neutron transmission of HDCR5 with different vol% of boron carbide addition[26]

4.5.2 Gamma ray transmission of high density cement mixed with 5 vol% crumb rubber and lead

The transmitted photon intensity in the presence of the shielding with different thicknesses was also investigated. The results revealed that the $\ln(I/I_0)$ value decreased with increasing shielding thickness, which complied with the Beer Lambert's law as shown in Fig. 4.11. It is also evident that the transmission was lower for shielding with higher lead content.

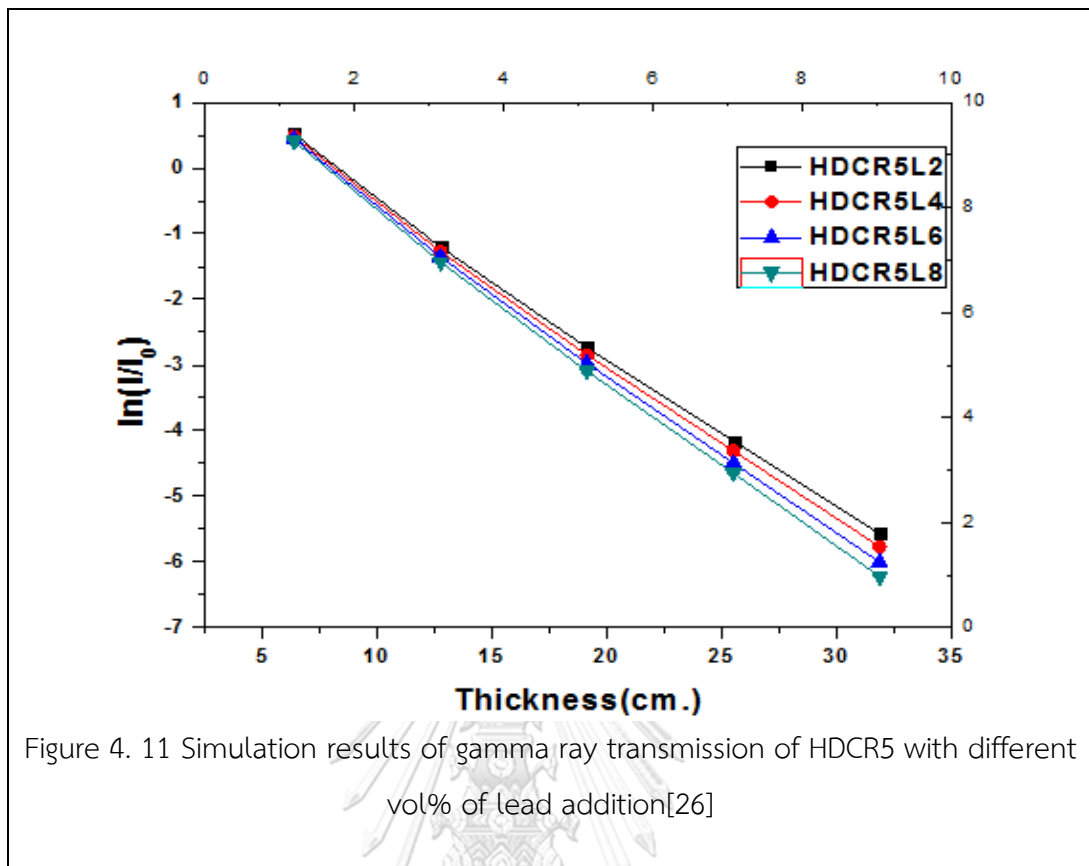


Figure 4. 11 Simulation results of gamma ray transmission of HDCR5 with different vol% of lead addition[26]

4.6 Determination of scattered gamma ray and secondary gamma ray from shielding materials

The buildup factor was studied to determine the scattered gamma ray and secondary gamma ray of shielding materials after gamma radiation interacted with materials. The narrow beam geometry (good-geometry) and the broad beam geometry (poor geometry) arrangements were set up to investigate the buildup factor of materials. The intensity of narrow beam is denoted by I_g and the intensity of broad beam is denoted by I_b . The gamma ray transmissions of narrow beam and broad beam revealed that the values of $\ln(I/I_0)_b$ and $\ln(I/I_0)_g$ reduced when the amount of crumb rubber content in high-density cement increased as presented in Table 4.1.

Table 4. 1 Gamma ray transmissions of narrow beam and broad beam geometries [27] ($I_{0b}=123863.333$ and $I_{0g} = 125572.667$)

Shielding type	I_b	I_g	$\ln(I/I_0)_b$	$\ln(I/I_0)_g$
HDCR5	22074.6	21427.0	-1.757	-1.768
HDCR10	24161.2	23575.7	-1.635	-1.657
HDCR15	24251.0	23977.0	-1.630	-1.656
HDCR20	24644.0	24508.7	-1.614	-1.634
HDCR25	27386.6	26374.7	-1.509	-1.560

The reason for the downward trends of $\ln(I/I_0)_b$ and $\ln(I/I_0)_g$ with increasing crumb rubber content was because of the reduction of barite quantities in the shielding materials, since Ba in barite is a heavy element with good gamma ray attenuation characteristic.

The samples of high-density cement and high-density cement mixed with various percentages of crumb rubber from 5 to 25% with 5% increment were also studied on the mean free path and the buildup factor. The experimental results are shown in Figs. 4.12, 4.13 and 4.14.

The average distance travelled by photons between any consecutive interactions (scattering or absorption) is called the mean free path parameter or MFP, which is in the other word the relaxation length. The results found that the mean free paths of HDC, HDCR5, HDCR10, HDCR15, HDCR20 and HDCR25 were 7.175, 7.182, 7.592, 7.670, 7.773 and 8.139 centimeters, respectively, as shown in Figure 4.12. The high-density cement without crumb rubber (HDC) had the lowest mean free path value ($\mu=0.1390 \text{ cm}^{-1}$), and the high-density cement mixed with 5 vol% crumb rubber (HDCR5) had the lowest MFP ($\mu=0.1392 \text{ cm}^{-1}$), compared to all other shielding with higher crumb rubber contents. These results indicated that adding more crumb rubber increased the mean free path quite substantially.

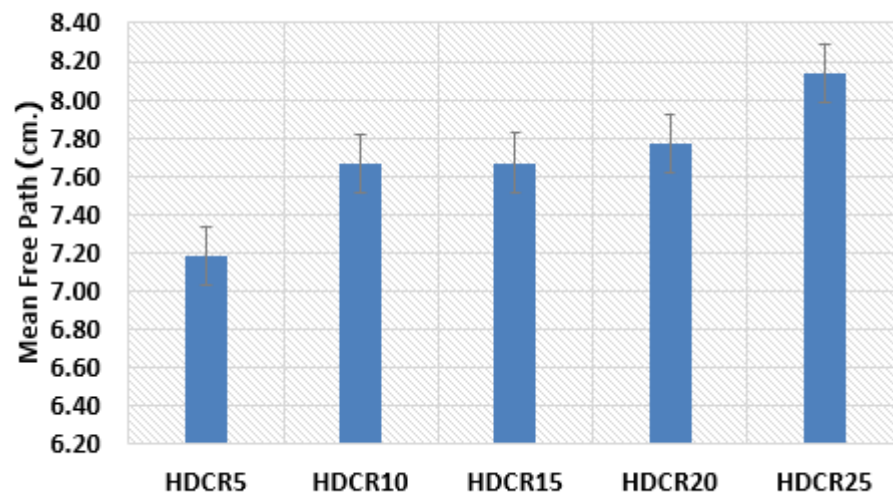
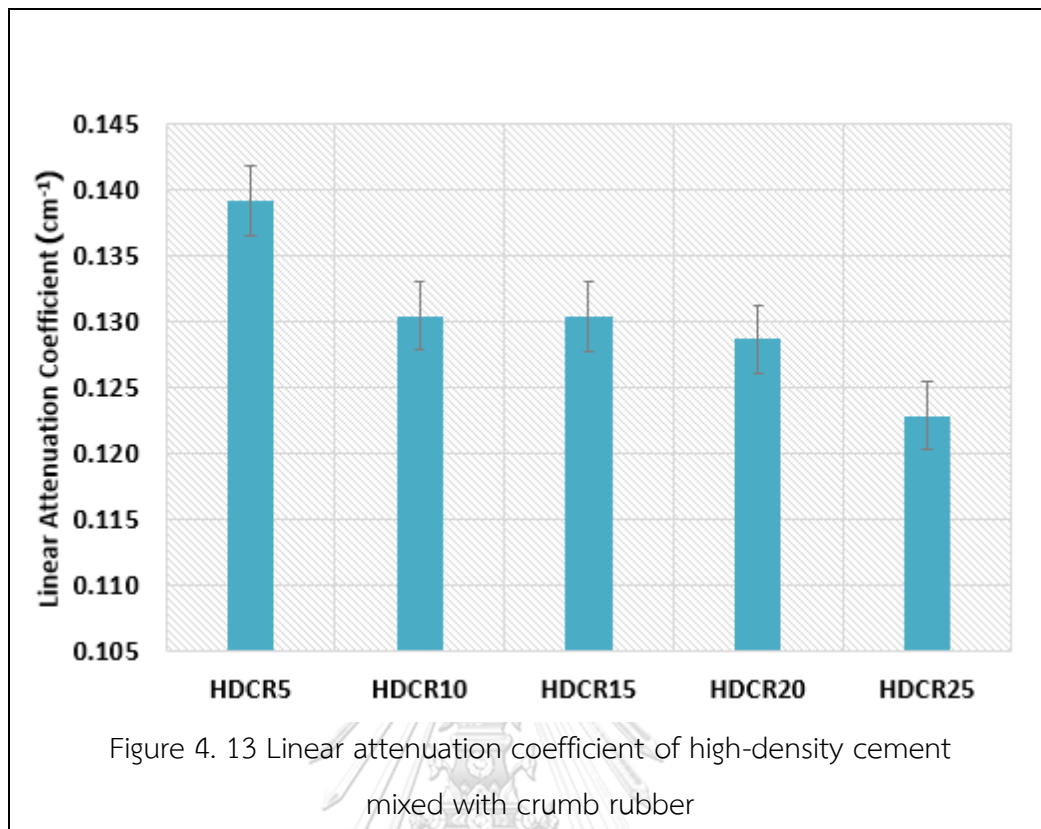


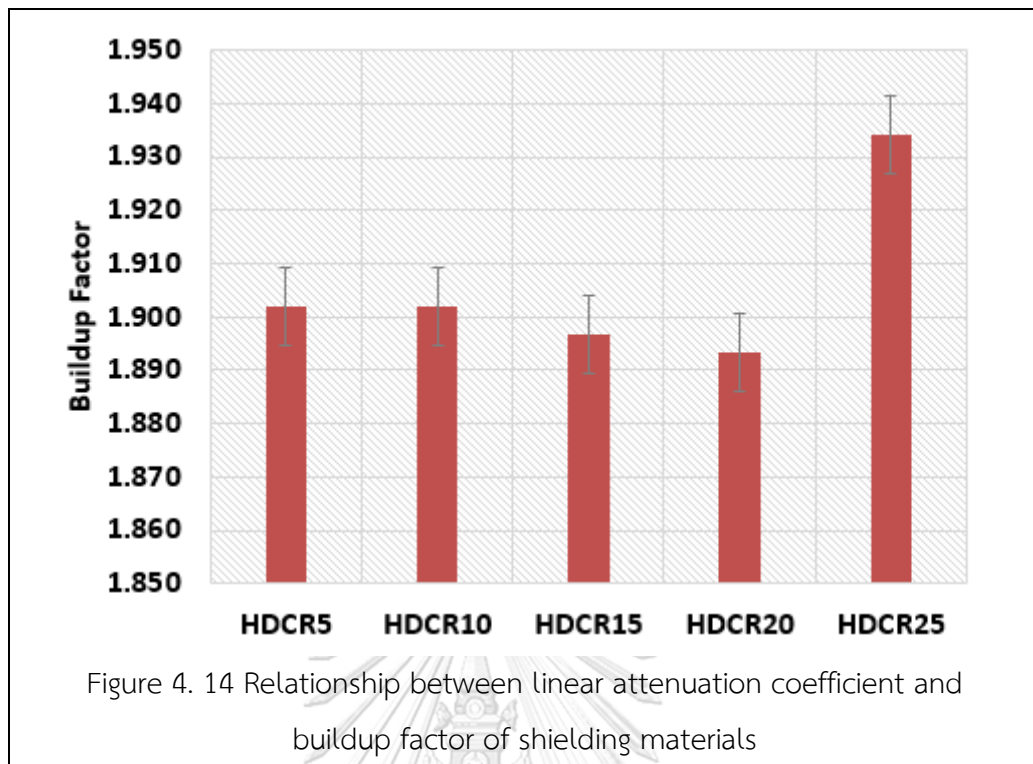
Figure 4. 12 Mean free path of gamma ray after addition of crumb rubber in high density cement

These behaviors can be explained that as the atomic density of rubber is lower than high-density cement (HDC) and as heavy elements in HDC have large scattering cross-sections for gamma rays compared to hydrogen and carbon atoms, the gamma radiation will be able to travel further before undergoing any interaction when adding more crumb rubber (and effectively reducing HDC).

The effect of crumb rubber addition on linear attenuation coefficient is shown in Fig. 4.13.



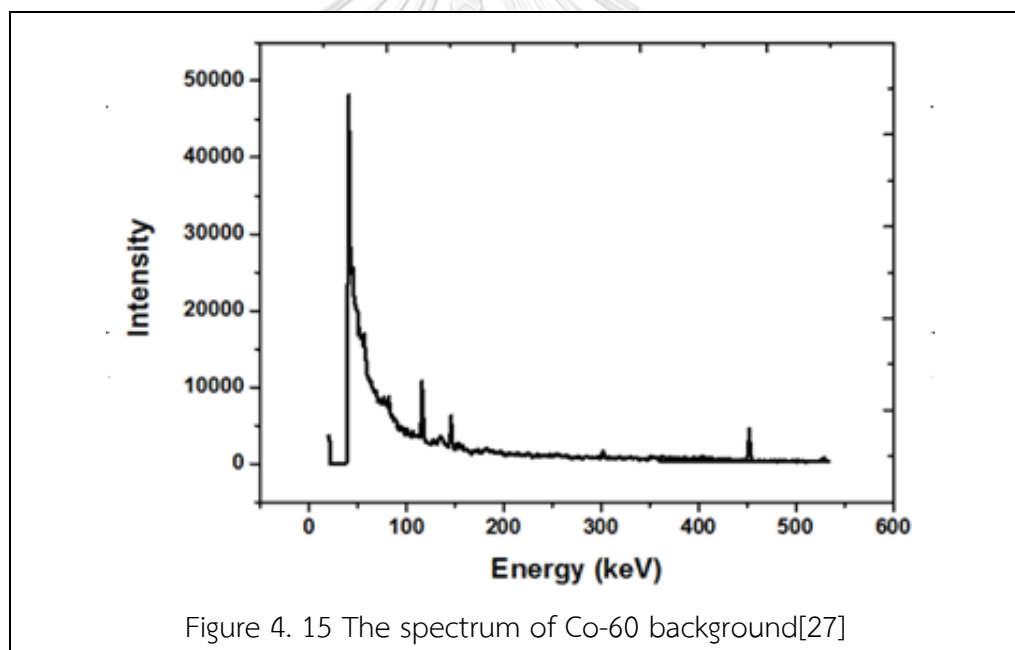
The linear attenuation coefficient is an indicator to describe the effectiveness of shielding material on gamma ray attenuation. The linear attenuation coefficient is also used to calculate the penetration and energy deposition by photons in shielding materials. The shielding materials which were high-density cement without crumb rubber and high-density cement with crumb rubber were evaluated on this parameter. The linear attenuation coefficients of high density cement mixed with 5, 10, 15, 20 and 25 vol% crumb rubber were evaluated to be 0.1392, 0.1304, 0.1303, 0.1286 and 0.1228 cm⁻¹, respectively. The results showed that the value decreased with increasing crumb rubber addition. The increasing crumb rubber percentage influenced the overall Z value and lowered the density of the shielding, resulting in less gamma ray attenuation. With respect to crumb rubber addition, the trend of the linear attenuation coefficient must be the opposite of the mean free path (MFP=1/μ).

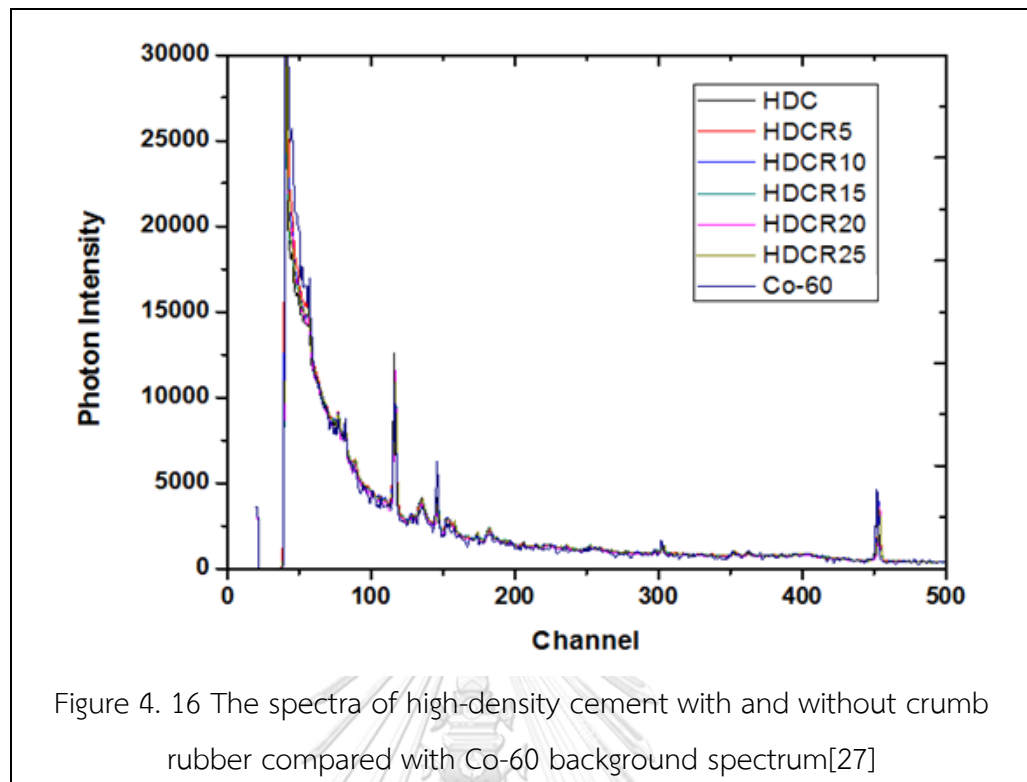


The buildup factors for various samples were obtained from the computation of the $\ln(I/I_0)_b$ and $\ln(I/I_0)_g$ values. The buildup factor experimental results indicated that the values for high-density cement mixed with crumb rubber at 5, 10, 15, 20 and 25 vol% were 1.044, 1.030, 1.025, 1.019 and 1.053, respectively. These values were inversely proportional to the mean free path values. The buildup factor values should normally be unity for the case of a collimate beam of monogenetic photon, and should usually be greater than 1 for all other cases due to gamma ray scattering with shielding materials. The reduction in the buildup factor when the crumb rubber content in high-density cement was up to 20 vol% was a highly advantageous feature since the addition of crumb rubber also reduced the secondary gamma ray and scattered gamma ray emissions. In this research, the evaluated buildup factor values of shielding materials were all close to unity, which can be explained that the secondary gamma ray and scattered gamma ray were not existent.

4.7 Determination of prompt gamma ray and secondary gamma ray of shielding materials

The gamma ray emissions can be released from the interaction between neutrons with shielding materials through neutron capture interaction process which have to be investigated for the radiation safety. The results of the PGNAA studies revealed the gamma ray spectra as shown in Figs. 4.15 and 4.16. The spectrum of Co-60 was used to determine the prompt gamma ray and secondary gamma ray emissions as illustrated in Fig. 4.15. The PGNAA spectra of HDC, HDCR5, HDCR10, HDCR15, HDCR20 and HDCR25 were similar. Comparison of the spectra of high-density cement mixed with crumb rubber and without crumb rubber to that of Co-60 background revealed that they were not different as illustrated in Fig. 4.16.





In conclusion, there were no detectable characteristics of prompt gamma ray and secondary gamma ray emissions from the Prompt Gamma ray Neutron Activation Analysis. This does not mean that there was no neutron capture interaction occurring in the shielding material. This means that the shielding material effectively shielded all of the generated prompt and secondary gamma ray due to the presence of the heavy (barite) and light (carbon and hydrogen) elements.

4.8 Investigation of the cracking mechanism of high-density cement mixed with crumbed rubber and lead particles

To improve the shielding performance of the high-density cement mixed with 5 vol% crumb rubber, lead particles were added at 2, 4, 6 and 8 % by weight. The photon attenuation experiments indicated that the lead particles played an important role to enhance the shielding material performance. However, after the high-density cement mixed with crumb rubber and lead particles were irradiated with gamma radiation and

neutron radiation, they cracked. The cracking problem was investigated to determine the cause.

In first step, the elemental composition of the lead particles was determined by Scanning Electron Microscope with Energy Dispersive Spectroscopy (SEM:EDS). The results found that lead particles consisted of lead element (85.74 wt%), oxygen element (7.84 wt%) and other elements (6.4 wt%) as illustrated in Table 4.2.

Table 4. 2 Weight and atomic percentages of elemental composition of the lead powder based on EDS analysis

Element	Weight %	Atomic %
O	7.84	51.26
Sn	2.88	2.52
Sb	3.52	3.02
Pb	85.74	43.18

4.8.1 Lead adhesion result

In order to study the adhesion between lead particles and high-density cement, the lead adhesion testing was conducted. The result of the experiment indicated a poor adhesion between lead particles and high-density cement mixed with 5 wt% crumb rubber as shown in Fig. 4.17. The poor mechanical interface was the underlying mechanism of the cracking problem. With the poor interface, lead particles behave similar to air pockets. When neutron radiation and gamma radiation interacted with materials, stresses were generated. Cracks would predominantly occur and expand in those weak areas containing lead particles with poor adhesion to concrete.



Figure 4. 17 After removal of lead powder from surface of dried shielding

In order to prevent the cracking problem with the existence of lead particles, surface properties of each particle must be improved to allow it to bond strongly with high-density cement. Improvements can include coating lead particles with an appropriate substance.

4.8.2 Analysis of elemental composition of high-density cement mixed with 5 vol% crumb rubber and various percentages of lead particles

The two techniques, SEM:EDS and XRD, were utilized to analyse the elemental composition of high-density cement mixed with crumb rubber and 0, 2, 4, 6 and 8% of lead particles.

4.8.2.1 Scanning Electron Microscopy and Electron Dispersive Microscopy results

SEM:EDS is capable of providing high magnification and high resolution imaging of samples at 5,000X magnifications. Fig. 4.18 displays the micrograph of high-density cement's microstructure.

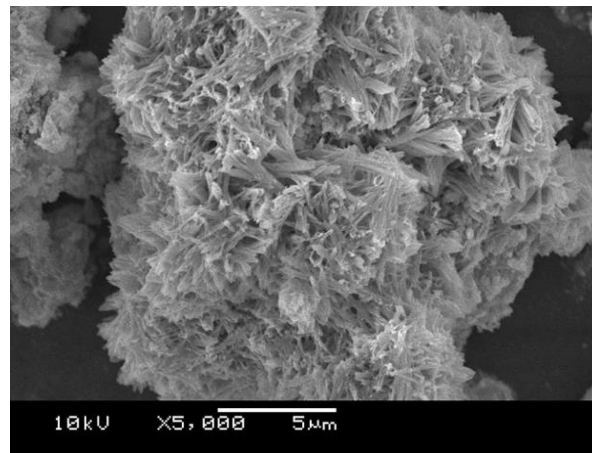


Figure 4. 18 SEM micrograph of high-density cement with 5,000x magnification

Figures 4.19 - 4.23 display micrographs of high-density cement mixed with various percentages of crumb rubber. Different microstructures can be observed. The microstructure of HDC exhibited the somewhat porous and needle-like structures. These microstructural features disappeared with varying degrees with crumb rubber addition. HDCR microstructures appeared to be less porous than HDC.

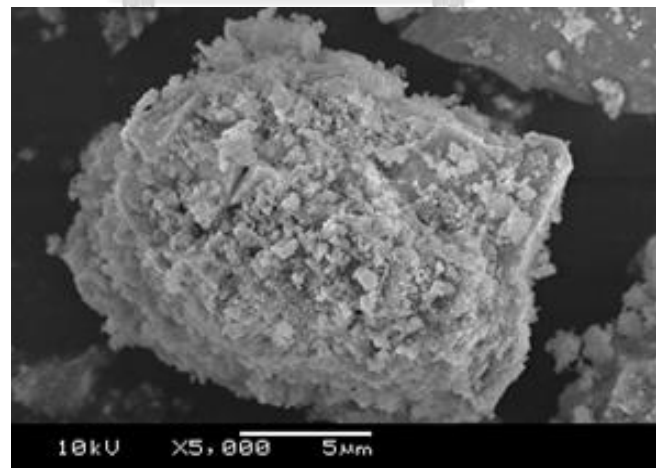


Figure 4. 19 SEM micrograph of high-density cement mixed with 5 vol% crumb rubber at 5,000x magnification

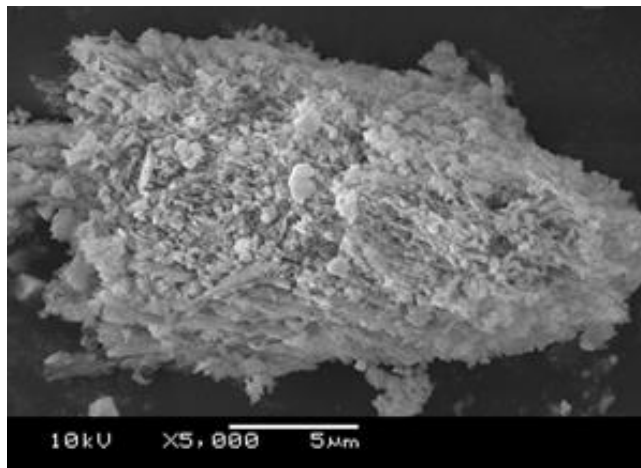


Figure 4. 20 SEM micrograph of high-density cement mixed with 10 vol% crumb rubber at 5,000x magnification

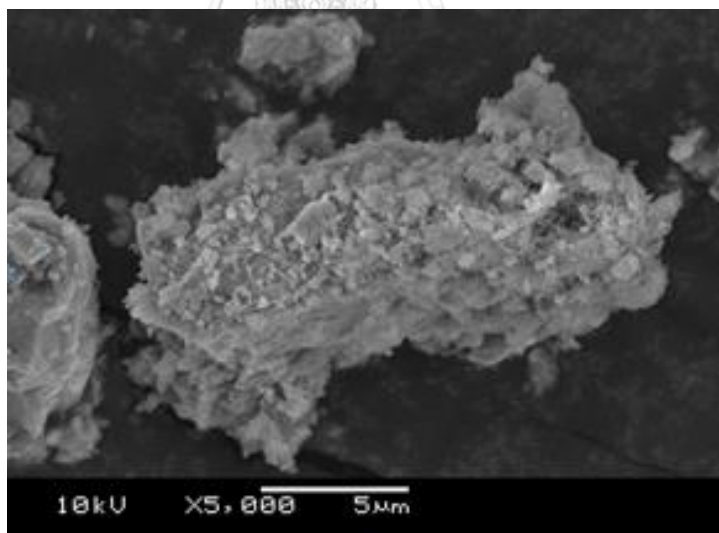


Figure 4. 21 SEM micrograph of high-density cement mixed with 15 vol% crumb rubber at 5,000x magnification

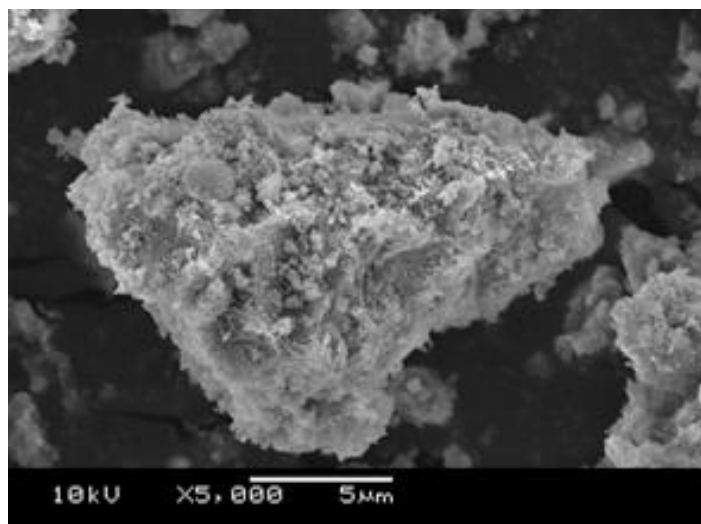


Figure 4. 22 SEM micrograph of high-density cement mixed with 20 vol% crumb rubber at 5,000x magnification

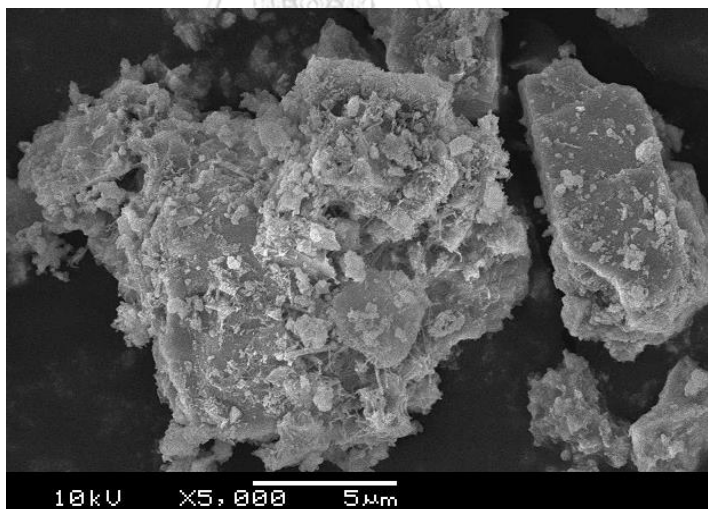
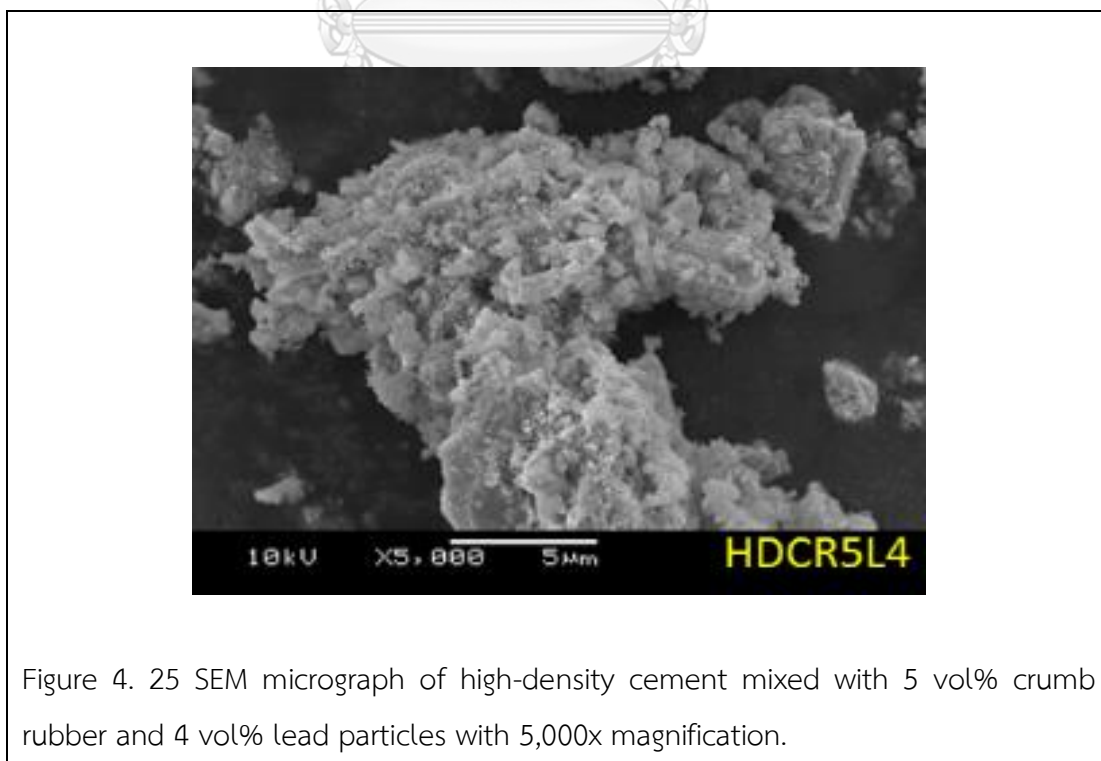
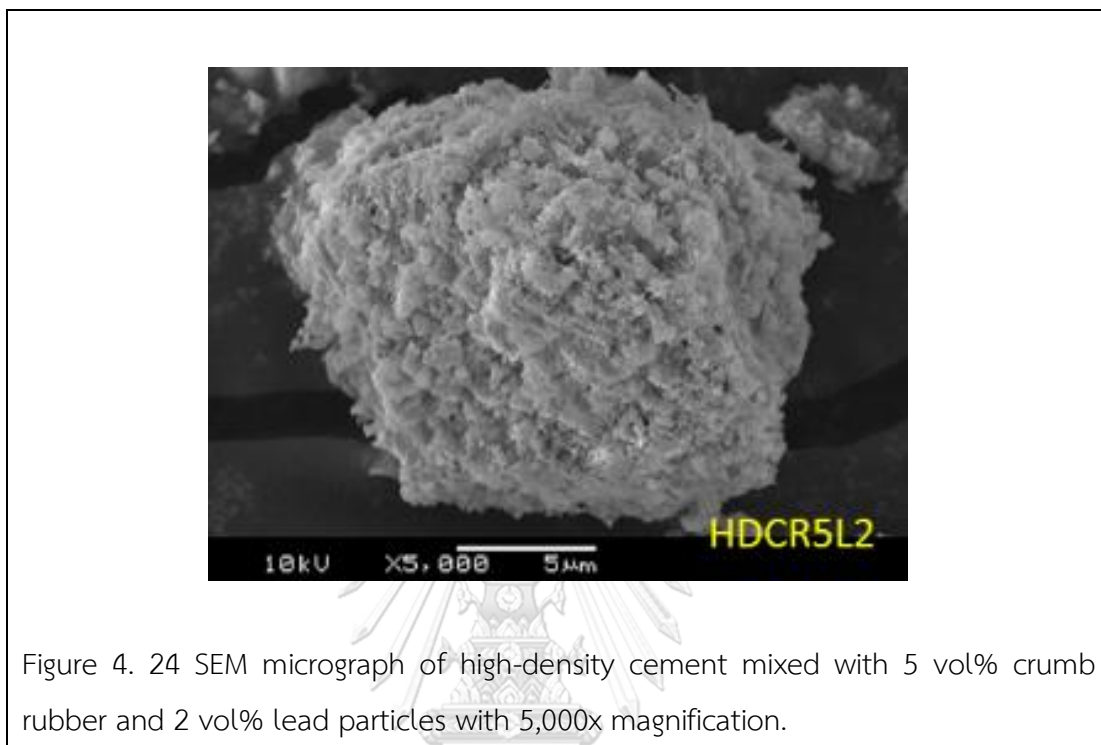


Figure 4. 23 SEM micrograph of high-density cement mixed with 25 vol% crumb rubber at 5,000x magnification

The microstructure images of high-density cement mixed with 5 vol% crumb rubber and lead powder from 2 to 8% with 2% increments are shown in Figures 4.24 - 4.28.

The lead addition resulted in noticeable changes in morphological characteristics. HDCR5Lx appeared to be more tightly packed than HDCRx.



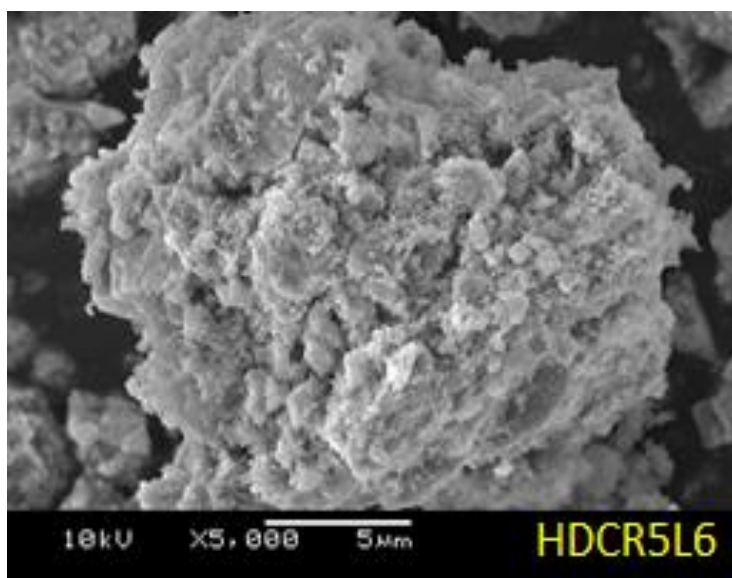


Figure 4. 26 SEM micrograph of high-density cement mixed with 5 vol% crumb rubber and 6 vol% lead particles with 5,000x magnification.

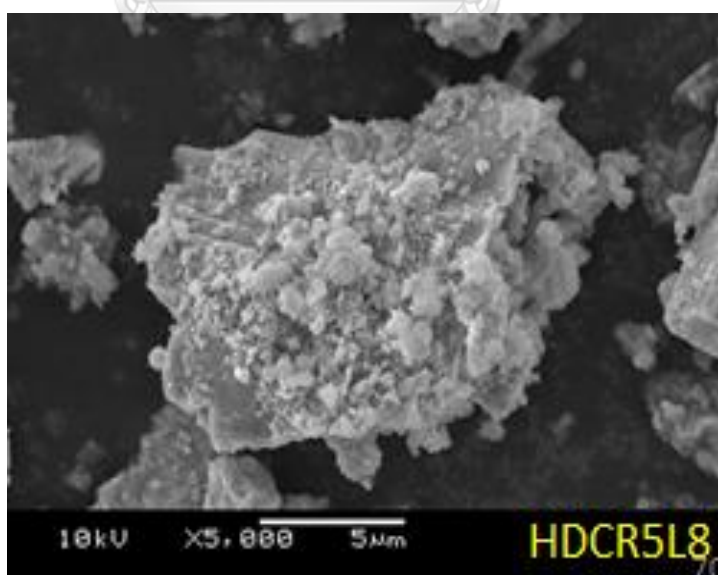


Figure 4. 27 SEM micrograph of high-density cement mixed with 5 vol% crumb rubber and 8 vol% lead particles with 5,000x magnification.

The EDS technique was utilized to investigate the elemental composition of high-density cement mixed with 5 vol% crumb rubber and 8 vol% lead particles. The results revealed that the sample composed of barium, oxygen, sulphur, carbon, nitrogen, lead, calcium, silicon and aluminum with following weight percentages: 35.69, 34.08, 9.27, 6.7, 5.41, 4.31, 2.75, 1.33 and 0.45%, respectively as illustrated in Table 4.3.

Table 4. 3 Weight percentages of elemental composition of HDCR25 and HDCR5L8 based on EDS analysis

Element	Weight %	
	HDCR25	HDCR5L8
C	4.86	6.70
N	4.64	5.41
O	15.00	34.08
Al	0.25	0.45
Si	0.21	1.33
S	10.87	9.27
Ca	1.54	2.75
Ba	62.64	35.69
Pb	-	4.31

The EDS results confirmed the presence of the added lead particles; however, the analyzed quantity of 4.31 wt% was lower than 5 wt%. This may indicate the inherent uncertainty in the analysis, or the analyzed small piece of sample obtained from the large piece of fabricated shielding material may have minor component inhomogeneity. The EDS spectrum of this sample is shown in Figs. 4.28 and 4.29.

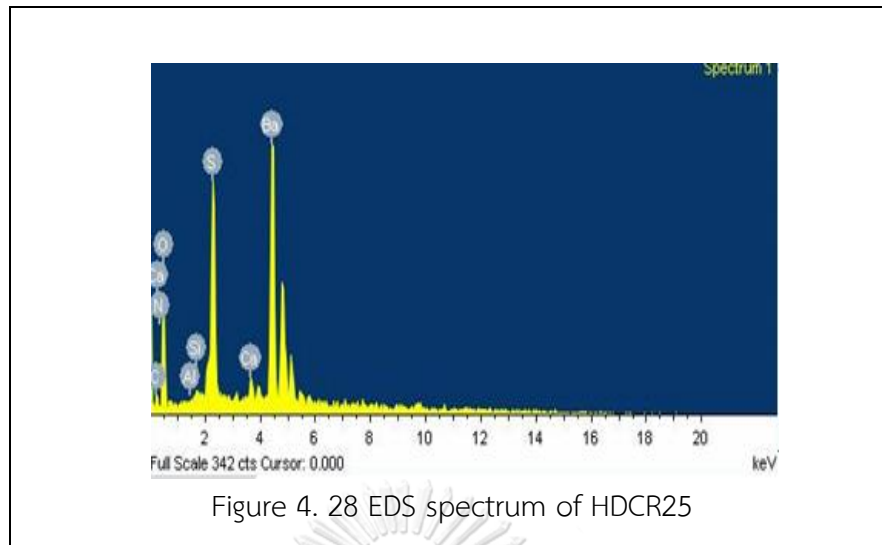


Figure 4. 28 EDS spectrum of HDCR25

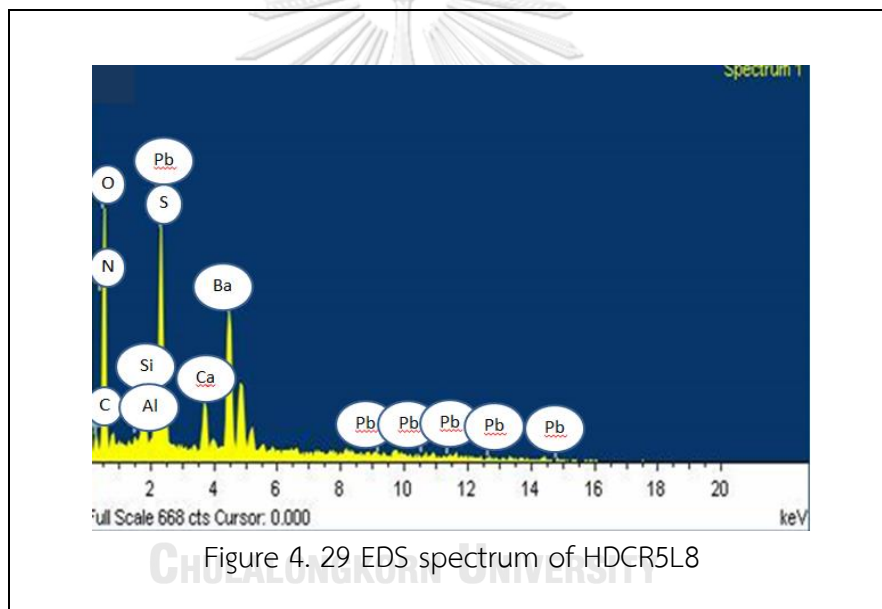


Figure 4. 29 EDS spectrum of HDCR5L8

4.2) X-ray Diffraction Technique

The X-ray diffraction results can characterize and identify crystalline phases, which are unique for each particular phase pattern and can be utilized to identify the substance. This technique was utilized to examine the cause of cracking of high-density cement mixed with crumb rubber and lead particles. Although the addition of lead particles can improve the gamma attenuation performance, the cracking problems rendered it quite unsuitable for actual applications in radiation working areas. Thus, the

investigation of HDCR5, HDCR5L2, HDCR5L4, HDCR5L6 and HDCR5L8 were carried out to determine the cause of the cracking as shown in Figs. 4.30 and 4.31.

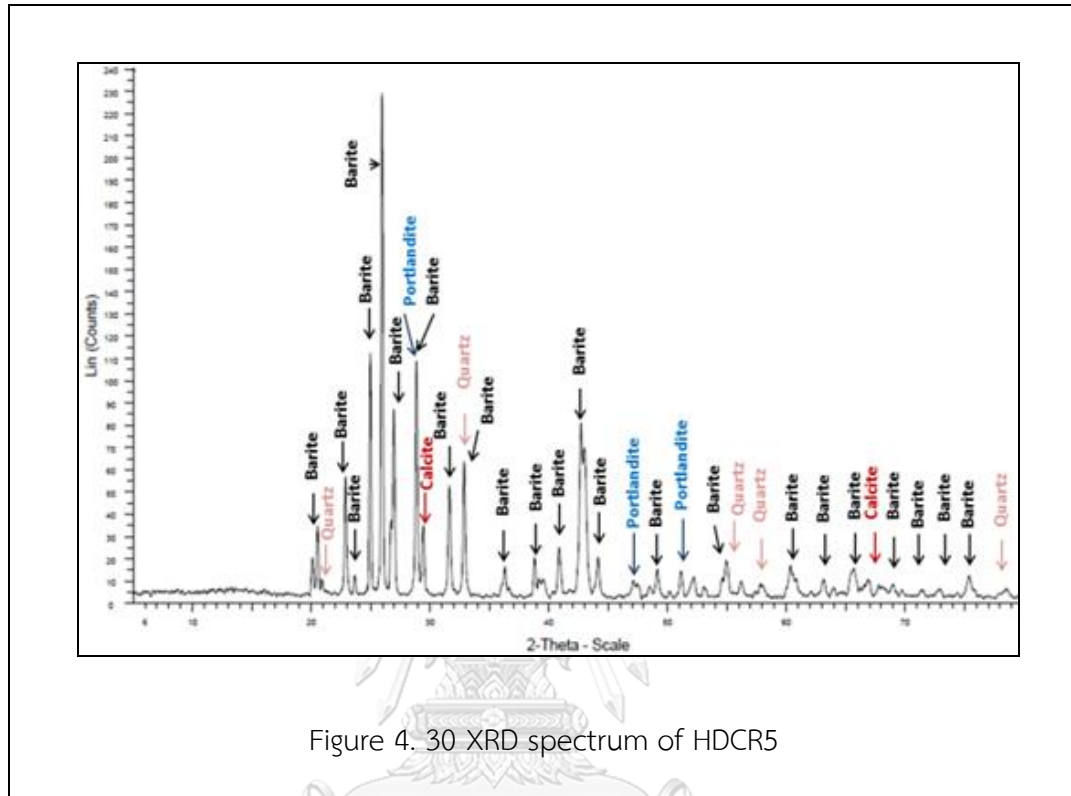


Figure 4. 30 XRD spectrum of HDCR5

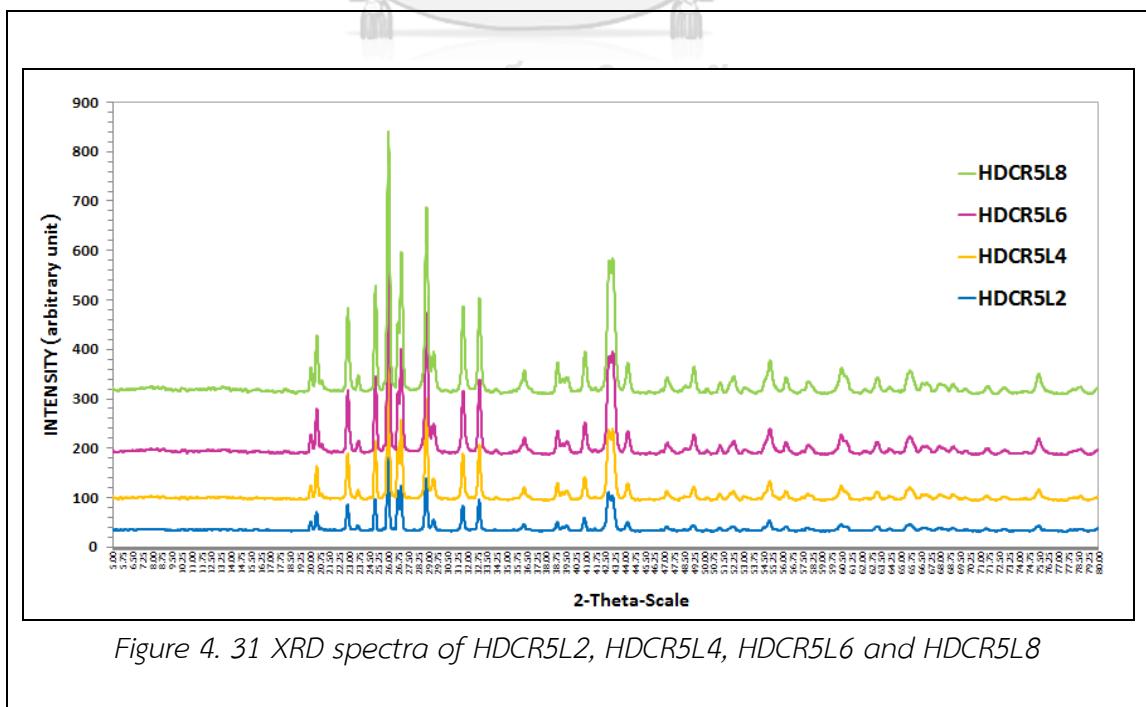


Figure 4. 31 XRD spectra of HDCR5L2, HDCR5L4, HDCR5L6 and HDCR5L8

The crystalline phases identified from the XRD technique indicated that HDCR5 consisted of barite (BaSO_4), portlandite [$\text{Ca}(\text{OH})_2$], quartz (SiO_2) and calcite (CaCO_3), which has the crystal structures of orthorhombic, hexagonal, cubic and rhombohedral, respectively. The analysed quantity of each phase is shown in Table 4.4.

For HDCR5L8, the crystalline phases were identified by the XRD technique and results were listed in Table 4.5. The results indicated that HDCR5L8 consisted of barite, portlandite, quartz, calcite, PbO_2 and Pb crystalline phases. As expected, the added lead powder in high-density cement resulted in the presence of PbO_2 and Pb.

Table 4. 4 Quantitative estimate of weight percentages of the mineral phases in HDCR5 and HDCR5L8 samples based on XRD analysis

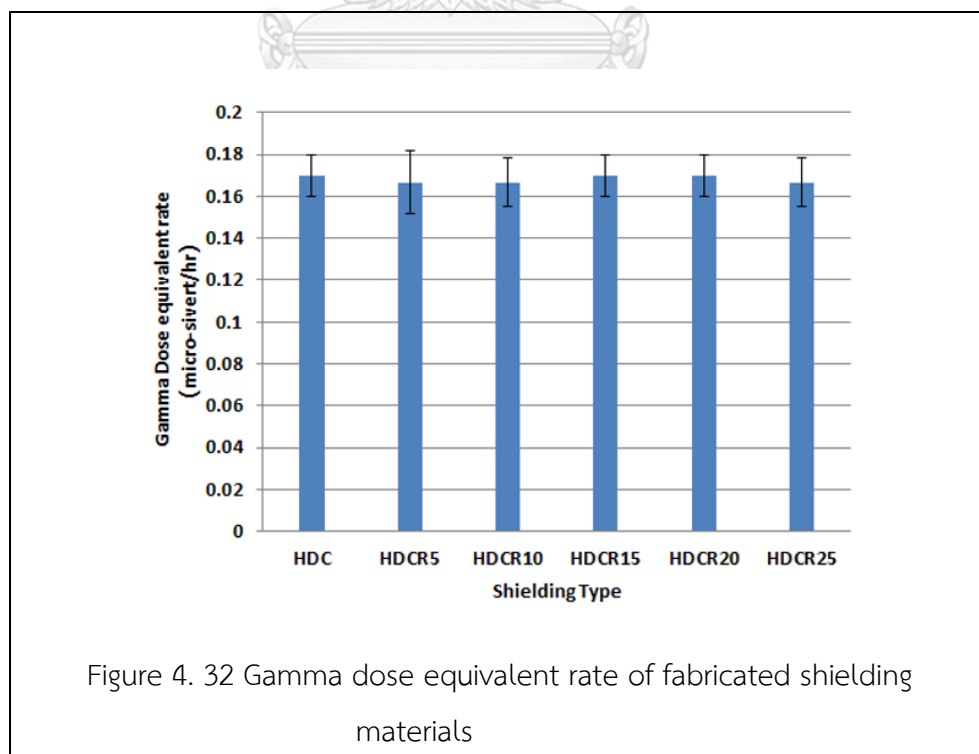
Phase	Chemical Formula	Quantity (wt%)	
		HDCR5	HDCR5L8
Barite	BaSO_4	75.029	72.769
Portlandite	$\text{Ca}(\text{OH})_2$	0.146	1.198
Quartz	SiO_2	8.343	5.240
Calcite	CaCO_3	16.482	20.558
Lead Oxide	PbO_2	-	0.108
Lead	Pb	-	0.128

The HDCR5L8 analysis results revealed approximately 0.24 wt% of Pb and PbO_2 , confirming the addition of lead particles. The inconsistency between the analyzed results and the added quantity of 5 wt% may be attributed to the uncertainty in the analysis. For example, the portlandite phase was analyzed to be 10 times more abundant in HDCR5L8 than in HDCR5. Moreover, certain amount of lead particles in a fine powder form might remain at the bottom of the crushed sample during the XRD analysis because of lead's higher density than high-density cement. These particles at the bottom may not be detected by the XRD technique.

Although the discrepancy between the analysed EDS and XRD results and the expected result occurred, both analytical techniques confirmed the presence of the added lead powder and the expected phases.

4.4 Dose rate evaluation

The shielding materials which were HDCR5, HDCR10, HDCR15, HDCR20 and HDCR25 were evaluated on the dose rates of transmitted gamma radiation and neutron radiation as shown in Fig. 4.32. The results found that the gamma dose equivalent rate of these materials were at most 0.51 micro-Sievert per hour, and that the photon dose rates of shielding materials composing of high-density cement mixed with crumb rubber were about the same compared with high-density cement, taking into account the standard deviation of the measurement. Crumb rubber in high-density cement had no effect on photon dose rate because carbon and hydrogen atoms could not effectively attenuate gamma radiation. Moreover, the replacement of crumb rubber in high-density cement resulted in the lowered density of HDCR, reducing its ability to attenuate gamma radiation.



For the neutron dose rate evaluation, the results revealed that neutron dose rates of HDC, HDCR5, HDCR10, HDCR15, HDCR20 and HDCR25 were not detectable with the neutron dose rate detector MGP Model HDS101 G/GN with the unit of count per second. Switching to the neutron detector NT-35-03 with the unit of micro-Sivert per hour could not detect the neutron dose rate either as illustrated in Fig. 4.33.

The cause of no detectable neutron dose rate may be due to the very low activity of the neutron source for the detectors to detect the transmitted radiation, as well as the low sensitivity of the neutron dose rate detectors.



4.5 Mechanical property of shielding materials by Compressive Testing Machine (CTM)

The compressive strengths of cubical specimens fabricated from high-density cement mixed with crumb rubber were determined after 28 days of curing time and the results are shown in Table 4.5. The results revealed that the average compressive strength of high-density cement was 15.03 N/mm^2 , and that the average compressive strength decreased with increasing crumb rubber content[27].

Table 4. 5 Compressive strengths of different types of shielding materials[27]

Shielding type	Crushing load (kN)			Compressive strength (N/mm ²)			Avg. Compressive strength (N/mm ²)
	1	2	3	1	2	3	
HDC	199.8	297.9	245.6	12.063	18.312	14.725	15.03
HDCR5	139.8	151.6	158.1	9.9770	9.7430	9.6790	9.80
HDCR10	142.5	169.7	174.9	8.3610	10.087	10.610	9.69
HDCR15	183.0	124.6	166.7	11.022	7.4120	9.9710	9.47
HDCR20	129.4	165.5	144.0	7.8980	10.001	8.6930	8.86
HDCR25	104.5	114.7	111.0	6.4330	6.9730	6.7910	6.73

The average compressive strengths of high-density cement mixed with crumb rubber at 5, 10, 15, 20 and 25 vol% were 9.80, 9.69, 9.47, 8.86 and 6.73 N/mm², respectively. These results were expected because the compressive strength of crumb rubber was much lower than that of high-density cement. With the presence of crumb rubber, the high-density cement mixed with 5 vol% crumb rubber exhibited the maximum average compressive strength[27]. Even though the average compressive strength of high-density cement materials was not as strong as expected due to the very fine size of barite (40 mesh or 420 microns), the database of mechanical property of this type of material can be utilized in other engineering applications in the further.

4.6 Economic data

The raw material costs of the shielding material composing of high-density cement mixed with crumb rubber were evaluated as shown in Table 4.6. However, the costs of the chemical additives, transportation, material testing and equipment were not included in the Table 4.6.

Table 4.6: Estimated cost of high-density cement mixed with crumb rubber

No.	Item	Cost (Bath)	Quantity of Shielding	Cost (Bath/shielding)
1	Mold	3700	15	246.67
2	Rubber	4000	40	100.00
3	Cement	2500	40	62.50
4	Barite	5000	40	125.00
Total cost				534.17

Table 4.6 showed the economic data of the shielding materials to be cost effective. These basic data can be applied to fabricate this type of radiation shielding materials for future uses.



CHAPTER VI

CONCLUSIONS

5.1 Conclusions of research

The shielding materials composing of high density cement mixed with crumb rubber had been designed to attenuate neutron and gamma radiation, especially the radiation that occurred from the photonuclear reaction in the particle accelerator. Different percentages of cement, crumb rubber and chemical additives influenced the neutron and gamma ray attenuation characteristics of the materials.

The addition of crumb rubber in high-density cement enhanced the performance of neutron shielding. The crumb rubber contains the large number of carbon and hydrogen light elements which are the effective materials to shield neutrons. In this research study, high-density cement mixed with 25 vol% crumb rubber exhibited the best performance to attenuate neutron radiation. This is because the collisions between neutrons and light atomic nuclides which are carbon and hydrogen atoms effectively slow down fast neutrons while the barium heavy elements constitutes to the moderation of fast neutrons into thermal neutrons. However, the inclusion of crumb rubber in high-density cement reduced the gamma radiation shielding capability, and the MCNP simulation results indicated that the transmitted photon flux of high-density cement mixed with 5 vol% crumb rubber was the lowest of all the samples.

The radiation attenuation experiments were performed to verify the performances of shielding materials. The addition of crumb rubber enhanced the neutron shielding efficiency; however, the quantity of crumb rubber greater than 5 vol% resulted in the decrease in the neutron shielding efficiency because of the reduction in barite composition in high-density cement. Moreover, water absorption in crumb rubber caused the shielding material to swell during fabrication, and some part

of crumb rubber could not be contained in the mold and a certain amount of carbon and hydrogen atoms were lost.

The high-density cement mixed with crumb rubber at 5 vol% was selected for additional studies to improve the photon and neutron shielding and to maintain the mechanical properties. Lead and boron carbide were selected as additives to high-density cement mixed with 5 vol% crumb rubber (HDCR5). Lead, which exhibits an excellent gamma attenuation characteristic, was mixed with HDCR5 with various percentages from 2 to 8% with 2% increment (HDCR5L2, HDCR5L4, HDCR5L6 and HDCR5L8). The addition of lead to HDCR5 improved the neutron and gamma ray attenuations especially the high-energy gamma ray. For boron carbide, with its excellent thermal neutron absorption, it was added to HDCR5 and was found to reduce the thermal neutron transmission. Barite and boron constituted to the moderation of fast neutrons into thermal neutrons to be captured by boron, as well as to provide the inelastic scattering process to attenuate gamma radiation.

However, high-density cement mixed with 5 vol% crumb rubber and more than 4 vol% lead powder experienced cracking problem under neutron and gamma radiation. The cause of cracking was investigated. The XRD spectra indicated that the addition of lead powder resulted in formation of portlandite and calcite phases. Moreover, the lead adhesion test result showed that the adhesion between lead and high-density cement was very poor, causing each lead particle to behave as an “air pocket” in high-density cement. These presented weak areas, resulting in generation and propagation of cracks. Surface properties of each lead particle must be improved to allow it to bond strongly with high-density cement. Improvements can include coating lead particles with an appropriate agent.

Gamma radiation can be emitted as a result of gamma and neutron interactions with matters. For gamma radiation, when gamma ray interacts with shielding materials, gamma radiation can be released from the Compton scattering process. This process was investigated for radiation safety design by studying the buildup factor parameter. The study revealed that the buildup factor values were close to unity, indicating that

the scattered gamma ray and secondary gamma ray were not present or were completely absorbed by the shielding materials, which confirmed that this shielding materials can be applied in the nuclear and radiation applications.

For neutron interactions, the neutron capture process can result in emission of prompt gamma ray and secondary gamma ray. These gamma ray emissions from the shielding materials were investigated using the prompt gamma neutron activation analysis (PGNAA). The PGNAA results indicated that the emission spectra of HDCR5, HDCR10, HDCR15, HDCR20 and HDCR25 were similar when compared to the Co-60 background spectrum. Although some neutron capture processes must have occurred inside the shielding materials, the heavy element (barite) and light elements (carbon and hydrogen) helped to absorb the prompt gamma ray and secondary gamma ray. These results confirmed the safety of the high-density cement mixed with crumb rubber which can be utilized as neutron and gamma ray shielding materials.

The compressive strength test was performed to evaluate the strength of shielding materials. It was found that the average compressive strength of shielding materials became lower with increasing crumb rubber addition. With the presence of crumb rubber, the high-density cement mixed with 5 wt% crumb rubber exhibited the maximum average compressive strength.

In conclusion, the new recycling method of waste rubber for radiation shielding purposes was presented to offer a new class of neutron and gamma radiation shielding material. This shielding material can be applied in nuclear science and engineering applications. This research study not only helps decrease environmental problems, but also magnifies the radiation safety in nuclear, radiation and other related works.

5.2 Recommendations for future research

The following recommendations are offered for future research on this topic.

1. In order to fulfill the evaluation of the shielding material capabilities, the lifetime of the shielding materials under neutron fluence should be evaluated.
2. The water absorption of crumb rubber should be studied to improve the effective material proportion of high-density cement mixed with crumb rubber.
3. The effect of barite and crumb rubber aggregate size should be studied to improve the neutron and gamma attenuation ability.





จุฬาลงกรณ์มหาวิทยาลัย
CHULALONGKORN UNIVERSITY



จุฬาลงกรณ์มหาวิทยาลัย
CHULALONGKORN UNIVERSITY

REFERENCES

1. Y. Kawashima, *PROPOSAL OF A SYNCHROTRON RADIATION FACILITY TO SUPPLY ULTRAVIOLET LIGHT, X-RAY, MeV-PHOTON, GeV-PHOTON AND NEUTRON*. Proceedings of FLS 2006, 2006: p. 24-26.
2. KL, V., et al., *EFFECT OF NATURAL RUBBER LATEX ON NORMAL AND HIGH STRENGTH CONCRETE*. INTERNATIONAL JOURNAL OF ADVANCE RESEARCH IN SCIENCE AND ENGINEERING, 2014. **3**(9): p. 12.
3. Grinys, A. and H. Sivilevicius, *Tyre Rubber Additive Effect on Concrete Mixture Strength*. Journal of Civil Engineering and Management, 2012 **Volume 18**(3): p. 393-401.
4. Lamarsh, J.R. and A.J. Baratta, *Introduction to Nuclear Engineering*. Third ed. 2014.
5. Lylia Hamidatou, et al., *Concepts, Instrumentation and Techniques of Neutron Activation Analysis* 2013, Intech.
6. *Neutron cross section*. Available from: <http://www.nuclear-power.net/neutron-cross-section/>.
7. *Development of an ultra-fast X-ray camera using hybrid pixel detectors*. 2011. [online] Available at: <http://Development of an ultra-fast X-ray camera using hybrid pixel detectors>. [Accessed 2 May 2017].
8. Library.sciencemadness.org. (2017). *Cite a Website - Cite This For Me*. [online] Available at: http://library.sciencemadness.org/lanl1_a/lib-www/la-pubs/00326397.pdf [Accessed 2 May 2017].
9. *INTERACTIONS OF GAMMAS*. 2016 1/29/99 [cited 2016 15 November]; Available from: http://www.hep.wisc.edu/~prepost/407/gamma/gamma_html.html.
10. McAlister, D.R., *Gamma Ray Attenuation Properties of Common Shielding Materials*. p. 14.
11. Yilmaz, E., et al., *Gamma ray and neutron shielding properties of some concrete materials*. 2011, ELSEVIER: ScienceDirect. p. 2204-2212.

12. Booth, T.E., et al., *A General Monte Carlo N-Particle Transport Code, Version 5*. 2005, The U.S. Department of Energy, National Nuclear Security Administration. Los Alamos National Security. p. 1-508.
13. Shultis, J.K. and R.E. Faw, *An MCNP Primer*. 2011.
14. Compuhigh.com. (2017). *Lesson01: Principles of Science*. [online] Available at: <http://www.compuhigh.com/demo/physsscilesson01.htm> [Accessed 2 May 2017].
15. Azam, A. *Hydration of Concrete and also define the Heat of Hydration* 2016 [cited 2016 15 October]; Available from: <http://megacivilengineering.blogspot.com/2013/09/hydration-of-concrete-and-also-define.html>.
16. Naseer, M.H. *CEMENT*. 2015 [cited 2016 15 October]; Available from: <http://petrotan.com/cement>.
17. Ayub, T., S.U. Khan, and F. AhmedMemon, *Mechanical Characteristics of Hardened Concrete with Different Mineral Admixtures: A Review*. The Scientific World Journal 2014. **Volume 2014**, (Article ID 875082): p., 15 pages.
18. Corrosionpedia. (2017). *What is Compressive Strength? - Definition from Corrosionpedia*. [online] Available at: <https://www.corrosionpedia.com/definition/1620/compressive-strength-material-science> [Accessed 2 May. 2017].
19. Corrosionpedia. (2017). *What is Tensile Strength? - Definition from Corrosionpedia*. [online] Available at: <https://www.corrosionpedia.com/definition/1072/flexural-strength> [Accessed 2 May. 2017].
20. Corrosionpedia. (2017). *What is Flexural Strength? - Definition from Corrosionpedia*. [online] Available at: <https://www.corrosionpedia.com/definition/5061/flexural-strength> [Accessed 2 May 2017].
21. Corrosionpedia. (2017). *What is Elastic Deformation? - Definition from Corrosionpedia*. [online] Available at:

<https://www.corrosionpedia.com/definition/2104/elastic-deformation>
[Accessed 2 May 2017].

22. Suparat, T., *Waste Tyre Management in Thailand: A Material Flow Analysis Approach*, in *School of Environment*. 2013, Asian Institute of Technology. p. 157.
23. Hird, A.B., P.J. Griffiths, and R.A. Smith, *Tyre waste and resources management: A mass balance approach*. 2002.
24. Banerjee, S., R. Yang, and C.E. Courchene, *Scanning Electron Microscopy Measurements of the Surface Roughness of Paper*. *Ind. Eng. Chem. Res.*, 2009. **Vol. 48**(No.9): p. 3.
25. *Introduction to Energy Dispersive X-ray Spectrometry (EDS)*. Available from: <http://cfamm.ucr.edu/documents/eds-intro.pdf>.
26. Aim-O, P., et al., *Monte carlo simulation of innovative neutron and photon shielding material composing of high density concrete, waste rubber, lead and boron carbide*. *Journal of Physics: Conf. Series* 860 (2017) 012043, 2017.
27. Aim-O, P., et al., *Buildup factor and mechanical properties of high-density cement mixed with crumb rubber and prompt gamma ray study*. *IOP Conf. Series: Materials Science and Engineering* 2017. **244** (012023): p. 8.
28. Wang, X.-Y. and K.-B. Park, *Analysis of compressive strength development of concrete containing high volume fly ash*. *Construction and Building Materials* 98 (2015) 2015: p. 810–819.
29. AHMED, B. and M. RAHMAN, *Assessment of Compressive Strength of Concrete Based On Combination of Different Sizes of Aggregate*. *International Journal of Advanced Structures and Geotechnical Engineering*, July 2015. **Vol. 04**(No. 03).
30. Google.co.th. (2017). *Technology, M.I.o., Principles of Radiation Interactions - Google Search*. [online] Available at: <https://www.google.co.th/search?q=Technology,+M.I.o.,+Principles+of+Radiation+Interactions&dcr=0&tbm=isch&tbo=u&source=univ&sa=X&ved=0ahUKEwihr7ifzuvXAhVETrwKHRTkAbwQ7AkIOg&biw=1366&bih=623> [Accessed 2 May 2017].



จุฬาลงกรณ์มหาวิทยาลัย
CHULALONGKORN UNIVERSITY



จุฬาลงกรณ์มหาวิทยาลัย
CHULALONGKORN UNIVERSITY

APPENDIX A

Neutron Flux to Dose Rate Conversion Factor NCRP38

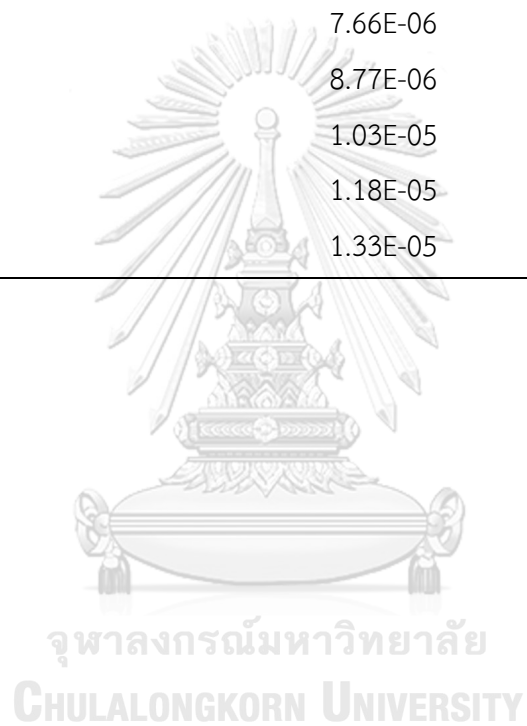
Energy,E (MeV)	DF(E) (rem/hr)/(n/cm ² -s)
2.5E-08	3.67E-06
1.0E-07	3.67E-06
1.0E-06	4.46E-06
1.0E-05	4.54E-06
1.0E-04	4.18E-06
1.0E-03	3.76E-06
1.0E-02	3.56E-06
1.0E-01	2.17E-05
5.0E-01	9.26E-05
1.0	1.32E-04
2.0	-
2.5	1.25E-04
5.0	1.56E-04
7.0	1.47E-04
10.0	1.47E-04
14.0	2.08E-04
20.0	2.27E-04

Photon Flux to Dose Rate Conversion Factors ANSI/ANS-6.1.1-1977

Energy,E(MeV)	DF(E) (rem/hr)/(p/cm ² -s)
0.01	3.96E-06
0.03	5.82E-07
0.05	2.90E-07
0.07	2.58E-07
0.1	2.83E-07
0.15	3.79E-07
0.2	5.01E-07
0.25	6.31E-07
0.3	7.59E-07
0.35	8.78E-07
0.4	9.85E-07
0.45	1.08E-06
0.5	1.17E-06
0.55	1.27E-06
0.6	1.36E-06
0.65	1.44E-06
0.7	1.52E-06
0.8	1.68E-06
1	1.98E-06
1.4	2.51E-06
1.8	2.99E-06
2.2	3.42E-06
2.6	3.82E-06
2.8	4.01E-06
3.25	4.41E-06
3.75	4.83E-06
4.25	5.23E-06
4.75	5.60E-06
5	5.80E-06

Photon Flux to Dose Rate Conversion Factors ANSI/ANS-6.1.1-
1977111(Continued)

Energy,E(MeV)	DF(E) (rem/hr)/(p/cm ² -s)
5.25	6.01E-06
5.75	6.37E-06
6.25	6.74E-06
6.75	7.11E-06
7.5	7.66E-06
9	8.77E-06
11	1.03E-05
13	1.18E-05
15	1.33E-05



APPENDIX B

DOSIMETRIC QUANTITIES[30]

Quantity	Definition	New Units	Old Units
Exposure	Charge per unit mass of air $1R = 2.58 \times 10^{-4} \text{ C/kg}$	-	Roentgen (R)
Absorbed dose to tissue T from radiation of type R $D_{T,R}$	Energy of radiation R absorbed per unit mass of tissue T $1 \text{ Gy} = 1 \text{ joule/kg}$ $1 \text{ Gy} = 100 \text{ rads}$	gray (Gy)	Radiation absorbed dose (rad)
Equivalent dose to tissue T, H_T	Sum of contributions of dose to T from different radiation types, each multiplied by the radiation weighting factor (W_R) $H_T = \sum_R W_R D_{T,R}$	Sievert (Sv)	Roentgen equivalent man (rem)
Effective Dose, E	Sum of equivalent doses to organs and tissues exposed, each multiplied by the appropriate tissue weighting factor (W_T) $E = \sum_T W_T H_T$	Sievert (Sv)	Rem

APPENDIX C

EXAMPLE OF MCNP INPUT FILE

1. High-Density Cement mixed Crumb Rubber 5 vo% (Neutron)

c Input File

```
1 0 -1 imp:n=1 imp:p=1 $Ambient
2 2 -2.826 -2 imp:n=1 imp:p=1 $HDCR5
3 3 -0.00125 -3 imp:n=1 imp:p=1 $air
4 3 -0.00125 -4 3 2 1 imp:n=1 imp:p=1 $Ambient
5 0 4 imp:n=0 imp:p=0 $outside the sphere
```

c Surface cards

```
c ##### Define Surfaces #####
1 RPP -8.35 -6.35 -1 1 -1 1 $ source
2 RPP -6.35 6.35 -6.35 6.35 -6.35 6.35 $ shield
3 RPP 6.35 8.89 -6.35 6.35 -6.35 6.35
4 SO 30 $Sphere Ambient
```

c

c Data cards

```
c ##### Define Materials #####
mode n p
```

phys:p

```
m2 6012 -0.040395 1001 -0.004515 8016 -0.00509 & Approximation WR
1001 -0.000965 8016 -0.083858 12000 -0.000322 13027 -0.001126& HDC
14000 -0.002814 16000 -0.029025 20000 -0.013507 26000 -0.012784&
56000 -0.8056
```

```
m3 6000 -0.000124 7014 -0.755268 8016 -0.231781 18000 -0.012827 $air
```

c

```
c ##### Define Source #####
```

c Source Am/Be energy definition. Point source. Isotropic.

```
sdef pos=-7.35 0 0 erg=d1
```

```

si1 h 0 0.5 1 1.5 2 2.5 3 3.5 4 4.5 5 5.5 6 6.5 7 7.5 8 8.5&
    9 9.5 10 10.5 11 11.5 12
sp1 d 0 0.15 0.08 0.09 0.06 0.100 0.15 0.107 0.101 0.11 0.102 0.15&
    0.07 0.12 0.05 0.08 0.10 0.05 0.02 0.03 0.04 0.02 0 0 0
c
c ##### Define Tallies #####
f2:n 2.1 $Tally neutrons on surface 2.1 (Xmax)
e2 0.5e-6 1e-6 0.5e-5 1e-5 0.5e-4 1e-4 0.5e-3 1e-3 &
    0.5e-2 1e-2 0.5e-1 1e-1 0.5 1 5 10 50 100
sd2 161.29
f12:p 2.1 $Tally Photons in cell 3
e12 0.5e-6 1e-6 0.5e-5 1e-5 0.5e-4 1e-4 0.5e-3 1e-3&
    0.5e-2 1e-2 0.5e-1 1e-1 0.5 1 5 10 50 100
sd12 161.29
nps 10000000

```

2. High-Density Cement mixed Crumb Rubber 5 vo% (Photon)

```

c Input File
1 0 -1 imp:n=1 imp:p=1 $Ambient
2 2 -2.826 -2 imp:n=1 imp:p=1 $HDCR5
3 3 -0.00125 -3 imp:n=1 imp:p=1 $air
4 3 -0.00125 -4 3 2 1 imp:n=1 imp:p=1 $Ambient
5 0 4 imp:n=0 imp:p=0 $outside the sphere
c
c Surface cards
c ##### Define Surfaces #####
1 RPP -8.35 -6.35 -1 1 -1 1 $ source
2 RPP -6.35 6.35 -6.35 6.35 -6.35 6.35 $ shield
3 RPP 6.35 8.89 -6.35 6.35 -6.35 6.35
4 SO 30 $Sphere Ambient
c

```



```

c Data cards
c ##### Define Materials #####
mode n p
phys:p
m2 6012 -0.040395 1001 -0.004515 8016 -0.00509 & Approximation WR
1001 -0.0034057 8016 -0.2960409 12000 -0.00113525 13027 -0.003973& HDC
14000 -0.0099341 16000 -0.1024651 20000 -0.045129 26000 -0.045129&
56000 -0.44023
m3 6000 -0.000124 7014 -0.755268 8016 -0.231781 18000 -0.012827 $air
c
c ##### Define Source #####
c Source Co energy definition. Point source. Isotropic.
sdef PAR=2 POS=-7.35 0 0 ERG=D1 AXS=0 5 0 EXT=D2 RAD=D3 $l source
SI1 L 1.1732 1.3325
SP1 D 1 1
SI2 -1.875 1.875
e0 1 100i 50
SP2 0 1
SI3 0 1.25
SP3 -21 1
c
c ##### Define Tallies #####
f2:p 2.1 $Tally photons on surface 2.1 (Xmax)
e2 0.5e-6 1e-6 0.5e-5 1e-5 0.5e-4 1e-4 0.5e-3 1e-3 &
0.5e-2 1e-2 0.5e-1 1e-1 0.5 1 5 10 50 100
sd2 161.29
f12:p 2.1 $Tally Photons in cell 3
e12 0.5e-6 1e-6 0.5e-5 1e-5 0.5e-4 1e-4 0.5e-3 1e-3&
0.5e-2 1e-2 0.5e-1 1e-1 0.5 1 5 10 50 100
sd12 161.29
tmesh

```

```

rmesh1:p flux
cora1 -8.35 20i 8.89
corb1 -6.35 20i 6.35
corc1 -6.35 20i 6.35
endmd
nps 10000000

```

3. High-Density Cement mixed with Crumb Rubber 10% (Neutron Dose Equivalent Rate)

c Input File

```

1 0 -1 imp:n=1 imp:p=1 $Ambient
2 2 -2.729 -2 imp:n=1 imp:p=1 $HDCR10
3 3 -0.00125 -3 imp:n=1 imp:p=1 $air
4 3 -0.00125 -4 3 2 1 imp:n=1 imp:p=1 $Ambient
5 0 4 imp:n=0 imp:p=0 $outside the sphere

```

c Surface cards

c ##### Define Surfaces #####

```

1 RPP -8.35 -6.35 -1 1 -1 1 $ source
2 RPP -6.35 6.35 -6.35 6.35 -6.35 6.35 $ shield
3 RPP 6.35 8.89 -6.35 6.35 -6.35 6.35
4 SO 30 $Sphere Ambient

```

c Data cards

c ##### Define Materials #####

mode n p

phys:p

```

m2 6012 -0.121185 1001 -0.013545 8016 -0.01527 & Approximation
1001 -0.000863 8016 -0.075031 12000 -0.000288 13027 -0.001007&
14000 -0.002518 16000 -0.002597 20000 -0.0012085 26000 -0.011438&
56000 -0.7208
m3 6000 -0.000124 7014 -0.755268 8016 -0.231781 18000 -0.012827 $air

```

c

```

c ##### Define Source #####
c Source Am/Be energy definition. Point source. Isotropic.
sdef pos=-7.35 0 0  erg=d1
si1 h 0 0.5 1 1.5 2 2.5 3 3.5 4 4.5 5 5.5 6 6.5 7 7.5 8 8.5&
    9 9.5 10 10.5 11 11.5 12
sp1 d 0 0.15 0.08 0.09 0.06 0.100 0.15 0.107 0.101 0.11 0.102 0.15&
    0.07 0.12 0.05 0.08 0.10 0.05 0.02 0.03 0.04 0.02 0 0 0
c
c ##### Define Tallies #####
f2:n 2.1  $Tally neutrons on surface 2.1 (Xmax)
e2 0.5e-6 1e-6 0.5e-5 1e-5 0.5e-4 1e-4 0.5e-3 1e-3 &
    0.5e-2 1e-2 0.5e-1 1e-1 0.5 1 5 10 50 100
sd2 161.29
c
c NCRP-38 Neutron flux-to-dose rate conversion factor
c units:mrem/hr per n/cm^2sec= (pSvcm^2/sec)(3.6e-4)
de2 2.5e-8 1e-7 1e-6 1e-5 1e-4 1e-3 1e-2 0.1 0.5 1 2.5 5 7 10 14 20
df2 3.676e-3 3.676e-3 4.464e-3 4.464e-3 4.309e-3 3.676e-3 3.572e-3 2.174e-2&
    9.259e-2 0.1315 0.125 0.156 0.147 0.147 0.208 0.227
c
f12:p 2.1  $Tally Photons in cell 3
e12 0.5e-6 1e-6 0.5e-5 1e-5 0.5e-4 1e-4 0.5e-3 1e-3&
    0.5e-2 1e-2 0.5e-1 1e-1 0.5 1 5 10 50 100
sd12 161.29
c
c Photon flux to dose rate conversion factors ANSI/ANS-6.1.1-1977
c units: (rem/hr)/(p/cm^2-s)
de12 0.01 0.03 0.05 0.07 0.1 0.15 0.2 0.25 0.3 0.35 0.4 0.45 0.5&
    0.55 0.6 0.65 0.7 0.8 1.0 1.4 1.8 2.2 2.6 2.8 3.25 3.75 4.25 4.75&
    5.0 5.25 5.75 6.25
df12 3.96e-06 5.82e-07 2.90e-07 2.58e-07 2.83e-07 3.79e-07 5.01e-07&

```

6.31e-07 7.59e-07 8.78e-07 9.85e-07 1.08e-06 1.17e-06 1.27e-06 1.36e-06&
 1.44e-06 1.52e-06 1.68e-06 1.98e-06 2.51e-06 2.99e-06 3.42e-06 3.82e-06&
 4.01e-06 4.41e-06 4.83e-06 5.23e-06 5.60e-06 5.80e-06 6.01e-06 6.37e-06&
 6.74e-06

c

nps 10000000

4. High-Density Cement mixed with Crumb Rubber 10% (Photon Dose Equivalent Rate)

c Input File

1 0 -1 imp:n=1 imp:p=1 \$Ambient
 2 2 -2.823 -2 imp:n=1 imp:p=1 \$HDCR10
 3 3 -0.00125 -3 imp:n=1 imp:p=1 \$air
 4 3 -0.00125 -4 3 2 1 imp:n=1 imp:p=1 \$Ambient
 5 0 4 imp:n=0 imp:p=0 \$outside the sphere

C Surface cards

C ##### Define Surfaces #####

1 RPP -8.35 -6.35 -1 1 -1 1 \$ source
 2 RPP -6.35 6.35 -6.35 6.35 -6.35 6.35 \$ shield
 3 RPP 6.35 8.89 -6.35 6.35 -6.35 6.35
 4 SO 30 \$Sphere Ambient

C Data cards

C ##### Define Materials #####

mode p

phys:p

m2 6012 -0.8079 1001 -0.0903 8016 -0.1018 & Approximation
 1001 -0.00358 8016 -0.31162 12000 -0.00119 13027 -0.00418&
 14000 -0.01045 16000 -0.10785 20000 -0.05019 26000 -0.04750
 m3 6000 -0.000124 7014 -0.755268 8016 -0.231781 18000 -0.012827 \$air

c

c ##### Define Source #####

c Source Co energy definition. Point source. Isotropic.

sdef PAR=2 POS=-7.35 0 0 ERG=D1 AXS=0 5 0 EXT=D2 RAD=D3 \$l source

SI1 L 1.1732 1.3325

SP1 D 1 1

SI2 -1.875 1.875

e0 1 100i 50

SP2 0 1

SI3 0 1.25

SP3 -21 1

c

c ##### Define Tallies #####

f2:P 2.1 \$Tally neutrons on surface 2.1 (Xmax)

e2 0.5e-6 1e-6 0.5e-5 1e-5 0.5e-4 1e-4 0.5e-3 1e-3 &

0.5e-2 1e-2 0.5e-1 1e-1 0.5 1 5 10 50 100

sd2 161.29

c

c Photon flux to dose rate conversion factors ANSI/ANS-6.1.1-1977

c units: (rem/hr)/(p/cm²-s)

de12 0.01 0.03 0.05 0.07 0.1 0.15 0.2 0.25 0.3 0.35 0.4 0.45 0.5&

0.55 0.6 0.65 0.7 0.8 1.0 1.4 1.8 2.2 2.6 2.8 3.25 3.75 4.25 4.75&

5.0 5.25 5.75 6.25

df12 3.96e-06 5.82e-07 2.90e-07 2.58e-07 2.83e-07 3.79e-07 5.01e-07&

6.31e-07 7.59e-07 8.78e-07 9.85e-07 1.08e-06 1.17e-06 1.27e-06 1.36e-06&

1.44e-06 1.52e-06 1.68e-06 1.98e-06 2.51e-06 2.99e-06 3.42e-06 3.82e-06&

4.01e-06 4.41e-06 4.83e-06 5.23e-06 5.60e-06 5.80e-06 6.01e-06 6.37e-06&

6.74e-06

c

nps 10000000

VITA

NAME: Ms. Pawitra Aim-O

SEX: Female

NATIONALITY: Thai

DATE OF BIRTH: 16 December 1978

PLACE OF BIRTH: Nakhon- Ratchasima

INSTITUTION ATTENDED:

Burapha University

2002-2005: Bachelor of Science (Environmental Health)

Sukhothai Thammathirat Open University

2009-2011: Bachelor of Science (Occupational Health and Safety)

Kasetser University

2004-2009: Master of Engineering (Safety Engineering)

Chulalongkorn University,

2014-2017: Doctoral of Engineering (Nuclear Engineering)

HOME ADDRESS: 156 Moo 4, Ta-oeng, Chokchai district, Nakhon-Ratchasima, Thailand, 30190, Tel 080-7302882

Email: pawitra_a@outlook.com